MECHANOMODULATION OF LYMPHATIC VESSEL CONTRACTILITY USING OSCILLATORY PRESSURE WAVEFORMS

A Dissertation
Presented to
The Academic Faculty

By

Anish Mukherjee

In Partial Fulfillment
of the Requirements for the Degree
Doctor of Philosophy in
Bioengineering

Georgia Institute of Technology

December 2020

MECHANOMODULATION OF LYMPHATIC VESSEL CONTRACTILITY USING OSCILLATORY PRESSURE WAVEFORMS

Approved by:

Dr. J. Brandon Dixon, Advisor
School of Mechanical Engineering
Georgia Institute of Technology

Dr. Levi Wood
School of Mechanical Engineering
Georgia Institute of Technology

Dr. Hanjoong Jo
School of Biomedical Engineering
Georgia Institute of Technology

Dr. Stanislav Emelianov
School of Electrical and Computer Engineering
Georgia Institute of Technology

Dr. Michael J. Davis
School of Medicine
University of Missouri

Date Approved: November 2, 2020

And once the storm is over you won't remember how you made it through, how you managed to survive. You won't even be sure, in fact, whether the storm is really over. But one thing is certain. When you come out of the storm you won't be the same person who walked in. That's what this storm's all about.

Haruki Murakami

To my mother - my inspiration and my pillar of support

ACKNOWLEDGEMENTS

undergraduate students working alongside me, Stephen Arjanto and Josephine Rudd, who have inspired me with their passion and dedication.

The administrative and research personnel in the Parker H. Petit Institute for Bioengineering and Biosciences (IBB) building have been instrumental in me completing my work. I would like to thank the amazing people at the Physiological Research Laboratory (PRL) for taking care of the research animals and always being there to help. I would like to especially thank Dr. Laura O'Farell and Dr. Richard Noel for always being there to share their experience and knowledge with me. I would like to thank Andrew Shaw for training me on the microscopy core and being patient and helpful with my many requests.

The Bioengineering program has offered me the freedom to explore my interests and develop myself as a researcher and as a person, for which I am really grateful. Being in the Bioengineering Graduate Association has helped me immensely in my research and professional life. On that note, a special thank you must go to Laura Paige for pushing me to engage more with the many opportunities the program has to offer, and being the glue that holds the Bioengineering program together.

I have been extremely fortunate to be brought up in a loving and supportive family. My parents have been a constant source of support and inspiration. Thanks to their sacrifice, I could focus on my work without having to worry about my needs, a privilege that I am really grateful for. I would also like to thank them for letting me pursue my passion and never imposing their wants on me. It cannot be easy to have your child stay so far away from you for so long, but I have the utmost gratitude and respect for their sacrifice. I would like to especially mention my cousin, Tipu, whose courage, dedication, and passion towards his craft has been a constant source of inspiration for me.

I have also had the fortune of having many great friends throughout my life, who have enriched my life with their presence and support. I would like to thank Ritwik, Rudra, and Debdutta (the original "Charu-goenda") for being there during the formative years of my life and still continuing to be there whenever needed. Thank you to Souravda, Monodeepda,

vi

Swarnavada and Suvadeepda for your guidance and friendship during the first, crucial, few years of my PhD. I would like to especially thank Shruti, Shashi, and Anusha for making the final few years of my PhD infinitely more bearable with their craziness and companionship. And, of course, thank you to Saurabh Nath for being a constant source of motivation, wackiness, intellectual partnership, and a bedrock of friendship I can always lean on.

I would especially like to thank Asha for Education, a non-profit organization working towards the education of underprivileged children in India. Being part of the organization has helped me stay connected with my roots in India, while also developing my leadership and communication skills. I have met numerous wonderful people while volunteering with Asha, many of whom have become extremely close friends.

And finally I would like to thank a very special person, Gareeyasee, for coming into my life at a crucial time and enriching my life to an extent I never expected. You make me a better person. The last two years have been more fun than they have any right to be because of your love, enthusiasm and support. I look forward to sharing many more years of my life with you.

TABLE OF CONTENTS

LIST OF FIGURES

LIST OF ABBREVIATIONS

LEC	Lymphatic Endothelial Cells
LMC	Lymphatic Muscle Cells
WSS	Wall Shear Stress
$\mathbf{P_{avg}}$	Average Transmural Pressure
ΔP	Pressure Gradient
NO	Nitric Oxide
NOS	Nitric Oxide Synthase
ROS	Reactive Oxygen Species
NIR	Near Infrared
ICG	Indocyanine Green
WSS	Wall Shear Stress
OWSS	Oscillatory Wall Shear Stress
CWT	Continuous Wavelet Transform
MLD	Manual Lymphatic Drainage
IPC	Intermittent Pneumatic Compression
CB	Compression Bandaging
OPW	Oscillatory Pressure Wave
ROI	Region of Interest

SUMMARY

The lymphatic system is a network of vessels and nodes transporting and clearing interstitial fluid, orchestrating the immune response, and facilitating lipid transport. An important component of the lymphatic system are the collecting lymphatic vessels which pump lymph through the body by virtue of their intrinsic contractility. The collecting lymphatic vessels are known to be sensitive to their mechanical microenvironment which dictates their contractility. However, relatively little is known about how collecting lymphatic vessel contractility is modulated by their oscillatory mechanical microenvironment and how this mechanosensitivity is affected by lymphatic injury. It is important to know the limits of the mechanomodulation of lymphatic vessels in both physiological and pathological circumstances, since an aberrant mechanical microenvironment is frequently associated with lymphatic dysfunction, such as in the case of lymphedema. The present work investigates the role of the oscillatory mechanical microenvironment in the modulation of collecting lymphatic contractility. The mechanomodulation of isolated collecting lymphatic vessels by oscillatory shear stress was investigated and optimal parameters of stimulation were identified for maximizing lymphatic function. The modulation of lymphatic vessels was also investigated in vivo in response to oscillatory pressure gradients mimicking pressure waveforms during massage. Massage-like pressure waveforms modulated collecting lymphatic vessel contractility, and this modulation was altered by lymphatic injury. Thus, the oscillatory microenvironment is shown to be an important regulator of lymphatic contractility and the present work provides clues on how the mechanomodulation of lymphatics can be harnessed to understand and improve therapeutic approaches to lymphedema.

CHAPTER 1

INTRODUCTION

The lymphatic system is a complex network of branching vessels and nodes that make up a secondary circulatory system of the human body next to the blood circulation. Lymphatic vessels (specifically, lacteals) were identified in dogs as early as 1622, in the form of "milky" vessels that existed in parallel with the blood circulation [1]. The lymphatics were initially regarded as a "sewage system" for the body, useful only for draining the capillary filtrate from the interstitium (the fluid-filled space between tissues) and recirculating it back into the bloodstream. In the years since then, the role of lymphatic vessels has been elucidated in a number of physiological and pathological situations where they are not only passive channels for the transportation of interstitial fluid, but active participants. The lymphatics are crucial for a successful immune response, facilitating the trafficking and maturation of immune cells. Intestinal lymphatics, specifically lacteals, are involved in the absorption as well as the transportation of lipids. They are also involved in a number of pathologies, most notably cancer, where their physiology and morphology are impaired, leading to aberrant lymphatic vessels that can exacerbate the pathological conditions. For that same reason, lymphatics have emerged as primary targets for treating a number of immune and cancer-related pathologies.

In spite of the importance of the lymphatic system in homeostasis, an understanding of how the network of lymphatic vessels functions as a coherent unit, combining the various mechanical and chemical cues that shape its physiology, is still in its infancy. While steady strides are being made in our understanding of the biology of lymphatic vessels in the context of immunology and cancer, equally important is their response to their mechanical microenvironment, since the mechanical microenvironment determines the physiology of lymphatics to a large extent. The degree to which lymphatic vessels can sense and respond

to their mechanical environment is called mechanosensitivity, and the alteration of lymphatic function in response to the mechanical microenvironment is called mechanomodulation. The intrinsic functional characteristics of the lymphatics, in tandem with extrinsic factors, determine the net flow of lymph through the lymphatic network which, in turn, can dictate the difference between physiological and pathological conditions in the lymphatics. Hence, this thesis will delve into the interactions of the lymphatic system with its mechanical microenvironment and will try to answer some questions regarding how lymphatic vessels are modulated by their environment and how the mechanomodulation is altered during pathological states.

1.1 Components of the Lymphatic System

Before going into the details of lymphatic mechanomodulation, it is important to understand what the different parts of the lymphatic system are. The lymphatic system begins with the lymphatic capillaries, also called initial lymphatics. Initial lymphatics are closed-ended vessels formed by a single layer of lymphatic endothelial cells (LECs) with a discontinuous basement membrane [3, 4, 5]. The endothelial cells are held together by specialized button-like junctions [6, 7] which provide structural integrity to the initial lymphatics, while allowing for the entry of fluid into the lymphatic capillaries. The button-like junctions cause the initial lymphatic endothelial cells to be apposed to each other, forming overlapping flap-like structures that are called primary lymphatic valves. The primary lymphatic valves are the sites of uptake of interstitial fluid into the lymphatic vasculature. A defining feature of these initial lymphatic endothelial cells is their connection to their surrounding extracellular matrix with anchoring filaments. During periods of excess interstitial fluid accumulation, the anchoring filaments open the primary lymphatic valves, which results in the movement of interstitial fluid into the initial lymphatics [8, 9]. The interstitial fluid is referred to as "lymph" once it enters the initial lymphatics and starts flowing through the lymphatic vasculature. Figure 1.1 shows the main components of the lymphatic vasculature
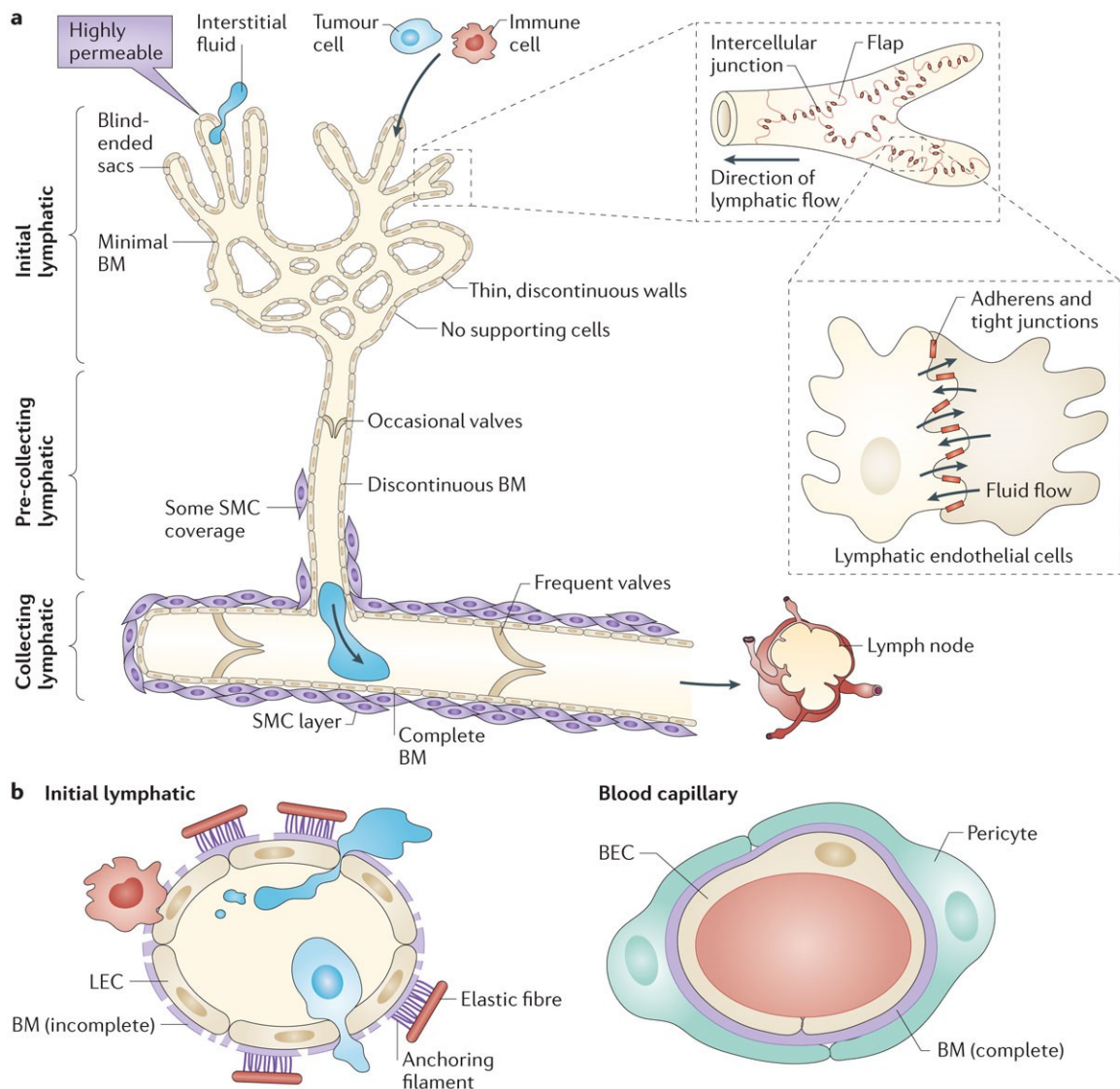
Figure 1.1: An overview of the various components of the lymphatic system. a) The organization of the lymphatic network is shown, starting from the initial lymphatic capillaries and moving to the pre-collecting and collecting lymphatics. The primary lymphatic valves in the initial lymphatics formed by the "button-like" junctions are highlighted. b) The initial lymphatic structure is compared to a blood capillary, showing a nearly absent basement membrane and the presence of special anchoring filaments that help in the formation of lymph by opening the primary lymphatic valves. The diagram is taken from Williams, 2014 [2].

with an emphasis on the structure of the initial lymphatic vessels. Figure 1.1b includes a comparison of the initial lymphatic capillaries with the blood capillaries to show the key structural differences.

The second major structure of the lymphatic network is the collecting lymphatic vessel (Figure 1.2). The initial lymphatics connect and form structures called pre-collecting lymphatics, which are characterized by a basement membrane surrounding the endothelial cells and sparse muscle cell coverage [10, 11]. These develop downstream into collecting lymphatic vessels, which are characterized by a complete basement membrane, lymphatic muscle cell (LMC) coverage, and well-developed valves (called secondary lymphatic valves) that ensure a unidirectional flow through the vessels [12, 13]. The collecting lymphatic vessel physiology is unique since they can spontaneously perform fast phasic contractions on top of the slow tonic constrictions that are also seen in blood vessels [14, 15]. The segment of a collecting lymphatic vessel between two valves is called a lymphangion, which is the basic, spontaneously contracting unit of the lymphatic vasculature. The lymphangions, with the assistance of the secondary lymphatic valves, ensure a unidirectional flow of lymph through the lymphatic vasculature.

The lymphatic vasculature is also interspersed with multiple lymph nodes. The lymph nodes serve as the point of exchange for nutrients and immune cells, also participating in the activation of the adaptive immune system [16, 5]. Afferent lymphatic vessels carry lymph, along with nutrients, chemokines, and cells, into the lymph nodes [17]. It is estimated that as much as half of all lymph is reabsorbed into the blood circulation by high endothelial venules within the lymph nodes as observed by the fact that efferent (outgoing) lymph has a higher protein concentration than afferent (incoming) lymph [18, 19, 20]. The rest of the lymph continues on its journey through the lymphatic circulation through the efferent lymphatic vessels.

1.2 The Collecting Lymphatics

Of these three components of the lymphatic system, collecting lymphatic vessels will be the major focus for this thesis. A hallmark of collecting lymphatic vessels is their ability to intrinsically contract and push lymph through the lymphatic vasculature. The fascinating intrinsic contractility of the collecting lymphatics makes it an interesting candidate for studying lymphatic function, especially considering the fact that the contractile activity of collecting lymphatics is highly regulated by both mechanical factors, such as the pressure and flow in and around the lymphatics (the lymphatic mechanical microenvironment), as well as chemical factors, such as nervous stimulation and the inflammatory environment around the vessels. While oftentimes the effects of mechanical and chemical factors are difficult to delineate in vivo, there is a convenient behavior of collecting lymphatics that allows us to study its response to its mechanical environment independent of the chemical cues that regulate lymphatic function; the collecting lymphatics can contract spontaneously even when dissected from the body of the animal and cannulated in a special preparation. Thanks to this behavior of the collecting lymphatics, steady strides have been made in understanding how they react to their mechanical microenvironment.

1.2.1 The Collecting Lymphatic Mechanical Microenvironment

The collecting lymphatic mechanical microenvironment is unique, especially compared to the mechanical conditions faced by blood vessels, and it is important to understand what makes collecting lymphatics distinct from their counterparts in the blood circulation. Both the collecting lymphatics and blood vessels are cylindrical (tubular) structures that experience time-varying transmural pressures (radial forces which stretch the walls of the vessels) and wall shear stresses (axial forces that act in parallel to the vessel walls). However, the lymphatic vessels, owing to their intrinsic contractility, are exposed to a unique mechanical microenvironment that sets them apart from the blood vasculature. Unlike blood
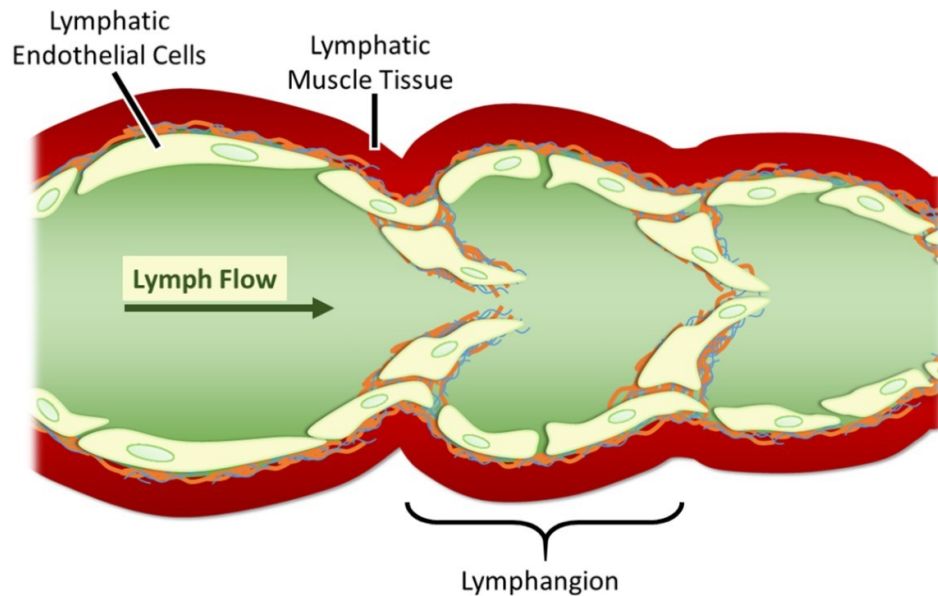
Figure 1.2: The structure of the collecting lymphatic vessels is shown. The vessels are primarily composed of lymphatic endothelial cells and lymphatic muscle cells. The presence of valves ensure a unidirectional lymph flow. The diagram is taken from Mukherjee, 2018 [21].

vessels, lymphatic vessels undergo both slow, long-term, tonic contractions as well as fast, short-term, phasic contractions. This unique intrinsic contractility of the lymphangions, combined with extrinsic factors such as muscle contractions, breathing, etc., subjects the lymphangions to highly oscillatory transmural pressures and wall shear stresses. During a typical contraction cycle, a lymphangion can contract up to 39% of its diameter, and while the average wall shear stress (WSS) over a contraction cycle is on the order of 0.6 dyn/cm^2, the peak shear stress is around 8 dyn/cm^2 as found in rat mesenteric lymphatics [22]. When exposed to edemagenic conditions [23, 24], or in response to elevated fluid loads due to high-fat meals [25], the flow rate, and thus the maximum wall shear stress, experienced by the vessels can increase 10-fold to about 5 to 40 dyn/cm^2 [23]. In comparison, the shear stress in the blood vasculature is far higher than those in lymphatics, with small arterioles having shear stresses exceeding 60 dyn/cm^2, and venules showing shear stresses of 20 dyn/cm^2 or higher [26, 27]. Hence, the lymphatic vessels are subjected to a

mechanical mechanical microenvironment characterized by low and oscillatory wall shear stress, albeit with maximum transient wall shear stress values that can approach those of the blood vasculature, especially during pathological conditions.

1.2.2 Metrics to Quantify Collecting Lymphatic Function

Lymphatics, while bearing structural similarities to blood vessels (especially the veins), are functionally quite different. In the absence of a centralized pumping unit akin to the blood circulation (the heart), the collecting lymphatics form a distributed pumping system consisting of a number of lymphangions in series. As mentioned before, lymphangions exhibit tonic as well as phasic contractions, thus being behaviorally similar to both blood vessels as well as the heart. Keeping in mind the behavioral similarities between the collecting lymphatics and the heart, it makes sense that a lot of metrics that have been used for defining the pumping function of the heart have made their way into the field of lymphatics as well [28, 29]. It is prudent to discuss some of these commonly used metrics that are useful in quantifying the contractile function of the lymphangions.

- Contraction frequency (Hz or contractions/minute)

- Contraction amplitude (μm)

- End diastolic diameter (μm) – the maximum diameter of the vessel over a contraction cycle

- End systolic diameter (μm) – the minimum diameter of the vessel over a contraction cycle

- Vessel tone (%) – the diastolic diameter of the vessel compared to the diameter of the vessel when it is maximally dilated (under calcium-free condition)

- Stroke volume (μm^3) – the volume of lymph pumped by a unit length of lymphangion per contraction

7

- End Diastolic Diameter (EDD)
- End Systolic Diameter (ESD)
- Contraction Frequency (CF)
- Contraction Amplitude (CA)

- Ejection Fraction (EF) = $\dfrac{EDD^2 - ESD^2}{EDD^2}$

- Fractional Pump Flow (FPF) = CF x EF
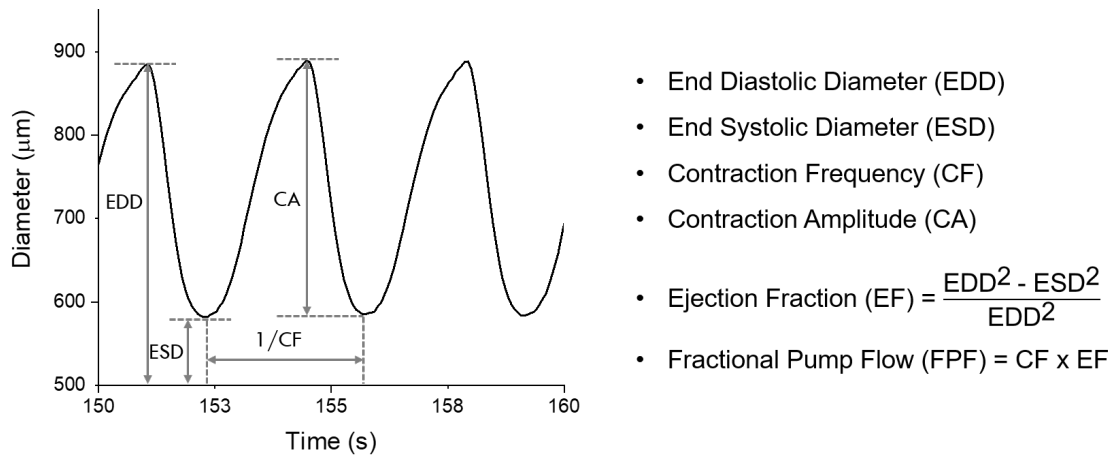
Figure 1.3: The lymphatic functional metrics are shown over a few typical contraction cycles of a lymphangion. The diameter tracing shows three contraction cycles of a lymphangion, and the four basic functional metrics - contraction frequency, contraction amplitude, end diastolic diameter, and end systolic diameter are shown in the graph. The two lymphatic transport metrics - ejection fraction and fractional pump flow, which are derived from the basic functional metrics, are defined in the figure legend.

- Ejection fraction (%) – the percentage of lymph pumped by a unit length of lymphangion per contraction

- Lymphatic pump flow (μm^3/s) – the volume of lymph pumped by a unit length of lymphangion per second. Mathematically, this is equivalent to (stroke volume x contraction frequency)

- Fractional pump flow (%/s) – the percentage of lymph pumped by a unit length of lymphangion per second. Mathematically, this is equivalent to (ejection fraction x contraction frequency)

The different lymphatic functional metrics are shown in Figure 1.3 over a few typical contraction cycles of a lymphangion.

8

a) Initial lymphatic

(i)

a) Collecting lymphatic

σ_{axial}

τ_{wall}

σ_{hoop}

(ii) τ_{wall}

NO
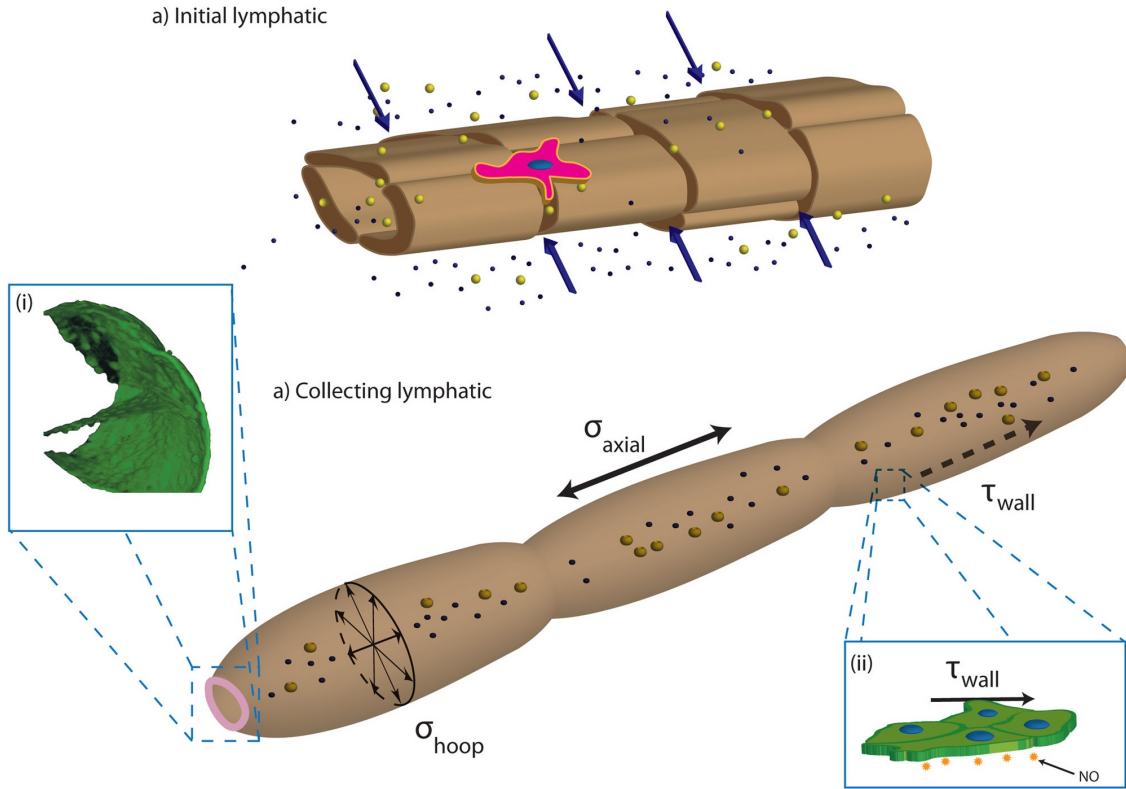
Figure 1.4: The different mechanical forces acting on initial and collecting lymphatic vessels are shown. Initial lymphatics are simple structures that are primarily exposed to intersitial pressures. The collecting lymphatics possess valves as shown by the confocal reconstruction in the inset, and they are exposed to a more complex milieu of forces, of which the wall shear stress (τ_{wall}), transmural pressure, represented as the hoop stress (σ_{hoop}), and axial stress (σ_{axial}) are the most important. The diagram is taken from Dixon, 2010 [30].

1.3   Mechanomodulation of the Collecting Lymphatics

The collecting lymphatic vessels possess the ability to sense their unique oscillatory mechanical microenvironment and change their contractile behavior accordingly, a property that is referred to as the mechanosensitivity of the lymphatics. The modulation of lymphatic contractility by mechanical forces is referred to as the mechanomodulation of the lymphatics. The two primary mechanical forces that affect the contractility of lymphangions are the luminal wall shear stress (WSS) and the transmural pressure [31, 32, 15]. The WSS (shown in Figure 1.4 as τ_{wall}) has the effect of applying a shearing force to the LECs lining the lumen of the lymphangion, which acts in the direction of the flow and parallel to

the endothelial cell layer. The WSS depends on the axial pressure gradient across the vessel or the rate of flow of the lymph (higher flow produces higher WSS), and the geometry of the lymphangion (a smaller cross-sectional area corresponds to a higher WSS for the same flow rate). The transmural pressure is the difference between the intralymphatic pressure (the pressure inside the lymphatic lumen) and the interstitial pressure (the pressure outside the lymphatic lumen). Transmural pressure exerts a radial hoop stress (shown in Figure 1.4 as σ_{hoop}) on the walls of the lymphangion, effectively radially stretching the lymphangion. A higher basal transmural pressure corresponds to an elevated stretch on the lymphatic endothelial cells and muscle cells. The collecting lymphatics are also exposed to a basal axial stress (shown in Figure 1.4 as σ_{axial}). An elevated axial stretch has also been shown to possibly affect lymphatic function [33, 34]. These forces have a significant impact on both the normal functioning of the lymphatic vasculature, as well as pathological conditions that may arise out of chronically elevated mechanical forces and/or reduced sensitivity to these mechanical forces [32, 15]. For the purpose of this thesis, we will delve into the details of the roles of WSS and transmural pressure on lymphatic mechanomodulation.

1.3.1 Wall Shear Stress

The luminal WSS is one of the most important regulators of lymphatic pump function, acting through the lymphatic endothelium to control the contraction of the LMCs. Studies on isolated lymphatic vessels have enabled us to isolate the effect of wall shear stress on lymphatic contractility. The pressure difference (also referred to as the pressure gradient), ΔP, across an isolated lymphatic vessel is frequently used as a substitute for the WSS, since qualitatively it provides similar information, while being easier to record and quantify. Early studies on the effect of WSS on the contraction of lymphangions suggested that the contractile frequency increased and the contraction amplitude decreased in rat iliac lymphatic vessels in response to an imposed constant pressure gradient [35]. The direction of the flow (decided depending on whether the pressure gradient was negative or positive)

was also implicated to be a deciding factor in whether the pump function was decreased or increased [36]. In 2002, Gashev et al. [37] quantified the effect of an imposed constant pressure gradient on the lymphatic pump function of rat mesenteric lymphatic vessels and thoracic ducts, while the average transmural pressure (P_{avg}) was being held constant. An imposed pressure gradient across the isolated lymphangion caused an inhibition of contractile function. A later study by Kornuta et al. [38] showed that a linearly increasing (ramped) pressure gradient across an isolated lymphangion can gradually inhibit lymphatic function, and this was concurrent with a stabilization of the average shear stress that the lymphangion was experiencing (Figure 1.5). Gashev et al. (2002) also showed that an increase in the pressure gradient across a lymphangion caused the frequency, ejection fraction, and fractional pump flow to decrease for both thoracic ducts and mesenteric vessels, with the thoracic ducts showing a more marked decrease in comparison to the mesenteric lymphatics (Figure 1.6). This well-documented decrease in lymphatic function by an imposed WSS is commonly referred to as "shear inhibition". The difference in the shear inhibition between thoracic ducts and mesenteric vessels implied a variability in the mechanosensitivity of the lymphatics based on the tissue bed from which the lymphatics originate.

The molecule that has been most extensively studied in the context of shear inhibition is nitric oxide (NO). Early studies performed on cultured LECs showed that endothelial cells can produce NO and upregulate inducible nitric oxide synthase (iNOS) expression in response to agonist stimulation [39]. The increased upregulation was proposed to cause lymphatic relaxation and hence control lymphatic tone, similar to the role played by NO in blood vessels. Indeed, in the work of Gashev et al. [37], blocking NO with an exogenous nitric oxide synthase (NOS) inhibitor, L-NMMA, partially reversed the flow-dependent contraction inhibition. While this study showed a role of NO in shear inhibition, it left the door open for the possibility of other molecules being involved in shear-dependent lymphatic modulation. Stimulation of NO production in lymphangions also reduced spontaneous transient depolarizations (which control lymphatic contractility) in LMCs, and this
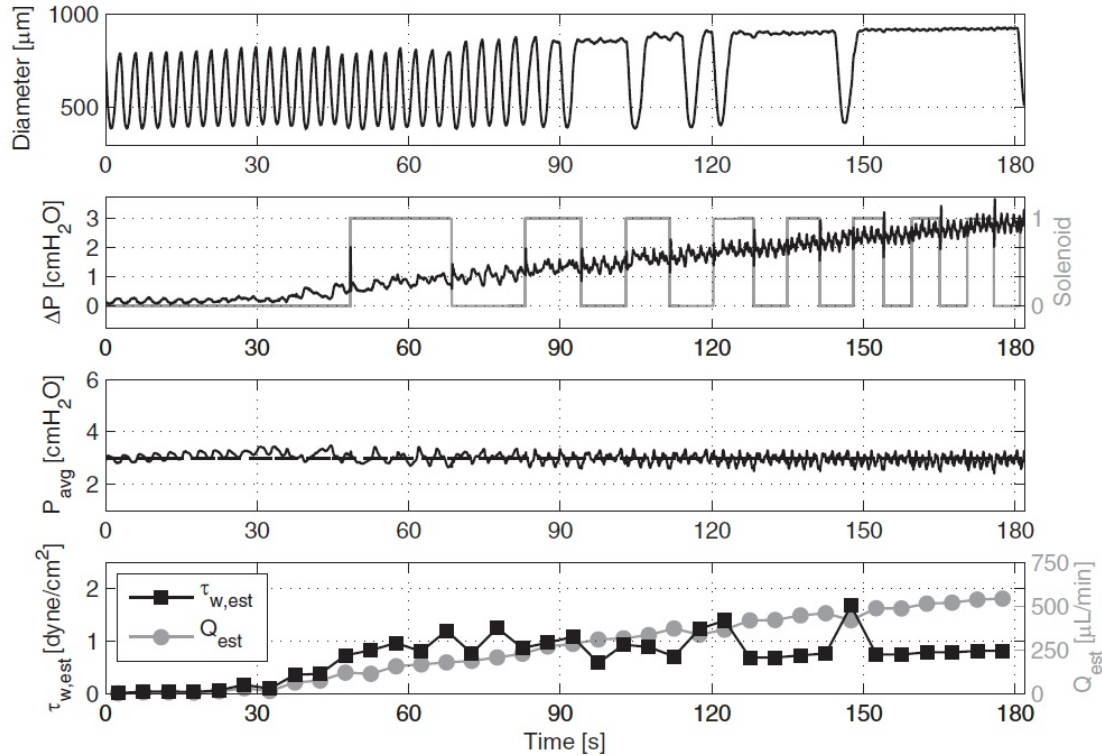
Figure 1.5: The inhibition of lymphatic contractions by an imposed wall shear stress is shown. The top panel shows the diameter tracing from a contracting lymphatic vessel, which captures the periodic contraction pattern of an isolated lymphatic vessel. The second panel shows an imposed pressure gradient that is being increased linearly. The third panel shows the average transmural pressure in the vessel, which is being held constant. The fourth panel shows the average estimated wall shear stress in the vessel. The figure is taken from Kornuta, 2015 [38].

effect was reversed by blocking NO. Thus, NO has a strong inhibitory effect on lymphatic contractility. Follow-up studies confirmed the inhibitory role played by NO in lymphatic contractility by genetically blocking basal NO production, which increased lymphatic contractility [40].

Other molecules, such as endothelial prostanoids [35], histamine [41], and reactive oxygen species (ROS) [42, 43] were also identified to play a role in the shear-induced functional changes in lymphatic vessels. Histamine was shown to be an important endothelium-derived relaxation factor (EDRF) that acts along with NO to inhibit lymphatic pumping [41]. While Gashev et al. previously showed that inhibition of NOS, and consequently NO
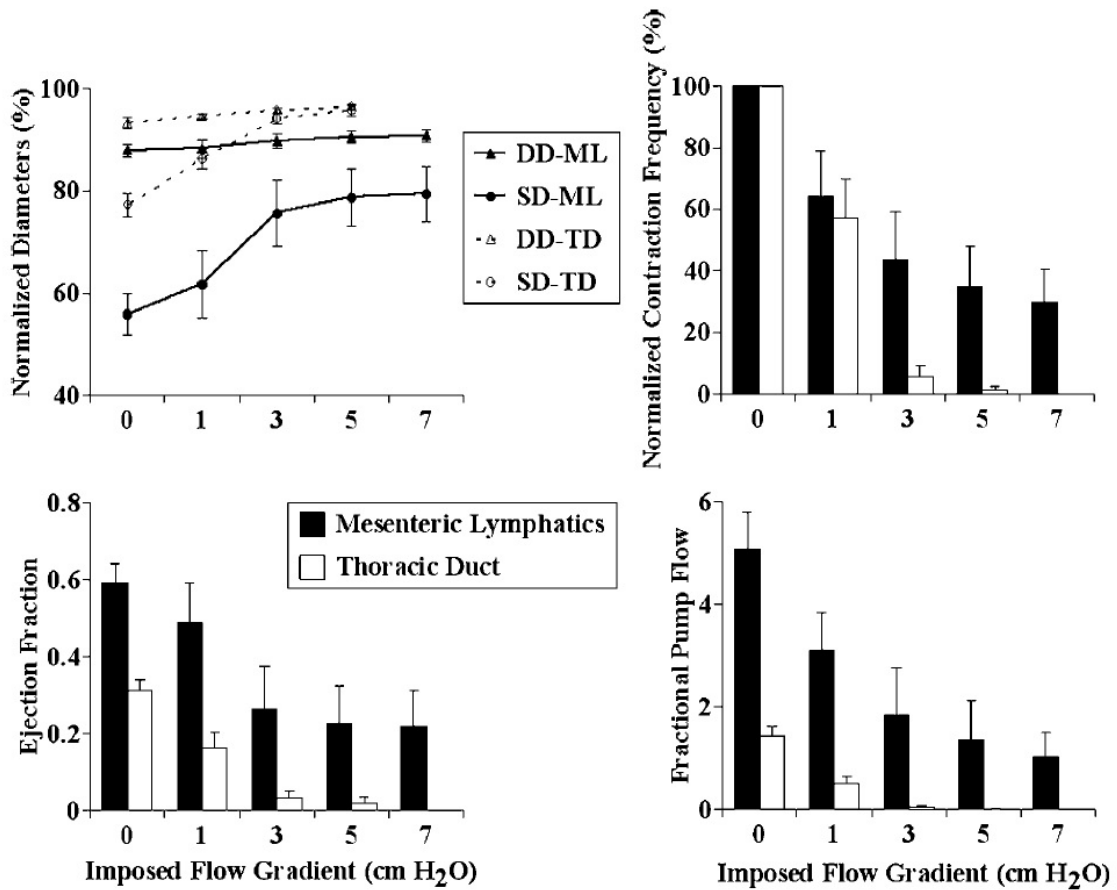
Figure 1.6: The effect of different constant pressure gradients on lymphatic function is shown. Metrics of lymphatic pumping such as contraction amplitude, frequency, ejection fraction, and fractional pump flow were all found to decrease in response to an increase in the imposed constant pressure gradient. Thoracic ducts showed a more marked decrease in function compared to the mesenteric collecting vessels. The figure is taken from Gashev, 2002 [37]

production, was not able to completely abrogate the flow-mediated relaxation of lymphatic vessels, blocking histamine and NO together completely eliminated the flow-dependent inhibition of lymphatic vessel contractility. Exogenously applied ROS have been shown to inhibit the contractile function of mesenteric lymphatics significantly [43]. Chronically increased flow in vivo has also been shown to increase the ROS concentration in LECs [42]. The overproduction of ROS that is induced by pathological mechanical forces (such as increased shear stress due to elevated lymph flow) can have long-term pathological effects on the collecting lymphatic function.

The role of shear stress in modulating lymphatic contraction is not simply a scientific curiosity that has been investigated in vitro and ex vivo. There are physiological benefits of lymphatics tuning their contractility to the prevalent shear stress environment, which is reflected in their lymph transport ability. In vivo experiments have shown that inhibition of NOS using an exogenous blocker (L-NMMA) reduced the lymph flow in initial lymphatics without affecting their structure [44]. When the collecting lymphatic vessels were ligated, the blockage of NOS did not cause a reduction in initial lymphatic flow. These findings suggested that NO is required for normal collecting vessel function, which affects the fluid transport across the lymphatic network. This role of NO in the regulation of lymphatic function was further investigated by Gasheva et al. [45], where the authors used phasically contracting vessels to generate flow (instead of an externally imposed flow) and compared them against non-contractile vessel segments. The phasically contractile vessels showed a lower tone than their non-contractile counterparts, which was consistent across transmural pressures ranging from 1-5 cmH$_2$O. NO was found to be the most important regulator of this flow-dependent vasodilation. Thus, one can see a picture of lymphatic self-regulation forming from all these studies, where the lymphatics can regulate their own function in a shear-dependent manner, with NO acting as a major player in this self-regulation. This idea was formalized as the pump-conduit duality of the lymphatic vessel using computational modelling and in vitro studies [46, 47]. Under this framework, lymphangions act as pumps when exposed to physiologically relevant pressure gradients, which are typically characterized by an elevated afterload. However, during pathological conditions such as edema, the direction of the pressure gradient can reverse, resulting in the lymphatic vessels acting more like conduits, characterized by a reduction in lymphatic pumping metrics. The transition to a conduit configuration reduces the resistance of the lymphatic vessels to flow, thus resulting in more efficient conduction of lymph through the lymphatic network.

It is important to mention that all the aforementioned studies were performed under constant shear stress conditions, while the lymphatic mechanical microenvironment is char-
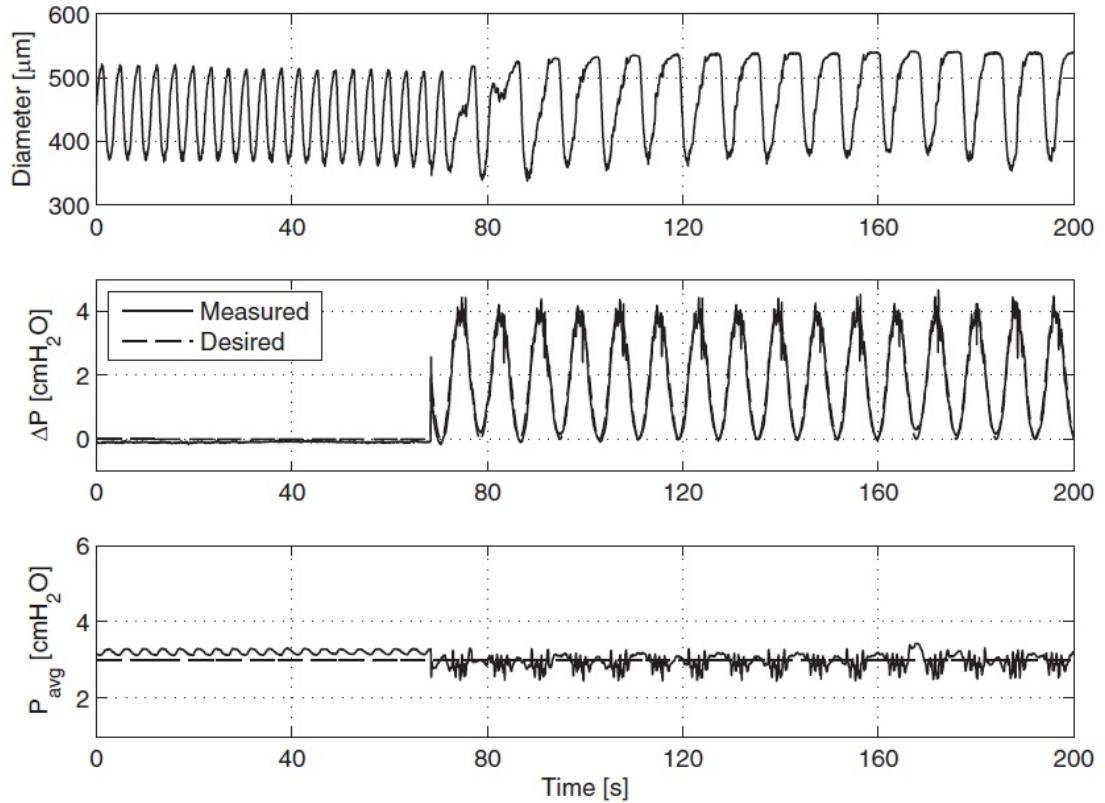
Figure 1.7: The entrainment of lymphatic contraction frequency to an imposed oscillatory pressure gradient is shown. The top panel shows the diameter tracing of the lymphatic vessel, the middle panel shows the imposed oscillatory pressure gradient, and the lower panel shows the average transmural pressure that is being held constant. The oscillatory pressure gradient was applied at the 70 s time point, after which the vessel was seen to entrain to the pressure gradient. The figure is taken from Kornuta, 2015 [38].

acterized by highly oscillatory shear stresses. In a more recent study, the lymphangions were found to "entrain" their contraction frequency to an externally applied oscillatory flow waveform at a constant transmural pressure, i.e. their contraction frequency matched the frequency of the externally applied oscillatory flow [38] (Figure 1.7). The entrainment was found to occur only for large amplitude oscillatory flow waveforms, and the blocking of NO or histamine did not block the entrainment. The oscillatory flow when applied on denuded vessels did not cause the vessel to entrain, thus showing that the endothelium is necessary for entrainment. Thus it is clear that the mechanomodulation of collecting lymphatics by oscillatory shear stresses cannot be simply explained by our current under-

15

standing of lymphatic mechanomodulation by constant shear stresses. When it comes to the question of how oscillatory shear stresses can modulate lymphatic function, we need other metrics and analysis techniques to quantify lymphatic behavior, and in this case the metric of entrainment becomes especially important. Chapter 2 of this thesis will attempt to investigate how oscillatory shear stress can modulate lymphatic contractility and what are the physiological benefits of this mechanomodulation.

1.3.2   Transmural Pressure

Transmural pressure has the opposite effect to WSS on lymphatic contractile function. Increasing the transmural pressure has the effect of increasing the pumping frequency and pump function of the lymphatic vessels until an optimum pressure is reached, after which the pumping frequency and pump function reduces with a further increase in transmural pressure. This behavior is expressed as a bell curve of the lymphatic pumping metric vs transmural pressure, which has been recapitulated in a number of different animals, including bovine, rat and mouse lymphatics [28, 29, 48]. The optimal modulation of lymphatic function by transmural pressure is thought to be driven by an optimal length-tension relationship that has been documented in most smooth muscle cells [49, 50, 51]. The isolated lymphatic vessels were also found to exhibit myogenic constriction and dilation in response to changes in transmural pressure, similar to that seen in blood vessels, where the diastolic diameter of the vessel slowly decreased after a sharp increase following a step increase in transmural pressure [52]. The amount of constriction was found to be higher when the pressure increase was effected from a lower baseline pressure, and enhancing the lymphatic contractility using substance P (an inflammatory mediator) increased the magnitude of the constriction. A ramped increase in transmural pressure elicited a rate-dependent response, where the contraction frequency (but not the amplitude) was found to be enhanced in response to a faster ramp.

However, the average transmural pressure in the lymphatics is not the only determining

16

factor for contractility. The preload (the transmural pressure upstream of a chain of lymphangions) and afterload (the transmural pressure downstream of a chain of lymphangions) can also affect lymphatic contractility. Increasing the preload slowly has the effect of increasing the end-diastolic diameter and stroke volume, while a sharp increase in preload is associated with a reduced stroke volume that slowly recovers over time [53, 54]. The length-tension relationship of lymphatic vessels were also studied using wire myography and revealed an increase in the active wall tension generated by isolated lymphatics in response to an increase in stretch [51, 49, 50, 55]. An acute increase in afterload was found to increase both tonic and myogenic constrictions in the upstream section of the isolated lymphatic vessels[54, 56]. While the endothelium is essential for flow-mediated changes in lymphatic contractility, it was shown that the endothelium is not required for the transmural pressure-dependent modulation of lymphatic pumping [57]. Thus, investigations into the effect of transmural pressure, and hence stretch, on collecting lymphatic function have mostly been focused on lymphatic muscle cells and the presence of stretch-activated ion channels that may lead to a transmural pressure-dependent control of contractility [58]. The effects of constant shear stress and transmural pressure on lymphatic contractility are represented in Figure 1.8.

While the response of lymphatic vessels to an acute increase in transmural pressure is well investigated, the response of lymphatics to an elevated level of transmural pressure for an extended duration has only been sparsely studied [60]. In response to a partial occlusion of a bovine mesenteric vessel in vivo for 3 days, the upstream segment of the vessel that had been exposed to an elevated pressure was found to have a higher systolic and diastolic diameter, as well as higher pump function than downstream vessels. The question of how lymphatics react long term to extended changes in their mechanical microenvironment is an important one in the context of lymphatic pathologies, specifically lymphedema. Pathologies related to lymphatic dysfunction, such as lymphedema, are associated with aberrant pressure and shear environments, which can have long-term consequences on lymphatic
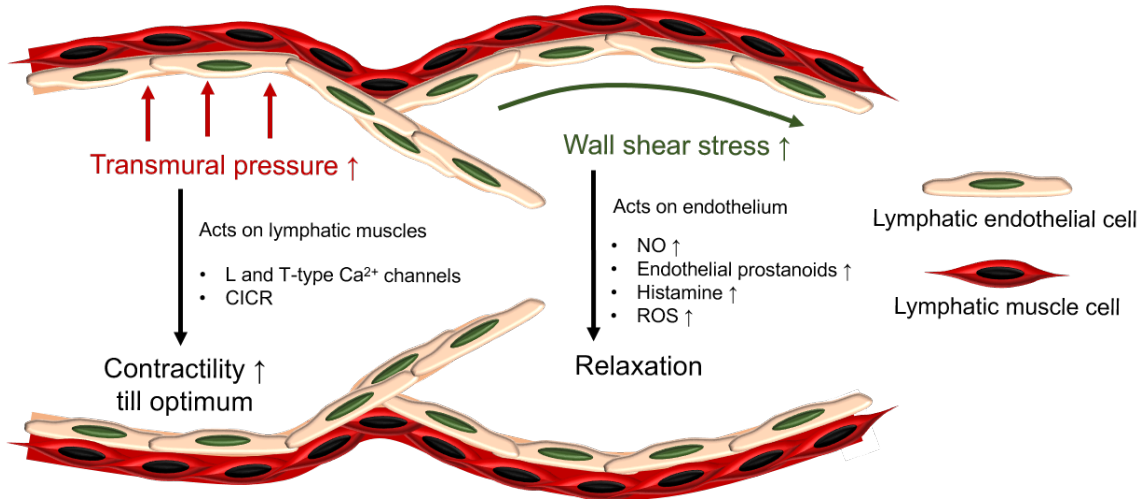
Figure 1.8: Collecting lymphatic vessels respond to the wall shear stress and transmural pressure acting on the LECs and LMCs respectively. The wall shear stress exerts a force parallel to the LEC layer and causes a relaxation and reduction in contractility of the lymphangions. The transmural pressure acts perpendicular to the wall of the lymphatics and controls the contractility by mostly affecting the lymphatic muscle cell layer. The diagram is taken from Mukherjee, in press [59].

function. The next section will delve into the literature on lymphedema, and this question will be visited during chapter 4, when we will discuss the long terms effects of an induced lymphatic injury on the mechanosensitivity and contractile function of the intact lymphatic network.

1.4 Lymphedema

As we have seen, the lymphatic vessels are highly sensitive to their mechanical microenvironment. The mechanical forces acting on the lymphatic vessels can modulate their pump function and ensure that the lymphatic vasculature is performing at an optimum level. Thus, it is no surprise that the dysfunction of lymphatic vessels is frequently accompanied by pathological shear stress and transmural pressure. The elevated mechanical forces are usually the result of some form of injury to the lymphatic system, or some other pathological condition in the body. The effect of these pathological forces is seen in a maladaptive re-modeling of the lymphatic vessels, leading to a loss of function or a loss in sensitivity to

mechanical forces, abnormal lymphangiogenesis, and/or malformations and remodeling. Lymphatic system function that is disrupted in this way can be caused by (and may cause) various pathologies in the human body including lymphedema, one of the most prominent lymphatic-related diseases.

The intrinsic contractile activity of lymphatics is crucial for the maintenance of interstitial fluid volume. When there is insufficient lymphatic drainage due to dysfunctional lymphatics, there can be a rapid accumulation of interstitial fluid. This can manifest as a unilateral swelling, usually of the extremities, called lymphedema [61]. Lymphedema can be both congenital, called primary lymphedema, or can be induced by an external injury, called secondary lymphedema. Secondary lymphedema is the most common form of lymphedema [62, 63], with breast cancer-related surgery being the leading cause in most developed countries and lymphatic filariasis being a major cause in most developing countries. In both cases, the net result is a disruption of the lymph flow by an obstruction/destruction of the lymphatic network. However, surgery-related secondary lymphedema is of primary concern for this thesis. Secondary lymphedema resulting from a surgical procedure is usually caused by the removal of lymphatic tissue (e.g. lymph nodes) and a secondary insult (e.g. radiation) that can damage the lymphatic vasculature and impair lymphatic pump function [63, 64]. What starts off as a reversible swelling of the extremities (treatable using physiotherapy) can progress into fibrosis, which is a hallmark of advanced lymphedema (Figure 1.9). Lymphedema is not only disfiguring, but also severely impacts the quality of life of the patients, reducing their freedom of movement and subjecting them to a lifelong usage of compression garments, physiotherapy, and other interventions to control the swelling.

1.4.1   Functional Changes in Collecting Lymphatics During Lymphedema

Lymphatic damage and lymphedema work hand-in-hand, exacerbating each other in a vicious cycle that starts with mild swelling due to tissue fluid retention, and ends with exten-
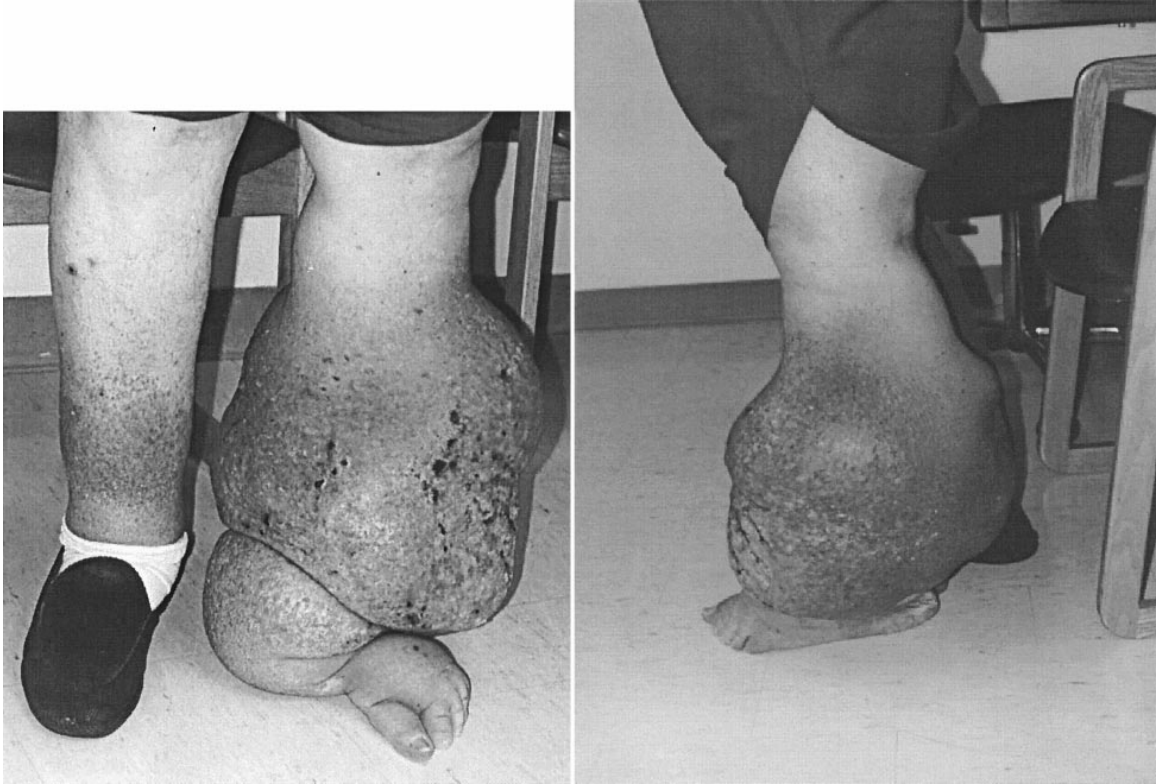
Figure 1.9: A patient with advanced leg lymphedema is shown. The patient is characterized by a unilateral swelling of the leg, with extensive fibrosis. The figure is taken from Rockson, 2001 [61]

sive fibrosis and extreme swelling. It is known that the conditions prevalent during lymphedema can lead to contractile dysfunction of the intact lymphatic network. This change in contractile behavior can be acute, particularly in response to a sudden change in the mechanical microenvironment in response to injury, or there can be long-term changes and remodeling due to sustained changes in the mechanical microenvironment. Some ex vivo studies have shown the functional remodeling of the collecting lymphatics in response to prolonged changes in the lymphatic mechanical microenvironment. When isolated mesenteric vessels were exposed to an elevated transmural pressure for about 3 days, their pump function, and diastolic and systolic diameters were all found to increase, resulting in a stronger lymphatic pump [60]. A study involving lymphatic injury in the hind limb of sheep showed that lymphatic injury can cause functional remodeling of collecting lymphatics, increasing the frequency and force generation while also decreasing the flow-mediated
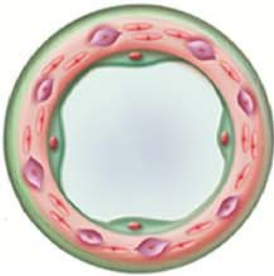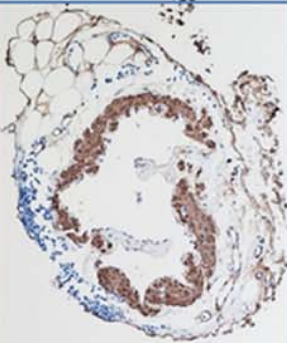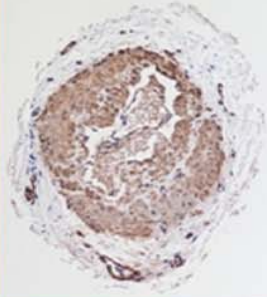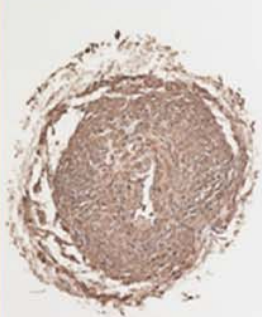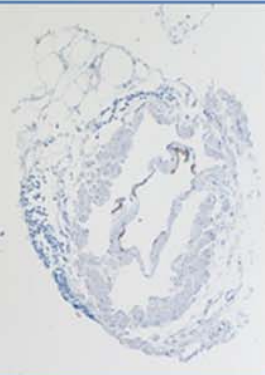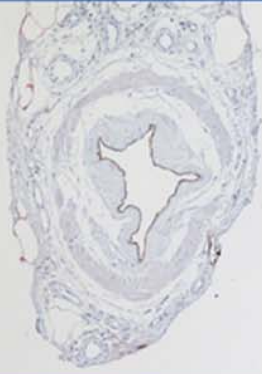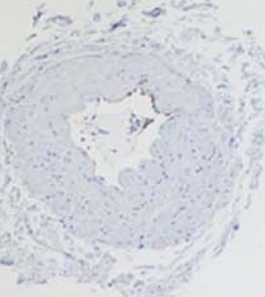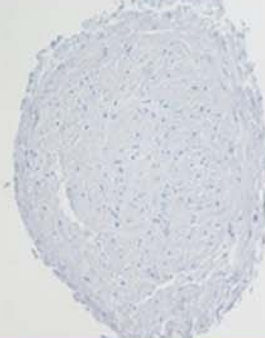
20

Figure 1.10: The various stages through which the collecting vessels undergo maladaptive remodeling in response to a pathological mechanical microenvironment are shown. The α-SMA staining, specific for LMCs, shows an initial thinning of the muscle layer (ectasis) followed by a gradual thickening (contraction) till the lumen gets almost completely occluded (sclerosis). Podoplanin staining, specific to LECs, is positive up to the ectasis stage but is absent at later stages. The figure is taken from Mihara, 2012 [65].

contraction inhibition [66].

As the aberrant mechanical conditions persist, the lymphatics can show long-term functional changes. In a murine model of tail lymphedema, it was found that chronic edema induced by a lymphatic injury had the effect of reducing fluid uptake by lymphatic capillaries, as well as a reduction in the contraction amplitude of the collecting lymphatics [67]. A reduction in contractile function has also been observed in humans with secondary lymphedema [68, 69]. Studies on lymphatic contractile function at various stages of lymphedema have revealed a decrease in lymphatic pumping pressure and contraction frequency [68, 70]. Collecting lymphatic vessels can also remodel as lymphedema progresses, starting from ectasis (enlargement of the lumen and thinning of the muscle layer), moving into contraction (narrowing of the lumen and thickening of the muscle layer), and eventually sclerosis (absence of any lumen, thickening of the muscle layer and fibrosis) [65] (Figure 1.10). While the molecular mechanisms dictating this remodeling and loss of function are not clearly understood, NO and reactive oxygen species (ROS) have been implicated in similar pathologies and may have a role to play in lymphedema-induced collecting lymphatic remodeling as well. Exposure of lymphatic vessels to chronically increased pulmonary flow has been shown to decrease the availability of NO and reduced NO-mediated relaxation of the thoracic duct [71]. This is probably mediated through a KLF-2 dependent increase in ROS, which compete with NO for bioavailability [42]. While the role of ROS in lymphatic function is not as well investigated as NO or other molecules, they has been found to inhibit contractions in isolated lymphatic vessels [43]. Prolonged exposure of lymphatic vessels to ROS can also possibly lead to endothelial dysfunction similar to that seen in blood vessels [72].

Thus it is abundantly clear that lymphedema leads to a progressive dysfunction of the collecting lymphatic contractility. It should be noted that the literature only focuses on the contractile activity of lymphatics as a measure of the severity of lymphatic dysfunction. There is another important metric of lymphatic contractile function, however, that may

have some importance in understanding how the lymphatic contractility may be manipulated during these pathological conditions. This metric is the mechanosensitivity of the collecting lymphatics, especially to their oscillatory mechanical microenvironment. The mechanosensitivity of lymphatics determines to what extent the collecting lymphatics can be modulated by their oscillatory mechanical microenvironment to enhance/optimize their function. The question of mechanomodulation becomes especially important when one realizes that the best treatment that we have for lymphedema right now is still the ancient tradition of massage and physiotherapy, with some modern advancements in the form of compression garments and intermittent pneumatic compression. Thus, modulating the mechanical environment of lymphatics is still the best available therapy for lymphedema, but little is known about how these oscillatory mechanical forces impact collecting lymphatic function. Thus, the question of mechanosensitivity and mechanomodulation of lymphatics to/by external oscillatory forces within the organism will be the focus for the 3rd chapter of the thesis, building off of the ideas laid out in chapter 2. In chapter 4, we will also try to understand how this mechanosensitivity changes due to lymphatic injury.

1.5   Imaging the Lymphatic System

Of course, none of the previously mentioned questions are answerable without the relevant technologies that allow us to image and quantify lymphatic function. Recent advances in imaging technologies have opened up a number of doors for assessing lymphatic structure and function that were impossible in the past. Previously, lymphatics could be imaged by sacrificing either the depth of penetration, spatial resolution, or the temporal resolution of the image. Techniques such as lymphoscintigraphy were used to image the lymph nodes, but their spatial resolution did not allow for the imaging of finer structures such as the collecting vessel network. Other established techniques such as magnetic resonance (MR) or X-ray lymphography were used to image the lymphatic network with decent spatial resolution, but at the expense of temporal resolution. The advent of near-infrared (NIR)
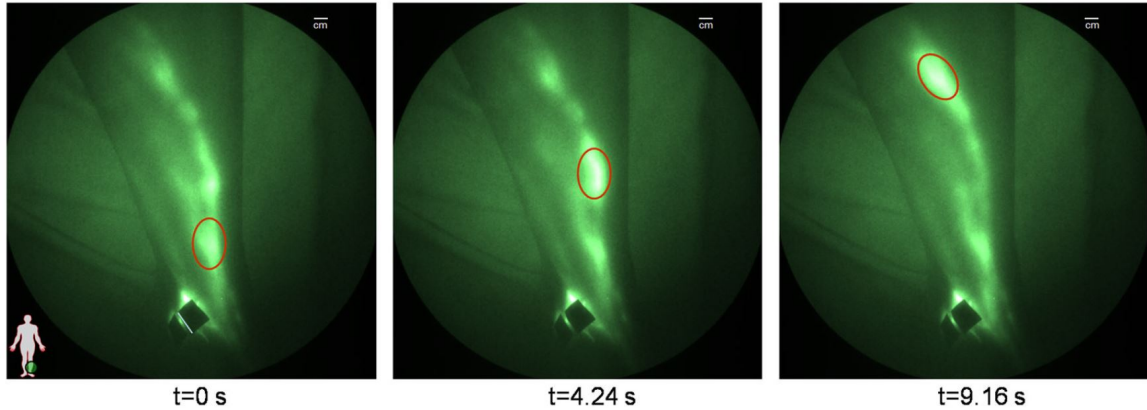
Figure 1.11: The transport of lymphatic dye through the leg collecting lymphatics of a healthy individual is shown. The dye travels as "packets" of fluorescence which can be used to quantify lymphatic function. The figure is taken from Rasmussen, 2010 [74].

fluorescence imaging thus came as a boon to the field of lymphatic imaging, allowing for imaging with a decent spatial resolution with good depth of penetration, while also enabling a high temporal resolution capture that allowed for the recording and quantification of collecting lymphatic function. A comparative study of different in vivo lymphatic imaging techniques can be found in the review paper by Munn and Padera [73].

For the purpose of this thesis, NIR imaging is the most important imaging modality since it allows us to effectively capture lymphatic pump function with a reasonable spatial and temporal resolution. Conventional fluorescence imaging has the advantage of offering high frame-rate capture of dye transport characteristics, thereby being suitable for the quantification of real time lymphatic function. However, it can have inherent disadvantages such as low spatial resolution and penetration depth. NIR imaging solves this problem by shifting the excitation/emission spectrum to the near infrared window (780 nm - 2500 nm), which is characterized by excellent penetration and low absorption of the excitation light by the skin. Thus, the superficial collecting lymphatics can be imaged with a decent spatial and temporal resolution using the NIR imaging method. Figure 1.11 shows "packets" of lymphatic dye which can be observed traveling along the leg lymphatics of a healthy individual and can be used for quantifying lymphatic function. The usage of NIR for imaging

lymphatic vessels was first demonstrated in a porcine model by Sharma et. al [75], where they introduced indocyanine green (ICG) conjugated with hyaluronan as a lymphatic specific contrast agent that could be used to quantify lymphatic function. Since then, ICG has been used to image the structure and function of the lymphatic network in humans, both in healthy and lymphedema patients [76, 77, 78, 74, 79]. Clear differences in the lymphatic structure and function can be observed between healthy and lymphedema patients using NIR imaging. A later study established LI-cor IRDye 800CW as a more suitable alternative to ICG for long-term lymphatic imaging since it has a minimal effect on lymphatic function [80]. Thus, NIR imaging is a powerful tool for imaging lymphatic function and assessing its changes in response to injury, and will be used in answering the questions that will be addressed in chapters 3 and 4.

1.6 Central Aims

The preceding discussion crystallizes into three questions which deserve special attention in regard to lymphatic contractility and mechanosensitivity. These are as follows:

1. How do lymphatics modulate their contractility in response to their oscillatory mechanical microenvironment and what does the aforementioned modulation mean for lymphatic function?

2. Can the lymphatics be optimally modulated in vivo to enhance/optimize their function using externally applied oscillatory pressures, similar to massage?

3. Can the modulation of lymphatic function by oscillatory pressures (akin to massage) be affected by lymphatic injury?

Equipped with the knowledge of the mechanosensitivity of lymphatics to constant (and to some extent oscillatory) forces, and the technological advances in lymphatic imaging, we are at a stage to answer these three questions. Thus, this thesis will be divided into three

central aims, designed to answer these three central questions. The hypotheses driving these three aims are:

1. Oscillatory shear stresses can optimally modulate lymphatic entrainment and pump function.

2. Oscillatory pressure waves, mimicking massages, can optimally modulate collecting lymphatic entrainment and function in vivo.

3. The mechanomodulation of lymphatic function by oscillatory pressure waves is altered by an injury to the lymphatic network.

The first aim will be the focus of chapter 2, where we will look at the modulation of lymphatic contractility by oscillatory shear stresses ex vivo. Chapter 3 will focus on the second question, where lymphatic mechanomodulation by oscillatory pressure waves will be investigated in vivo. Chapter 4 will look at how the mechanosensitivity of the lymphatics to oscillatory pressure gradients can change in response to lymphatic injury.

CHAPTER 2

EX VIVO MODULATION OF COLLECTING LYMPHATIC CONTRACTILITY

2.1 Background

Lymphangions, the basic functional units of the collecting lymphatic system, exhibit intrinsic phasic and tonic contractility and they respond to mechanical stimuli by modulating their contractility according to the prevailing microenvironment [31, 32]. Let us recapitulate some crucial knowledge about lymphatic contractility and mechanosensitivity from the previous chapter. There are primarily two types of mechanical forces that need to be considered in the lymphatic system – the hoop stress exerted on the wall due to the transmural pressure and the wall shear stress (WSS) in the lumen of the collecting lymphatic vessels due to lymph flow. The transmural pressure has a direct influence on the contraction frequency, the end systolic and diastolic diameter of the vessel, as well as other pumping metrics like ejection fraction. The general trend is an increase in the contraction frequency and pump function as the transmural pressure is increased from zero to an optimal pressure, after which a further increase in pressure causes a reduction in pump function [28, 29, 48]. The wall shear stress is another equally important factor in modulating both the tonic and phasic contraction of the lymphangions [35, 37]. Gashev et al. showed that both the chronotropic (phasic contractility) and inotropic (tonic contractility) responses of the lymphatic vessels were negatively affected by an imposed pressure gradient [37]. Numerous studies since these original ones have confirmed the findings of Gashev et al. that imposed flow decreases both the contraction amplitude and the contraction frequency [45, 41, 81], a phenomenon referred to as shear inhibition. The region chosen for the study can affect the response of the lymphatic vessels to the WSS as well. Rat thoracic ducts were seen to significantly inhibit their contraction with large, favorable pressure gradients, but these

pressure gradients had a minimal effect on the contractility of rat mesenteric and cervical lymphatics [82].

Experimentally, it is easier to control the pressure gradient across the vessel than the flow rate through it and hence previous studies have mostly focused on using the pressure gradient as a means to impose WSS on the vessel. In these studies, the vessels were cannulated in a specialized vessel chamber, and the flow was controlled through the vessel by controlling the pressures at the inlet and the outlet of the cannulae. However, in these experimental setups, it was not possible to take into consideration the exact WSS being applied to the vessel. The relationship between the applied pressure gradient across the vessel chamber and the WSS applied to the vessel is highly dependent on the diameter of the vessel and the pressure drop that occurs along the pipette tips used for cannulating the vessels. Most importantly, these studies also did not take into consideration the minor losses between the pipette tips and the vessels (the pressure loss that happens as the fluid transitions from the cannulae to the lymphangion), which can be significantly higher than the pressure losses due to the cannulae and the vessels taken together. Mathematically, the relationship between the applied pressure gradient and the various losses in the system can be expressed in a simplified form as

$$\Delta P_{chamber} = \tau_{wall} D_{vessel}(1 + \frac{R_{cannulae}}{R_{vessel}}) + f(Q, D_{cannuale}, D_{vessel})$$

In this equation, $\Delta P_{chamber}$ is the pressure gradient across the vessel chamber, τ_{wall} is the WSS on the vessel, $R_{cannulae}$ and R_{vessel} are the hydraulic resistances of the cannulae and the vessel respectively, Q is the net flow rate across the vessel chamber, and $D_{cannulae}$ and D_{vessel} are the diameters of the cannulae and vessels respectively. Thus, in the absence of the minor losses represented by $f(Q, D_{cannulae}, D_{vessel})$, the relationship between the pressure gradient across the vessel chamber and the actual WSS on the vessel is usually a simple linear relationship. However, the addition of the significant minor loss, which depends on the

vessel diameter, makes the relationship between $\Delta P_{chamber}$ and τ_{wall} a nonlinear one. The nonlinear relationship makes it difficult to compare the results (concerning the impact of flow on lymphatic function) across different studies that use slightly different setups or even possibly within the same study if vessels with different geometries are being studied with the same setup. Thus, it is important to investigate the mechanosensitivity of the lymphangions with respect to the WSS experienced by the lymphangions, if we want to compare the results even across different tissue beds. This is the first thing that will be attempted in this chapter; defining the shear inhibition of the lymphatics in terms of the WSS that they are experiencing and quantifying them as a measure of lymphatic mechanosensitivity to constant or ramped WSS.

The next thing to note is that although all the previous studies have looked at lymphatic contractility under constant shear stress conditions, the actual microenvironment of the lymphatics in vivo is highly oscillatory as described in chapter 1. A study by Kornuta et al. first tackled the problem of the modulation of lymphatic contractility by an oscillatory WSS (OWSS) [38]. The study showed that lymphatic vessels synchronized their contractions to an imposed OWSS ex vivo, i.e. the contraction frequency of the vessels was modulated to match the frequency of the applied OWSS. This synchronization of the vessel contractility with an externally imposed OWSS is referred to, in this chapter, as "entrainment". In this chapter, we will investigate in detail how the lymphangions are entrained by OWSS with different frequencies and amplitudes and will look at the phenomenon of entrainment as a measure of lymphatic mechanosensitivity to oscillatory WSS. Not only that, the importance of entrainment in the most basic function of a lymphangion, which is enabling flow through the lymphatics, will also be investigated.

To investigate the aforementioned questions, a data analysis package was developed to investigate the response of lymphangions to an OWSS in the frequency domain using continuous wavelet transform. The response of the lymphatic vessels to dynamic forces were analyzed by looking at their frequency domain response, which allowed for the quantifica-

tion of their entrainment to externally applied oscillatory forces. The ability of a lymphatic vessel to entrain its contractions to an externally applied OWSS was hypothesized to be dependent on its sensitivity to the WSS and its intrinsic contraction frequency (the average frequency with which the vessel contracts when no flow is applied to its lumen). The specific parameters of the applied OWSS (frequency and amplitude) were also hypothesized to affect the overall pumping performance of the lymphatic vessels through the mechanism of entrainment, that is elucidated in this work.

2.2 Methods

2.2.1 Experimental Setup

All experiments were performed on thoracic ducts isolated from male Sprague-Dawley rats that weighed between 280–300 gm. All procedures performed on the rats were reviewed by the Institutional Animal Care and Use Committee (IACUC) at Georgia Institute of Technology. The proposed procedures were found to comply with the Institute's Policy for Humane Care and Use of Laboratory Animals, and were approved by the IACUC at Georgia Tech (protocol number A14069). The thoracic duct was chosen since it has been observed that they show more sensitivity to shear stress variations than mesenteric lymphatic vessels [82] and was previously used to demonstrate the phenomenon of entrainment [38]. The presence of valves could introduce nonlinearities in the perfusion system that was used to control the pressure gradient across the vessel, which could lead to erratic behavior and large steady state errors in the applied pressure gradient. Hence, vessel segments devoid of lymphatic valves (i.e., portions of lymphangions) were chosen for the study to avoid the nonlinearities that may impact the performance of the isolated vessel perfusion system. The isolated vessels were cannulated in a vessel chamber and immersed in and perfused with physiological salt solution (PSS). Two micro-pipette tips mounted on the vessel chamber were used to cannulate the isolated thoracic duct. The size of the thoracic ducts ranged between 500 μm to 900 μm. Keeping this in mind, pipette tips with approximately 450 μm diameter were

30
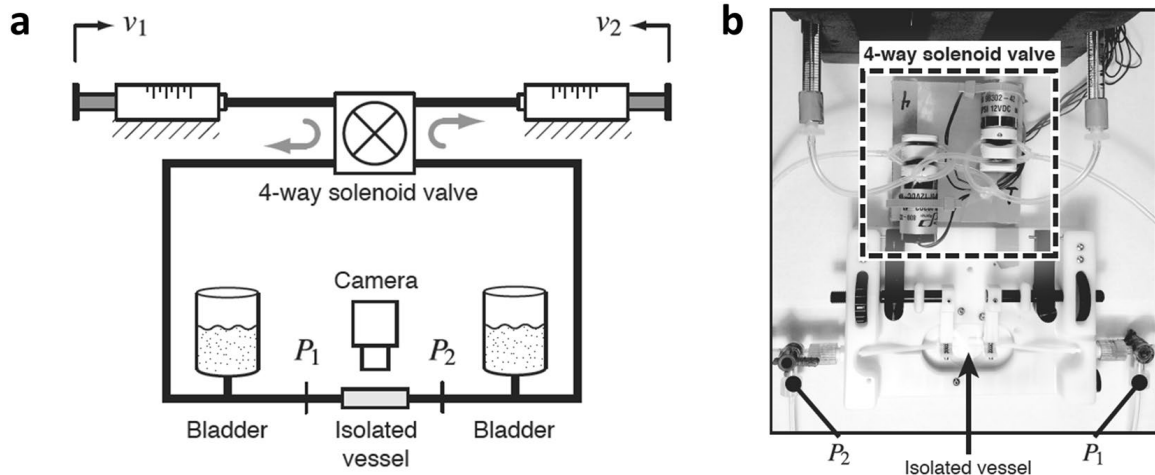
Figure 2.1: The ex vivo lymphatic vessel perfusion system. (a) The basic control scheme of the perfusion device is shown in the schematic. The syringes enabled the flow through the system and helped maintain the inlet and outlet pressures. The solenoid valves ensured unidirectional flow through the chamber, from the inlet to the outlet. Pressure transducers P1 and P2 recorded the pressure at the inlet and outlet of the vessel chamber. A feedback loop, using the pressure readings, ensured that the inlet and outlet pressures were maintained at the desired values. (b) The top view shows the tubing connections from the perfusion system to the vessel chamber, the location of the isolated vessel in the chamber and the inlet and outlet ports of the vessel chamber. The figure has been adapted from Kornuta, 2015 [83].

chosen.

The experimental setup consisted of a commercially available vessel chamber from Living Systems Instrumentation, connected to a custom perfusion system. The perfusion system allowed for the independent control of the average transmural pressure (P_{avg}) in the vessel and the pressure gradient (ΔP) along the vessel chamber through explicit model predictive control [83] as shown in Figure 2.1. The vessel chamber connected to the perfusion system was mounted on an inverted microscope, which was used to capture bright-field images of the contracting vessel as it was exposed to various flow conditions. The vessel chamber was heated using electric heating pads and the temperature was maintained around 38º C using a thermocouple and a temperature controller. To ensure that the composition of the media did not change during the experiments, fresh media was recirculated in the chamber using a peristaltic pump, running at a flow rate of 0.3 mL/min.

The mechanical conditions inside the vessel were controlled by the perfusion system that utilizes linear motors, gas-tight syringes and solenoid valves to control the pressures at the inlet and outlets of the vessel chamber, P1 and P2 respectively [83]. Analog pressure transducers were used to detect the inlet and outlet pressures in real time and control the device. The average transmural pressure in the vessel was calculated as the average of the inlet and outlet pressures, (P1 + P2)/2. The pipette tips were resistance matched and the length of the tubes connecting each pipette to the external tubing was matched to ensure that the hydraulic resistance of the pipettes, along with the connecting tubing, were equal. An equal hydraulic resistance in both the pipettes ensured that the pressure drops in both pipettes were the same. An equal pressure drop in both pipettes, in turn, ensured that the relationship between the pressure gradient across the vessel and ΔP was not dependent on the direction of the flow through the vessel. It should be noted that the relationship between the pressure gradient across the vessel and ΔP was still nonlinear, but not dependent on the flow direction, which ensured that any additional nonlinearities due to unequal pressure drops in the vessel, depending on the flow direction, could be avoided.

Depending on the average transmural pressure and pressure gradient that were applied to the vessel, it was possible that in certain instances the pressure at one of the ends of the vessel chamber could drop below 0 cmH$_2$O, which can raise concerns about the vessel lumen partially collapsing during the experiments. However, it should be noted that the pressures recorded by the transducers were at either end of the vessel chamber, which were not the same as the pressures at the end of the cannulated vessels themselves. The pressure drop across the vessel could be calculated from a knowledge of the diameter and length of the vessel, and the flow rate through the vessel, assuming a Poisuielle approximation for a low Reynold's number flow (which was applicable for these experiments). An example calculation of the approximate pressure drop across the vessel is presented here. Assuming a vessel with a diameter of 500 μm (considering a thoracic duct) and a peak flow rate of 9 μL/s through the lumen (representative flow rate calculated from experimental recordings

of the syringe positions), the wall shear stress produced was about 5 dynes/cm^2, which is in the physiological range for the thoracic ducts. The pressure drop across a vessel segment of 5 mm length (a representative length of the vessels that were used for the experiments) was about 0.2 cmH$_2$O for the aforementioned mechanical conditions, which was an order of magnitude lower than the total pressure drop across the system of about 4–8 cmH$_2$O. Hence, the pressure at either end of the vessel never reached 0 cmH$_2$O even during peak flow, thus eliminating the concern of the vessel collapsing during any of the experiments. Visually, the vessels were never seen to collapse during the experiment either.

2.2.2   Protocols

Each vessel was first stepped through average transmural pressures (P$_{avg}$) of 1, 3, 5, and 7 cmH$_2$O under a zero pressure gradient (ΔP) over 12 minutes to precondition them. This was done to ensure that the vessel isolation and cannulation process did not damage the vessel and that the reference contraction frequencies for the vessel could be determined, which was useful in the subsequent steps. After preconditioning, the vessel was subjected to 5 minute and 15-minute ΔP ramps from 0–9 cmH$_2$O at a P$_{avg}$ of 3 cmH$_2$O. The vessels were then taken through a series of oscillatory flow waveforms with different frequencies and amplitudes. Each step consisted of 5 minutes of zero ΔP, followed by 5 minutes of oscillatory ΔP at a P$_{avg}$ of 3 cmH$_2$O. The P$_{avg}$ was chosen as 3 cmH$_2$O for all the aforementioned protocols since the contractile function of the thoracic duct (determined by the contraction frequency and fractional pump flow) was found to be optimum near this pressure [32]. At no point was the vessel subjected to a retrograde flow. The frequencies of the applied flow waveforms were 0.075 Hz, 0.2 Hz, and 0.35 Hz. Since the intrinsic contractile frequencies of the isolated vessels under a P$_{avg}$ of 3 cmH$_2$O were around 0.3 Hz, the frequency values that were chosen covered a range that went from subphysiological to supraphysiological for the specific P$_{avg}$ that the vessels were being subjected to, and were hence referred to as "low", "medium", and "high" applied frequencies. The amplitudes of

the ΔP were chosen to be 4, 6, and 8 cmH$_2$O, which corresponded to "low", "medium", and "high" shear stresses as compared to the critical shear stress at which inhibition occurs, typically between 3–7 cmH$_2$O for the rat thoracic duct (the critical shear stress is a metric of lymphatic mechanosensitivity which will be defined later at the appropriate section).

2.2.3   Data Analysis

The data was acquired in the form of brightfield videos of the vessels. The videos were acquired by a non-inverted microscope at 4x magnification. The videos were then processed frame by frame in MATLAB®. Each frame was binarized using a window-based thresholding algorithm that helped distinguish the vessel from the background as shown in Figure 2.2a-b. Image processing was performed on the thresholded and binarized images to remove any noise due to particles floating in the chamber. The upper and lower boundaries of the vessel in the binarized image were calculated at all locations along the vessel and the diameter at each location was calculated by subtracting the upper boundary from the lower boundary. The diameters thus detected were aggregated over time to form diameter tracings (Figure 2.2c) that were then subsequently analyzed at each location along the vessel. Once the diameter data was obtained as a function of time and location, the tracings were filtered using an averaging low-pass filter to remove any noise due to the resolution of the image or errors during the binarizing step. The MATLAB® code for processing the images and obtaining the diameter data is provided in Appendix A.

Traditional time domain techniques to analyze entrainment, namely looking solely at the average contraction frequency, only provide binary information regarding entrainment without providing any information about how the OWSS parameters affect the degree of entrainment. Time domain techniques also do not provide any information about the relative presence of a particular frequency component in the overall signal, which is crucial for defining a nondimensional measure of entrainment. Hence, frequency domain analysis techniques, such as continuous wavelet transform, are essential in studying the amount of
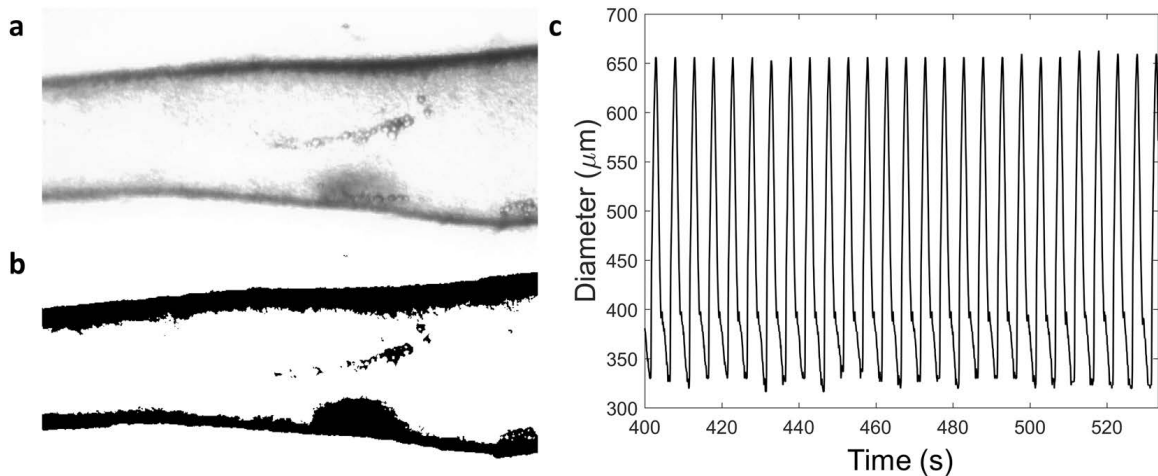
Figure 2.2: The data analysis workflow used to obtain the diameter tracings from the bright-field images. (a) Brightfield images of the vessels were acquired using an inverted microscope. (b) Binarized images of the vessel, isolated from the background, were obtained by thresholding the brightfield images. The binarized images were used to detect the diameter of the vessel at different locations along the vessel. (c) Going through all the frames in the video, the diameter was obtained as a function of time for all the locations along the vessel.

entrainment of a lymphangion to a spectrum of OWSS waveforms with different frequencies and amplitudes.

The diameter tracings were analyzed with Continuous Wavelet Transform (CWT), as shown in Figure 2.4. CWT is a frequency-based analysis technique that allows for the decomposition of a signal into its constituent components at different frequencies and times. The most commonly used tool in the analysis of frequency domain information is the Fourier Transform (FT), but it is only useful for calculating the magnitude of the frequency content of the data over a specific time window. When the spectral information is needed as a function of time, a modification to this method can be used, which is called the "Short Time Fourier Transform" (STFT). In this technique, the spectral information is obtained over user-defined time windows within the data, where the windows overlap with each other by an amount defined by the user. Hence, it is apparent that in this method, the temporal resolution is limited by the amount of overlap, and the user-defined nature of the time window can introduce subjectivity into the results of the transform. Ideally, a smaller time window can be used when the data is rich in higher frequencies and a larger

window should be used when the frequency in the data is more concentrated in the low frequencies, so as not to miss out on any information. These problems can be avoided using CWT as it accounts for the varying time and frequency resolutions in the data without any user intervention, thus reducing human interference and subjectivity to the analysis. It provides higher temporal and frequency resolution, thus enabling the study of the spectrum of the signal with higher fidelity. The MATLAB® code for calculating the CWT from the diameter data is provided in Appendix A.

The coefficient of a CWT is a representation of the magnitude of a component of the data at particular frequencies and times. The higher the magnitude of the CWT coefficient at a specific frequency and time (referred to as power), the greater the magnitude of that frequency component at that particular time. Hence, considering the entrainment of a vessel to an externally applied OWSS, the power at the applied OWSS frequency is representative of the component of the vessel contraction at the applied frequency and could be used as a measure of entrainment. However, the power at the applied frequency is also dependent on the contraction amplitude of the vessel at a particular time. Ideally, the entrainment of the vessel to the OWSS should be a nondimensional quantity that is independent of the contraction amplitude, since it is a measure of the relative importance of the frequency component at the applied OWSS over other frequency components that may be present in the diameter tracings. Hence, the percentage of power at the applied frequency at a particular time is defined as a nondimensional measure of the entrainment, since it is independent of the diameter of the vessel and is representative of the relative magnitude of the applied frequency component compared to the other frequency components.

2.2.4   Calculation of Wall Shear Stress

The axial pressure gradient across the vessel chamber in which the lymphatic vessel is cannulated is not reliable for estimating the wall shear stress in the lumen of the vessel, as mentioned before, because of the nonlinear relationship between the wall shear stress

and ΔP. There are minor losses associated with the sudden expansion of the pipette tip into a much larger vessel lumen. The pipette tip diameter is fixed, but the vessel diameter is variable, and hence the effective pressure drop across the vessel becomes a function of the vessel diameter. Hence, the shear data for these experiments were obtained from the information of the positions of the syringes which were measured in near-real time. Due to a low resolution of the location data of the syringe positions (due to hardware limitations of the sensors used to track the syringes), the positions of the syringes were tracked in 3-second intervals to obtain an average syringe velocity over that time interval. After this time-averaged syringe velocity (V_{avg}) was obtained, the flow rate, Q, was calculated from the knowledge of the inner radius, r of the syringe as

$$Q = \pi r^2 V_{avg}$$

From the diameter tracings of the vessel, an average diastolic diameter of the vessel (D_{diast}) was calculated by fitting a quantile regression curve that estimated the upper envelope of the diameter data. Using this diameter value, the representative wall shear stress was calculated as

$$\tau_{wall} = \frac{32\mu Q}{\pi D_{diast}^3}$$

Where μ is the dynamic viscosity of water at 38º C which is around 6.78 mdyn-s/cm2. Given the low Reynolds number (i.e. Re $<$ 1) and low Womersley number (Wo $<<$ 0.1) for these flows [84], and the fact that relatively straight vessel segments without valves were chosen, the Poisuielle flow approximation could be used to get an appropriate estimate of the applied WSS. The MATLAB® code for calculating the WSS from the syringe positions is provided in Appendix A.

Given the fact that the estimated shear stress was an average shear stress over a 3 second time interval, this technique for estimating the wall shear stress was only useful for usage with slowly varying ΔP, such as those applied during the ramp ΔP protocol (as described
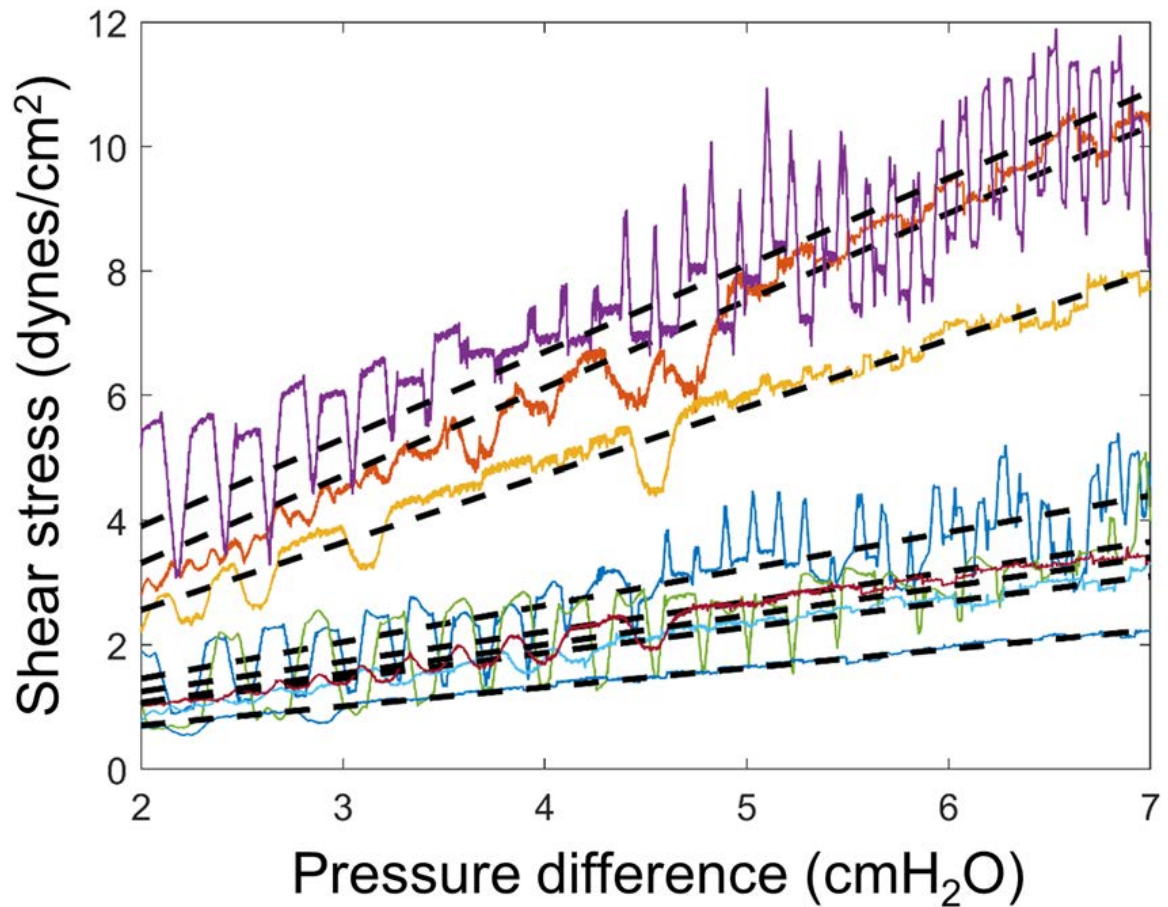
Figure 2.3: For the ramp shear stress experiments, the wall shear stress is plotted as a function of the pressure gradient. The 8 colored plots represent 8 different vessels on which the ramp protocol was applied. The dashed lines represent linear fits to the shear stress vs pressure gradient plots. The linear fit between the shear stress and the pressure gradient across the system was used to convert between the pressure gradient and shear stress for the oscillatory flow experiments.

before in the protocols section). Once the shear stress data was obtained for the ramp experiments, it was used to find the relationship between ΔP to WSS to be used in the conditions where an OWSS was applied. The relationship between ΔP and WSS was obtained by plotting the ramp shear stress as a function of ΔP and then fitting straight lines to them using linear regression analysis, as shown in Figure 2.3. The ΔP to WSS relationship was obtained for each vessel individually. The slope and offset of the fitted lines were used to calculate the OWSS from the oscillatory ΔP for each vessel. The advantage of calculating the OWSS in this way was that there was no reliance on using the ΔP across the system for calculating the OWSS, hence eliminating the variability introduced in the signal due to changes in the vessel diameter, and the accompanying minor losses.

2.3   Results

2.3.1   Characterization of Wall Shear Stress Sensitivity

To determine the wall shear stress sensitivity, the isolated lymphatic vessels were exposed to favorable pressure gradients that were linearly increased in magnitude over fixed time intervals (0 to 9 cmH$_2$O over 5 min and 15 min) while holding the transmural pressure constant at 3 cmH$_2$O. Thus, the ΔP was increased as a ramp function, and hence this protocol is referred to as the ramp protocol. Vessel contraction frequency over time was calculated using CWT, which is a frequency domain analysis technique that provides the spectral content of a waveform as a function of frequency and time. The magnitude of the wavelet coefficients represents the presence of a particular frequency component in the waveform at a particular time. An example spectrogram for a diameter tracing of a contracting vessel at a single location along the vessel is shown in Figure 2.4a. The colorbar represents the magnitude of the CWT coefficients. At any particular point in time, the frequency at which the magnitude of the coefficient (hereby referred to as "power") is the highest was defined as the "dominant frequency" at that time point, which is represented in Figure 2.4b. The other peaks in the CWT represent other prominent frequency components

39
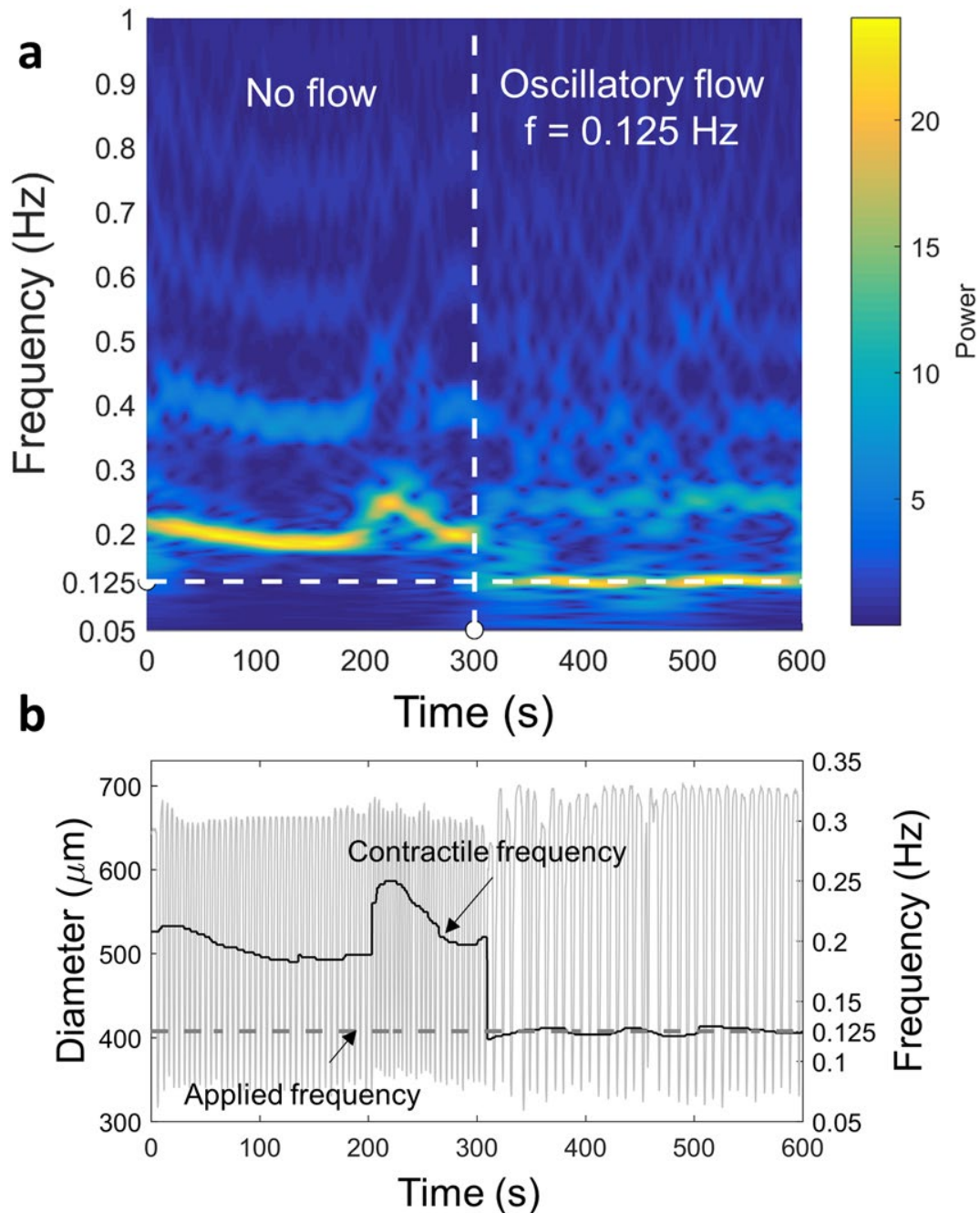
Figure 2.4: The frequency domain analysis method for diameter data. (a) Continuous wavelet transform (CWT) provides a detailed frequency domain information. The colorbar represents the magnitude of the CWT coefficient which is referred to as the power. The vertical dashed line represents the time at which imposed oscillatory flow begins and the horizontal dashed line represents the frequency of the imposed flow. (b) The frequency information can be easily isolated from the CWT. The calculated frequency is shown as a function of time and is overlaid on top of the diameter variations. For this particular experiment, the vessel was not exposed to flow at the start of the experiment ($\Delta P = 0$) and at 300 seconds an imposed oscillatory flow was applied to the vessel at the frequency indicated in the figure. The average transmural pressure was held constant at 3 cmH$_2$O

in the diameter tracing, which can occur at the harmonics. The use of CWT allows for subsequent analyses of the response of the lymphangion to different OWSS conditions, by studying the relative magnitudes of the different frequency components as a function of the frequency and amplitude of the applied OWSS.

From previous work, it is known that there is quite a bit of variability in the WSS that is necessary to inhibit contraction in thoracic duct segments which are taken from different rats [38]. Hence it is important to establish the WSS sensitivity of each vessel prior to exposing them to OWSS in order to determine the extent to which each vessel's unique shear sensitivity is responsible for their entrainment to oscillatory flow. To this end, the response of the thoracic ducts to a ramped shear stress was analyzed with CWT to obtain the shear sensitivity information (Figure 2.5a). The dominant frequency was obtained as a function of time from the CWT of the diameter tracings for the ramp experiment(Figure 2.5b). The imposed WSS was then obtained as a function of time for the ramp protocol by reading the syringe position of the perfusion system, assuming Poiseuille flow, and using the diastolic diameter of the vessel, as described previously in the methods section and in previous literature [38]. A linear fit between the WSS and time was obtained, assuming that the imposed WSS is zero at the start of the shear ramp.

With the fitted shear stress data being obtained, the dominant frequency was then plotted as a function of the shear stress to obtain the shear sensitivity (Figure 2.5c). The relationship between frequency and WSS appeared to follow a power law function of the form f = at^b, where f was the frequency, t was the time, and a and b were the parameters to be optimized. Curves of this nature, when fitted to the frequency vs WSS data, had an average r-squared value of about 0.9, which indicated that the power law model provided a good approximation to the shear-frequency relationship over the ranges tested.

The shear sensitivity of the vessels was represented by a "critical shear stress", which was defined as the shear stress at which the frequency of contraction drops down to half of the intrinsic frequency of contraction of the vessel. The critical shear stress was obtained
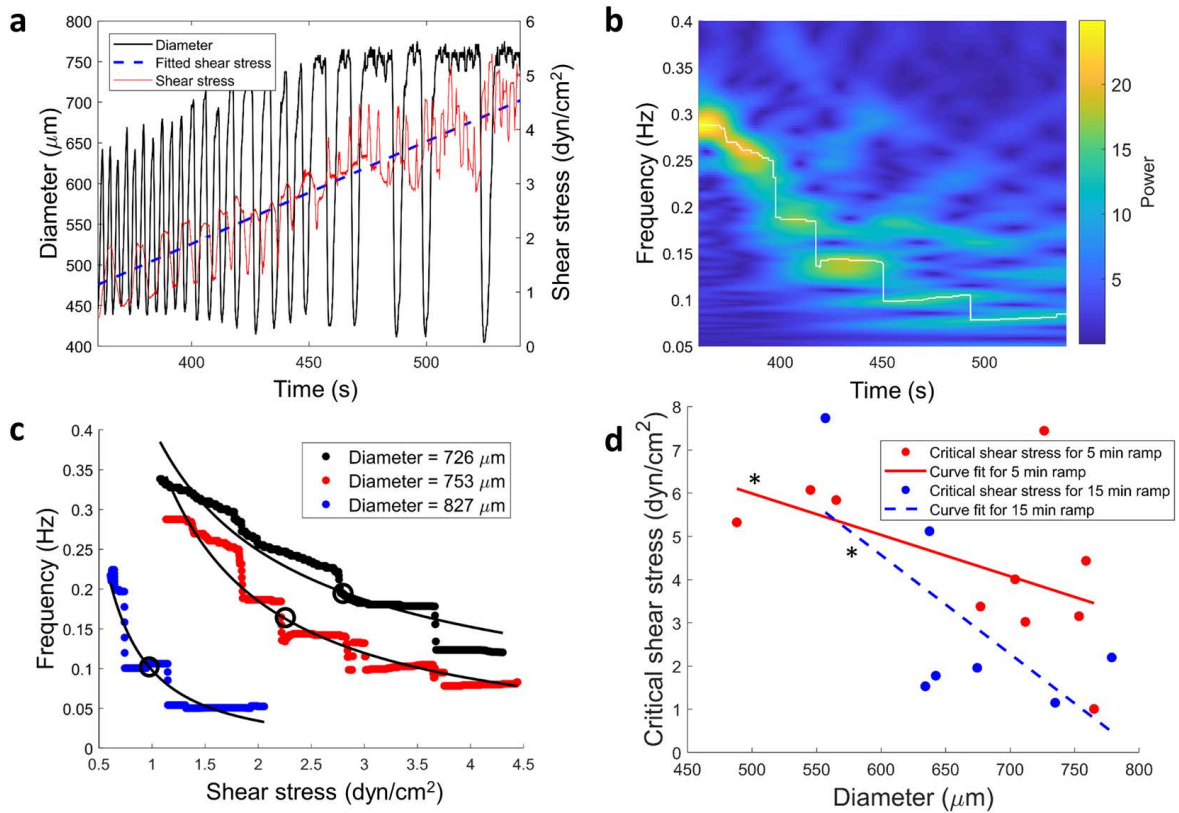
Figure 2.5: The critical wall shear stress of the vessel negatively correlates with the passive vessel diameter. (a) The diameter tracing is shown (in black) along with the applied WSS (in red) and fitted WSS (in blue). The contraction frequency of the vessel went down with time when a ramped WSS was applied to the vessel. (b) The CWT spectrogram of the diameter tracing is provided, with the white tracing highlighting the dominant frequency of contraction. The decrease in frequency with shear stress was quantified from the dominant frequency information. (c) The frequency is plotted as a function of the shear stress, and a power law curve is fitted to the data. The critical shear stress points, where the frequency is half of the intrinsic frequency are marked with the black circles. Representative fitted curves are shown for three different vessels and a dependence on the diameter of the vessel can be readily seen. (d) The critical shear stress is plotted as a function of the diameter of the thoracic duct for the two different shear stress ramps applied to the vessels (N = 9 for 5 min WSS ramp and N = 7 for 15 min WSS ramp) and the significance of the correlation is represented by the asterisk (*). Linear regression curves were fitted to the data and showed a significant negative correlation (Spearman correlation coefficient of 0.7454 and 0.787 with p values of 0.0133 and 0.0357 respectively for 5 min and 15 min ramps). The regression did not depend significantly on the rate of the ramp applied (p = 0.8629). Fisher's r-to-z transformation was used to calculate the significance of the correlation coefficients (*p<0.05).

from the power law relationship relating the frequency of contraction of the vessels to the imposed WSS. A higher critical shear stress for a vessel means that it takes a higher WSS for the vessel to inhibit its contraction by the same amount as that required by a vessel with a lower critical shear stress. Hence, the shear sensitivity is inversely related to the critical shear stress. The critical shear stress ranged between 0.1 to 10 dynes/cm^2 for the vessels tested. When the critical shear stress was compared between vessels with different average diastolic diameters, it was found to be strongly and significantly correlated to the average diastolic diameter of the vessel, irrespective of the rate of the ramp waveform applied to the vessel (Figure 2.5d). The Spearman correlation coefficient, calculated between the critical shear stress and the diastolic diameter, and were found to be 0.7454 and 0.787, with p values of 0.0133 and 0.0357 respectively for the ramp waveforms applied for 5 min and 15 min. The significance of the correlation coefficients were calculated using Fisher's r-to-z transformation. The shear sensitivity was not found to be significantly related to the rate of the ramped shear stress applied to the vessel (p = 0.8434).

2.3.2   Sensitivity of Entrainment to OWSS Parameters

To study the effect of variations in the frequencies and amplitudes of the OWSS on the entrainment response of the lymphangions, the spectral distribution of the power in the diameter data, and how it changes with the frequency and amplitude of the shear stresses applied to the vessel, was investigated using CWT. The percentage of power at a particular frequency is representative of the prevalence of that frequency component compared to the other components. The percentage of power at the applied OWSS frequency is thus indicative of the "strength of entrainment" of the vessel to the applied frequencies. OWSS with three different frequencies of 0.075 Hz, 0.2 Hz, and 0.35 Hz were imposed on the isolated thoracic ducts. These values were chosen to be reflective of frequencies that were less than, comparable to, and above the typical intrinsic contraction frequency of isolated pressurized rat thoracic ducts at an average transmural pressure of 3 cmH$_2$0. These three frequencies
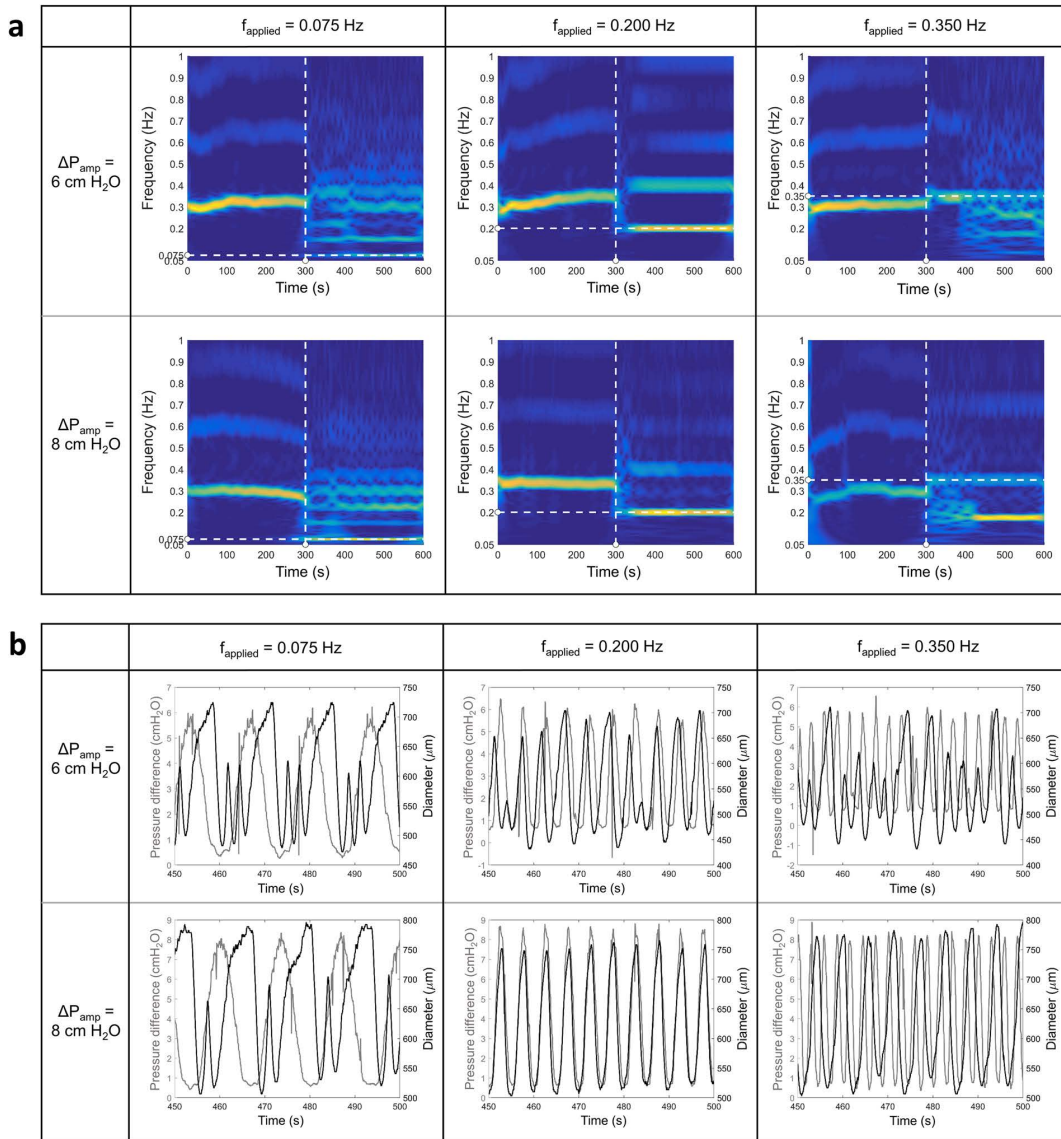
Figure 2.6: Representative CWT spectrograms, and diameter and pressure gradient tracings for the three applied frequencies of 0.075 Hz, 0.2 Hz, and 0.35 Hz, and two pressure gradients having amplitudes of 6 cmH$_2$O and 8 cmH$_2$O. (a) The vertical dashed line represents the time at which the OWSS was applied and the horizontal dashed line represents the frequency of the applied OWSS. The graphs show a clear dependence of the entrainment, represented by the percentage of power in the applied frequency component, on the applied frequency (comparing between the columns) and the magnitude of the OWSS (comparing between the rows). When the applied frequency exceeded the intrinsic frequency of contraction of about 0.3 Hz (bottom right panel), the maximum power was seen to be concentrated at half the applied frequency instead of the applied frequency. (b) The pressure and diameter tracings for the vessel are overlaid on top of each other, with pressure being represented by the gray line and diameter by the black line. The dependence of the entrainment on the applied frequency and shear stress is represented by the pressure and diameter tracings. When the applied frequency was greater than the intrinsic frequency of contraction, the vessel contracted at half the applied frequency (bottom right panel).

44

were also combined with three different amplitudes of the imposed pressure gradient waveform (ΔP_{amp} = 4, 6, and 8 cmH$_2$0, where ΔP is the pressure gradient measured across the vessel chamber in which the vessel is cannulated).

An observation of the CWT spectrograms for a single vessel at different applied frequencies and amplitudes, as shown in Figure 2.6a, reveals that the extent of entrainment of the vessel to the applied OWSS depends on both the frequency of the applied waveform and the amplitude of the pressure gradient. An interesting thing to note is that for an applied frequency of 0.35 Hz, the maximum power did not occur at the applied frequency, but rather at half the applied frequency which is 0.175 Hz. This phenomenon is seen for a lot of vessels that have an intrinsic contraction frequency less than 0.35 Hz. This suggests that the entrainment seen in the vessels may actually be an effect of shear inhibition, effected when the WSS rises above the critical shear stress. Since the frequency of oscillation of the OWSS is more than the vessel's intrinsic contraction frequency, the vessel gets entrained at a lower frequency, which is seen to be half the applied frequency. These spectrograms hence show an entrainment of the vessel contraction to the applied OWSS that depends on the applied frequency as well as the intrinsic contraction frequency. Furthermore, the power is higher when the applied pressure gradient is higher, indicating that the entrainment is higher at higher shear stresses.

The entrainment of thoracic ducts to the applied OWSS was investigated with respect to the difference between the intrinsic frequency of contraction and the applied frequency, as well as the applied shear stress normalized to the critical shear stress of the vessel (Figure 2.7a). The effect of the frequency difference (calculated as the intrinsic frequency minus the applied frequency) on the entrainment of the vessel to the oscillatory flow was investigated by dividing the dataset into 3 windows corresponding to applied frequencies that were higher than (0.3 Hz to 0.1 Hz), similar to (0.1 Hz to 0.1 Hz), and lower than (0.1 Hz to 0.3 Hz) the intrinsic frequency (Figure 2.7b). An unbalanced two-way ANOVA test was performed with an alpha level of 0.05 to obtain the statistical significance of the entrain-
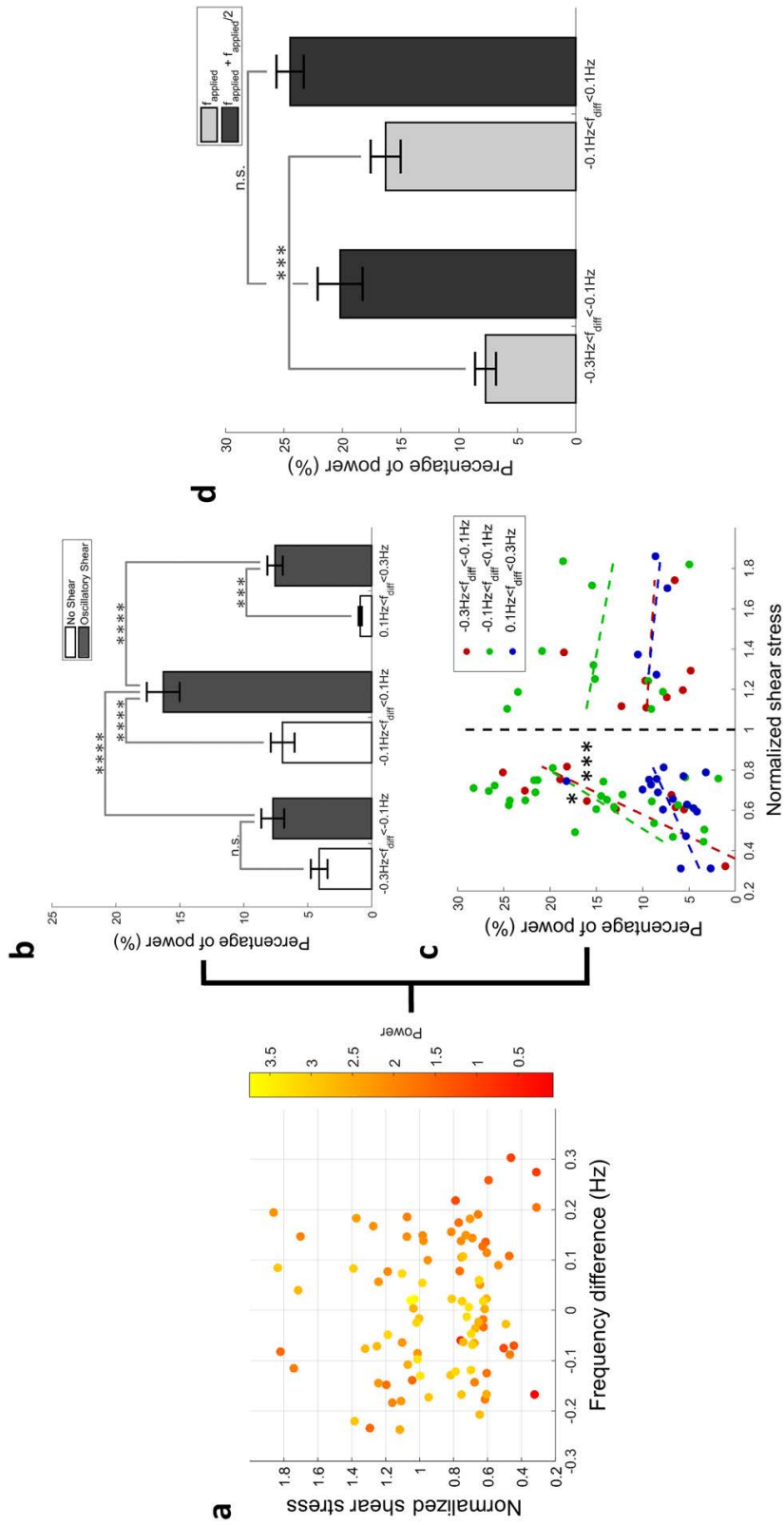
Figure 2.7: The entrainment of the vessel depends on both the frequency and magnitude of the imposed OWSS. (a) The percentage of power representing the entrainment is shown with respect to both the frequency difference and the shear stress difference (total N = 94, distributed between the three frequency and three pressure gradient conditions). (b) The percentage of power is shown at different ranges of frequency under no shear and oscillatory shear conditions, along with the standard error. (c) The entrainment is shown with respect to the normalized shear stress (amplitude of the applied OWSS normalized to the critical shear stress of the vessel). The dashed vertical line signifies the threshold at which the applied shear stress is equal to the critical shear stress. The percentage of power was significantly correlated to the normalized shear stress when the applied shear stress was below the critical shear stress, for similar and high applied frequencies. (d) The percentage of power at the applied frequency was compared to the sum of the percentage of power at the applied and half the applied frequency. When the sum of the percentage of power at both the applied frequency and half the applied frequencies are considered, there was no significant difference between the high and medium applied frequencies. This suggests that more power was present at half the applied frequency components when the externally applied frequency was more than the intrinsic frequency of contraction of the vessel. Unbalanced two-way ANOVA was performed to compare the group means between the different frequency and flow conditions (*p<0.05, **p<0.005, ***p<0.0005, ****p<0.00005). Fisher's r-to-z transformation was used to calculate the significance of the correlation coefficients (*p<0.05).

46

ment with respect to the frequency difference and the flow conditions (vessels exposed to no shear or OWSS). The entrainment of the vessel to the OWSS was evident from the significantly increased percentage of power in the applied frequency between no shear and oscillatory shear conditions (p = 0.0002, 2.07e-08 and 0.0028 for the three frequency groups). The entrainment was found to be maximum when there was minimal difference between the intrinsic frequency of contraction and the applied frequency. The percentage of power at low applied frequencies was found to be significantly lower than when the applied frequencies were similar to the intrinsic contraction frequency (p = 3.77e-08), demonstrating that the entrainment was hampered at low applied frequencies. The significant difference in the entrainment between the applied waveforms with higher and similar frequencies compared to the intrinsic frequency was lost when the power at both the applied frequency and half the applied frequency were considered (Figure 2.7d). This suggested a higher concentration of power at half of the applied frequency when the OWSS had a higher frequency than the intrinsic frequency and demonstrated that the vessels are contracting at half the applied frequency when the OWSS frequency exceeded the intrinsic frequency.

To investigate the effect of the magnitude of the applied shear stress on the entrainment, the amplitude of the applied OWSS was normalized with respect to the critical shear stress for each vessel so as to incorporate the unique mechanosensitivity of each vessel into the analysis. The entrainment was found to be significantly correlated to the normalized shear stress applied to the vessel (using Fisher's r-to-z transformation) in the similar and high frequency bands (r-squared values of 0.1643 and 0.6141 with p = 0.0399 and 0.0073 respectively) when the maximum applied shear stress was less than the critical shear stress (Figure 2.7c). The entrainment was not significantly correlated to the normalized shear stress of the vessels when the maximum applied shear stress was above the critical shear stress, suggesting that there was no added benefit to entrainment from a higher OWSS when the WSS was already above the critical shear of the vessel.

To determine if vessels other than the thoracic ducts might exhibit entrainment proper-

ties, preliminary studies with OWSS were performed on two mesenteric lymphatic vessels to test their entrainment. Mesenteric vessels have been shown in the literature to be less sensitive to the same pressure gradients compared to thoracic ducts [32]. The mesenteric vessels were subjected to oscillatory pressure gradients with an amplitude of 4 cmH2O and frequencies of 0.125 Hz and 0.0625 Hz, similar to the OWSS that the thoracic ducts were exposed to. The diameter and pressure tracings, the CWT of the diameter tracings, and the tracing of the power at the applied and intrinsic contraction frequencies are shown in Figure C.1. From the diameter tracings, it can be seen that the vessel contraction frequency changed with the application of the oscillatory pressure gradient, and the change was dependent on the applied frequency. This change in frequency was reflected by a decrease in the power at the intrinsic frequency and an increase in the power at the applied frequency. However, this entrainment to the applied oscillatory pressure gradient was much weaker than that observed in the thoracic ducts. The lower entrainment in mesenteric vessels could be attributed to their lower shear sensitivity compared to thoracic ducts (Figure C.2). For the same magnitude of the applied ramped WSS, the thoracic ducts exhibited a much stronger inhibition of contraction compared to the mesenteric vessels, a result which is supported by the literature [32, 82].

Four parameters of lymphatic contractility; contraction amplitude, contraction frequency, ejection fraction (which represents the percentage of lymph that is pumped by the lymphangion per contraction), and fractional pump flow (which represents the percentage of lymph that is pumped by the lymphangion per second); were investigated as a function of the frequency of the OWSS applied to the vessel and the flow condition ((vessels exposed to no shear or OWSS)), as seen in Figure 2.8. An unbalanced two-way ANOVA test was performed with an alpha level of 0.05 to test for the statistical significance of the entrainment with respect to the frequency difference and flow conditions. The contraction amplitude (Figure 2.8a) was significantly higher in response to the applied OWSS when the applied frequency was similar to the intrinsic contraction frequency ($p = 0.046$). The contraction
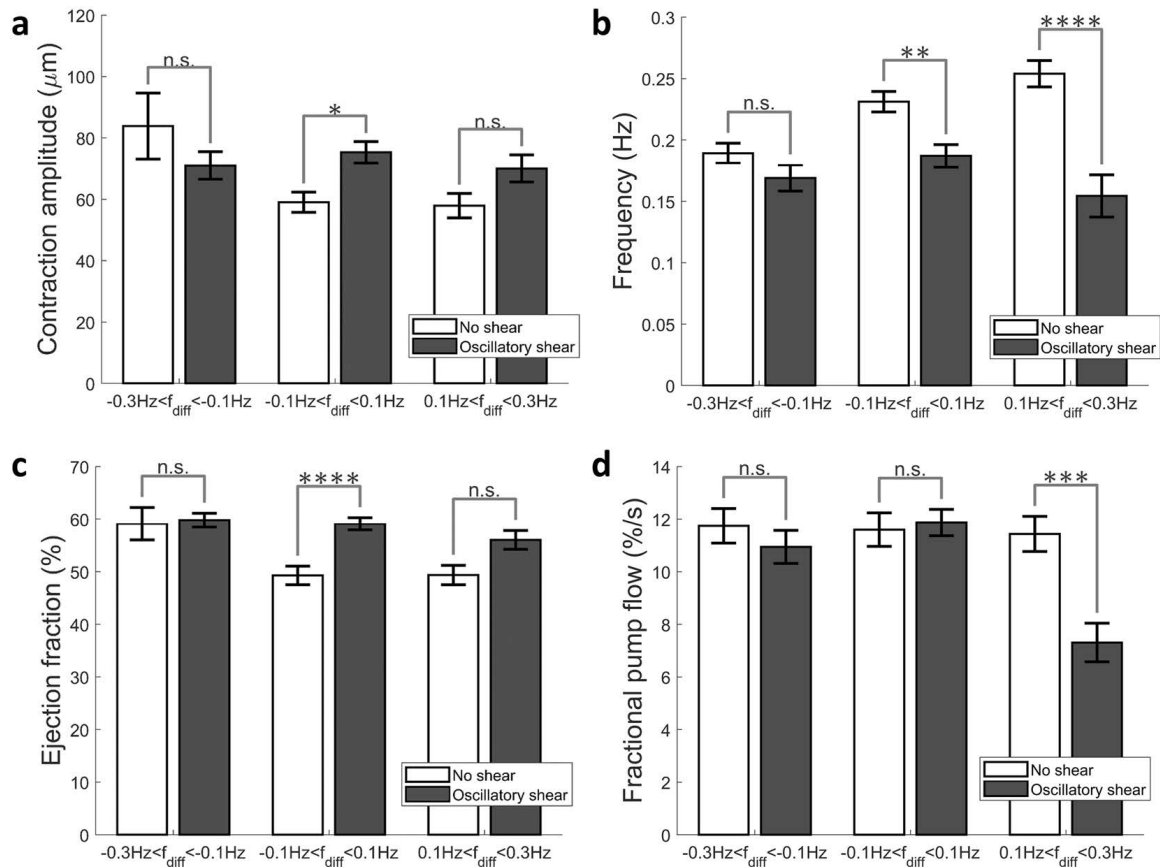
Figure 2.8: Four parameters of contractility; contraction amplitude, contraction frequency, ejection fraction and fractional pump flow; are modulated by the OWSS, depending on the frequency difference (N = 94). (a) The contraction amplitude was significantly higher (p = 0.046) for the similar applied frequencies and were not significantly different at other frequencies. (b) The contraction frequency was significantly lower for similar (p = 0.0056) and lower (p = 8.86e-08) applied frequencies. (c) The ejection fraction (percentage of lymph pumped per contraction) was significantly higher (p = 3.84e-05) at similar applied frequencies. (d) The fractional pump flow (percentage of lymph pumped per second) was significantly lower when low-frequency OWSS are applied (p = 2.8e-04).Unbalanced two-way ANOVA was performed to compare the group means between the different frequency and flow conditions (*p<0.05, **p<0.005, ***p<0.0005, ****p<0.00005)

frequency (Figure 2.8b) was found to be significantly lowered in response to the applied flow for the similar (p = 0.0056) and low (p = 8.86e-08) applied frequencies, with a greater decrease in the case of low applied frequencies. The ejection fraction (Figure 2.8c) was found to significantly increase when the applied frequency was close to the intrinsic frequency (p = 3.84e-05). The fractional pump flow (Figure 2.8d), representing the rate of fluid pumped as a result of lymphatic contractility (percentage of the fluid volume per second) was found to be significantly lower when the applied frequency was less than the intrinsic frequency (p = 2.84e-04). The increase in the ejection fraction for similar applied frequencies is possibly a consequence of the increased contraction amplitude at those frequencies (Figure 2.8a). Since the ejection fraction does not change significantly for the low applied frequency, the lowering of the fractional pump flow at low applied frequencies is possibly a consequence of the contraction frequency of the vessel getting lowered as a result of their entrainment to the imposed OWSS (Figure 2.8b).

2.4 Discussion

When exposed to an imposed pressure gradient ex vivo, lymphatic vessels are known to inhibit their contractile activity [35, 37]. The shear-mediated inhibition of the contractility of the lymphangions, similar to the flow-mediated dilation seen in blood vasculature, was reported to be endothelium-dependent and was reported to be dependent on the tissue bed from which the lymphatics were isolated [82]. In vitro studies have also shown the involvement of the lymphatic endothelium in this flow-mediated response [85, 86]. However, the actual WSS magnitudes at which this contraction inhibition occurs have been limited to one report on a small set of vessels [38]. This shear-dependent inhibition of lymphatic contractility is considered to be an important mechanism in their transition from a pump to a conduit for lymph, depending on the external forces, in order to optimize their lymph flow [46, 47]. In this work, the frequency of contraction of the vessels was found to be inversely related to the shear stress in the vessel, as shown in Figure 2.5c. Under sufficiently high

shear stresses, the vessel might stop contracting altogether. The critical shear stress which was introduced in this work can, therefore, be defined as an indicator of a threshold for the pump-conduit transition of the lymphatic vessels. Furthermore, this critical shear stress is inversely related to the diameter of the vessel, indicating that larger vessels are more sensitive to the wall shear stress. This alludes to an adaptation of the lymphangions to their own unique microenvironment in order to optimize their lymph transport capabilities.

The synchronized contraction of lymphangions to pump lymph has long been observed in vivo and has been suggested as being important for the optimal transport of lymph depending on the mechanical load that the vessels are being subjected to [87, 88]. The lymphatic vessels seem to have developed so as to utilize the propagation of depolarization waves along the lymphatic muscle layer for their contraction, facilitated by the electrical decoupling between the lymphatic endothelial and muscle cell layers [89]. Further, the role of endothelium-derived relaxation factors like nitric oxide and histamine in the flow-mediated dilation have been investigated [37, 45, 41, 81], and their presence was found to be correlated to the shear stress applied on the vessels. Computational models have also shown that the presence of these mechanisms for sensing and responding to the lymphatic microenvironment could facilitate the coordinated pumping of lymphangions [90, 91]. Previous work from our group has shown that the application of OWSS can cause entrainment in the contraction of lymphangions, and the entrainment is lost if the shear stress is sufficiently low [38]. Hence the existing literature suggests that the entrainment of contraction between lymphangions is affected at least in part by the shear sensitivity of the lymphangions, thus implicating flow-mediated dilation as a causative factor in the coordinated contraction of a chain of lymphangions.

The idea that entrainment is caused by flow-mediated dilation is supported by the result as represented in Figure 2.7d where the percentage of power in the applied frequency, representing the degree of entrainment, was found to be significantly higher when the applied frequency was close to the intrinsic frequency of contraction. This indicated the presence of

an optimum frequency of contraction that the lymphatic vessels have developed, possibly as a result of their microenvironment. If the entrainment is a result of inhibition of contraction by flow, it is not possible for the vessel to contract with a frequency higher than its intrinsic contraction frequency. This was supported by our observation that when a frequency of 0.35 Hz was applied to a vessel having an average intrinsic contraction frequency of about 0.3 Hz or lower, the vessel was unable to contract at the imposed frequency, and thus ended up contracting at half the applied frequency, effectively inhibiting its contraction at every other applied OWSS peak. Further supporting a mechanism implicating flow-mediated dilation in entrainment is the observation that the extent of entrainment of the vessel to the imposed OWSS was highly correlated with the ratio of the amplitude of the imposed WSS and the critical shear stress. The higher the amplitude of the OWSS, the stronger was the synchronization. Interestingly, this correlation was lost when comparing vessels in which the amplitude of the imposed WSS was above the measured critical shear stress, suggesting that elevating the WSS above this critical shear value has no benefit in terms of further increasing the entrainment.

It should be noted that the OWSS-induced entrainment is an active physiological response of the vessels to an imposed shear stress, and not an artifact of the system, as has been shown by Kornuta et al. in his original work [38]. Inhibition of the contractility of the vessels by using calcium-free media completely eliminated the entrainment of contractions to OWSS, showing that the active contractility of vessels is required for entrainment. During the experiments, the vessels were always subjected to small transmural pressure fluctuations over the OWSS (due to limitations in the perfusion system), which could affect their contractility. To show that these small transmural pressure fluctuations did not affect lymphatic entrainment to OWSS, the vessels were artificially subjected to oscillatory transmural pressures with an amplitude of less than 1 cmH$_2$O at zero shear stress. The oscillatory transmural pressure did not induce entrainment or any change in the contractility of the vessels, thus showing that the observed entrainment was solely caused by the applied

OWSS.

The response of the lymphangions to an OWSS is hypothesized to be dependent on the lymphatic endothelium. The role of the endothelium in shear-induced entrainment was established in a previous study [38] where denuded thoracic ducts were found to have an altered response to OWSS. In these experiments, the vessel contraction amplitude was hampered significantly as a result of the denudation as can be seen from the diameter tracings in Figure C.3. A CWT analysis revealed that the power at the applied frequency was lowered when the vessel was denuded. The power at the applied frequency in the denuded vessels was in the same range as the power at the applied frequency for a vessel with a calcium free media exhibiting no contractions, suggesting that any motion at the frequency of the flow waveform was not due to vessel contraction but passive fluctuations in the diameter due to the small transmural pressure fluctuations in the system. However, in the absence of an imposed waveform, the denuded vessel still exhibited strong intrinsic contractions, albeit at a reduced frequency. The absence of strong entrained contractions in the denuded lymphatic vessels under flow, even when intrinsic contractions are present under no flow conditions, suggests that the endothelium is required for entrained contraction of the lymphatic vessels to an OWSS.

The shear-dependent vasodilation of blood vessels is well documented [92, 93, 94] and similar phenomena have been observed in lymphatic vessels in the form of shear induced inhibition [46, 95]. The role of the endothelium was established in the shear-induced inhibition, in the form of the involvement of endothelium derived relaxation factors like nitric oxide (NO) and histamine [37, 45, 41, 81]. However, NO and histamine may not be the only molecules involved in the shear dependent response of lymphangions. Other molecules such as reactive oxygen species (ROS) have been shown to be implicated in shear-induced mechanotransduction through the endothelium for blood vessels [96, 97] and ROS have been shown to inhibit spontanous lymphatic contractions [43]. Further it has been shown that NO is not obligatory for the flow mediated dilation in the radial artery [98], which

alludes to mechanisms other than NO that may be involved in the endothelium-dependent shear-induced mechanotransduction. Further studies need to be done to delineate the mechanisms for shear-induced entrainment.

Studies have shown that mesenteric vessels respond less to the same pressure gradient compared to thoracic ducts [32]. The inhibition of the contraction frequency by an imposed WSS is not as pronounced for the mesenteric vessels as it is for the thoracic ducts, for the same pressure gradient. However, these studies did not account for the shear stress on the vessel lumen, which is dependent on the flow rate through the vessel and the diameter of the vessel. The flow rate through the vessel is not only dependent on the pressure gradient across the vessel chamber, but the overall resistance of the vessel chamber system. The total resistance of the vessel chamber depends on i) the vessel diameter, ii) the resistance of the pipette used for the vessel cannulation which is determined by its shape, and iii) the diameter difference between the pipette orifice and the vessel diameter. To determine if the apparent lower sensitivity of the mesenteric vessels recorded in the literature is indeed a property of the vessel and not due to the aforementioned discrepancy between the pressure gradient and the wall shear stress, a comparison was done between the average shear stress experienced by a thoracic duct and a mesenteric vessel for the same pressure gradient. It was found that the shear stress experienced by the mesenteric vessels for the same pressure gradient was in the same order of magnitude as the thoracic duct, and in some cases even higher (Figure C.2). Moreover, it was seen that the mesenteric vessel contractions were never completely inhibited, and the reduction in contraction frequency at the same shear stress was also less in comparison to the thoracic ducts. The lower entrainment of mesenteric vessels in response to OWSS (Figure C.1) is also consistent with the lower sensitivity of mesenteric vessels to wall shear stress. Like the thoracic ducts, the lower shear sensitivity of the mesenteric vessels can translate to a lower percentage of power at the applied frequency. The regional variability in the shear sensitivity of lymphatic vessels and its effect on the entrainment of lymphatic vessels to OWSS needs to be investigated further in

future work.

The potential physiological benefit of these unique features of lymphatic vessel entrainment to OWSS is perhaps best illustrated in Figure 2.8. In a chain of lymphangions, one would expect the frequency of the flow waveform resulting from the ejection of fluid from an upstream vessel to be similar to the frequency of the contractility of the adjacent vessel, due to the propagation of action potentials along lymphatic muscle cells adjacent to one another, even across the lymphatic valves [99]. Similar contraction frequency between adjacent lymphatics has also been observed in vivo [88] and it has previously been suggested with experimental data that the flow-mediated dilation could assist in the coordination of contraction between lymphangions [45]. Thus, the ability to dynamically respond to flow, and the fact that the kinetics of this response is optimized to occur on time scales similar to the vessel's intrinsic contraction frequency, might provide a mechanism to enhance ejection fraction and optimize lymphatic pumping even in the presence of lymphatic contractile coordination via electrical coupling of lymphatic muscle cells. This is supported by Figure 2.8a which shows that there was a significant increase in the ejection fraction when the externally applied flow was oscillating at a frequency close to the intrinsic frequency of contraction of the vessel. Similarly, Figure 2.8b shows a significant reduction in the fractional pump flow when the applied flow frequency was lower than the intrinsic contractile frequency of the lymphangion, due to the externally applied OWSS lowering the contractile frequency below its intrinsic value. Computational modeling that incorporates these dynamic responses, with values from actual experimental data such as those reported here, could shed light on the benefit of this flow-mediated entrainment, possibly by preserving the energy expenditure by lymphatic muscle cells and enhancing overall lymph transport.

The literature has also shown that the mechanosensitivity of lymphangions to shear stress is hampered in pathological states that have been related to impaired lymphatic transport, such as those that might occur in the case of metabolic syndrome [100, 101] and as a result of aging [102, 103]. The entrainment of lymphangions to shear stress could thus also

be hampered during cases of lymphatic endothelial dysfunction that affects flow-mediated dilation, thus leading to deficient pumping in the lymphatics or the unnecessary expenditure of energy by lymphatic muscle cells. This could provide a mechanism for reduced lymphatic pump flow during conditions of lymphatic dysfunction, possibly leading to impaired tissue-fluid homeostasis and other complications that may arise due to a compromised lymphatic system. Thus, the physiological consequences of impaired flow-mediated dilation to lymphatic pump performance in the context of disease is an important area of future study.

2.5   Interim Summary

This chapter shows that the lymphatic mechanomodulation by OWSS is dependent on both the intrinsic shear sensitivity of the lymphatics as well as the parameters of the OWSS (frequency and amplitude) that stimulate the lymphatics. The shear sensitivity of the lymphatics, represented by the critical shear stress, represents a threshold after which the entrainment of the vessel to the flow can no longer be modulated any further. Optimum frequencies of the OWSS, which maximally entrained lymphatic contractions, were found to be close to the intrinsic contractile frequencies of the vessels. Increases in entrainment at the optimum frequency conditions were concurrent with increases in the contraction amplitude and ejection fraction of the vessels, and low OWSS frequencies significantly impacted the fractional pump flow of the vessels through the phenomenon of entrainment. While it is clear that entrainment is an important metric of the shear sensitivity of lymphangions to OWSS and is relevant to the modulation of the pump function of the vessels in response to different OWSS, the fact remains that these experiments were done on isolated lymphatic vessels with tightly controlled mechanical conditions. The obvious question that arises out of this is "do lymphatics also entrain optimally to oscillatory forces in vivo and what does it mean for the lymphatic transport function?"

These questions become even more important in the context of lymphedema. Physiotherapy is still the most effective modality of lymphedema treatment in terms of the

reduction of volume of the affected limb, where externally applied oscillatory forces are used to drive lymphatic flow in the affected limb. However, little is known about how the oscillatory pressures applied during physiotherapy can modulate lymphatic function, and if there are optimal conditions which can maximally stimulate lymphatic contractility. Hence, in the next chapter, we will investigate the modulation of lymphatic contractility by oscillatory pressure waves, similar to those applied during physiotherapy.

CHAPTER 3

IN VIVO MODULATION OF LYMPHATIC CONTRACTILITY

3.1 Background

As seen in the previous section, the entrainment of collecting lymphatic vessels to oscillatory shear stresses is a combination of the parameters of the oscillatory flow being applied (frequency and amplitude) and the intrinsic contractile frequency and mechanosensitivity (critical shear stress) of the vessels. Thus the mechanical microenvironment of the lymphatics are important in determining collecting lymphatic function and, following from that, it also means that it is possible to modulate lymphatic function by altering the mechanical microenvironment. It is not just scientific curiosity that drives the question of how lymphatic contractions may be modulated; there are tangible practical benefits of this knowledge, especially considering that the primary modality of treating lymphedema is by applying external forces to control the swelling of the affected region of the body. We are, of course, talking about physiotherapy, which works on the premise of applying external forces to modulate the physiology of our body and, in turn, deliver a therapeutic effect [104].

As mentioned before, a common consequence of lymphatic dysfunction is a debilitating disease called lymphedema, which is marked by a unilateral swelling of the extremities of the body, typically an arm or a leg [61, 105]. Physiotherapy is the most commonly used modality for treating the swelling due to lymphedema. Physiotherapy for lymphedema (also referred to as "complete decongestive therapy") is usually administered in three different forms; i) manual lymphatic drainage (MLD) has a trained physiotherapist apply a massage to the affected region, ii) compression bandaging (CB) applies a static compressive force using a specialized garment to reduce interstitial fluid accumulation, and iii)

intermittent pneumatic compression (IPC) uses a specialized garment to apply a spatiotem-porally oscillating pressure wave (OPW) to the affected limb. MLD, CB, and IPC, either individually or in conjunction, have been shown to facilitate a significant reduction in the limb volume of lymphedema patients [106, 107, 108, 109].

These studies, however, have focused on the effect of MLD and/or IPC on the net vol-ume reduction of the affected limb, without elucidation of the underlying mechanisms that lead to this volume change. For example, how do the pressures applied during physio-therapy affect collecting lymphatic function? Since isolated lymphatic vessels have been shown to exhibit optimally entrained contractions to external oscillatory shear stresses [21], it is important to ask whether collecting lymphatic vessels can be optimally modulated us-ing an OPW in vivo and if that has any benefits to lymph drainage and volume reduction. Only a few studies have attempted to investigate the effect of MLD and IPC on collecting lymphatic contractile function and have shown transient improvements in the lymphatic uptake and lymph velocity in both affected and non-affected limbs [110, 111]. However, no studies have quantified how lymphatic function may be modulated by optimizing IPC, thereby potentially enhancing lymphatic contractile function and, possibly, overall lymph drainage. IPC is of particular interest in this work, since it has the most potential for being optimized for enhancing lymphatic function by customizing the spatiotemporal frequency of the OPW applied by this device. Hence this chapter will describe the modulation of lymphatic vessels by OPW in vivo using a rodent model, and try to delineate the impact of this modulation on lymphatic transport function.

3.2 Methods

3.2.1 Animal Model

Male Sprague Dawley rats were used to test the effect of OPW on rat tail lymphatic vessels. There are, typically, a total of 4 collecting lymphatic vessels running along the rat tail, two on either side. This symmetrical distribution of the collecting lymphatics in the rat tail

make them ideal for isolating the effects of the OPW on the lymphangions in one particular side. The collecting lymphatics on the left side of the tail were imaged for function while being stimulated with the OPW. A 2.4 cm long segment was chosen immediately proximal to the pressure cuff for imaging the lymphatics.

3.2.2   Pressure Cuff System

A pressure cuff system was designed to exert spatiotemporally varying oscillatory pressure waveforms on the rat tail. Figure 3.1a shows a schematic of the pressure cuff system. The system consists of a series of 3 commercially available occlusion cuffs (Kent Scientific®) that were designed for blood pressure measurements on the rat tail. The occlusion cuffs were pressurized using two syringe pumps through a series of two-way solenoid valves. The solenoid valves were programmed to switch between two states (on or off) in order to control the path of the air flow from the syringe to the selected pressure cuffs. The solenoid states were controlled by a programmable NI data acquisition and control inter-face (NI USB-6002) that was connected to a PC. The solenoids and the syringe pumps were controlled directly through a MATLAB® program implemented on a PC. The control algorithm is a simple proportional control scheme that controlled the velocity of the syringe (the MATLAB® control code is provided in Appendix B). Typically, one pump was set to control the pressure in the 3 pressure cuffs while the other resets. This ensured that one of the pumps was ready to operate when the other pump ran out of air, thus enabling a longer duration of operation for the system. Figure 3.1b shows the typical pressure distribution in the three cuffs.

The OPW was designed to simulate the effect of an IPC on the rat tail, albeit in a controlled manner. The pressure in the cuffs could be controlled independently by sequential switching of the solenoids. Thus, both the temporal frequency and the propagation speeds of the OPW could be controlled independently. The temporal frequency was the frequency of the pressure waveform in each cuff and were varied between 0.05 Hz, 0.1 Hz, and 0.2
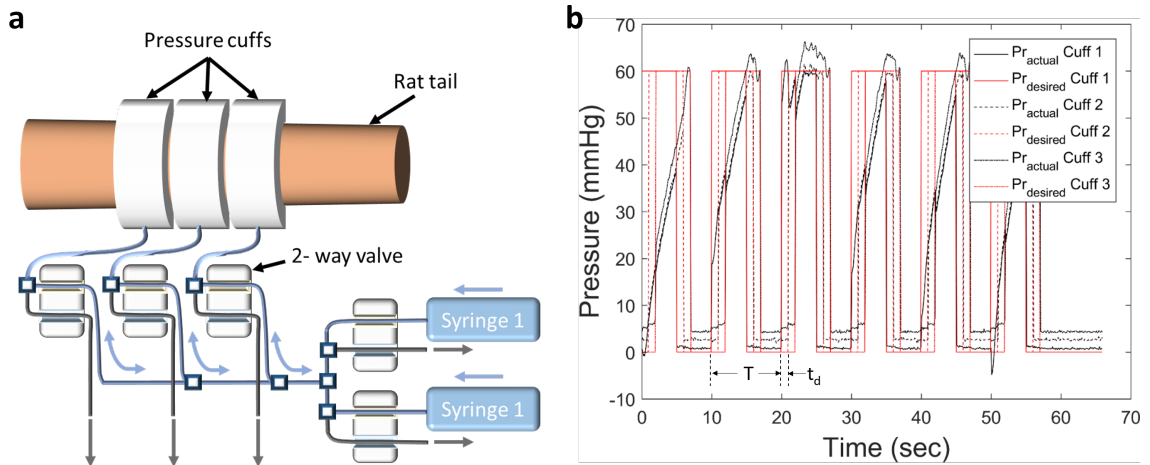
Figure 3.1: The schematic of the pressure cuff system and the applied OPW. a) A schematic of the pressure cuff system is shown. The three pressure cuffs were connected to two syringe pumps through a series of 2-way valves (solenoids) that controlled the flow of air. Through proper switching of the solenoids and selection of the pumps, independent control of the pressure in each pressure cuff was achieved. b) The oscillatory pressure wave is shown for each pressure cuff independently. T is the time period of the pressure wave in each cuff, and t_d is the time delay between the pressure cuffs.

Hz. The propagation speed was calculated from the time delay between the cuffs (t_d) as $17/t_d$ mm/s (the width of each cuff was 17 mm). Thus, the three time delays of 2 s, 6.67 s, and 10 s translated to OPW propagation speeds of 8.5 mm/s, 2.55 mm/s, and 1.7 mm/s respectively.

3.2.3   Data Acquisition

All the data were collected in the form of the near-infrared (NIR) fluorescence from an injected NIR dye. The NIR dye used for this purpose was prepared by conjugating the commercially available IRDye® 800CW to 20 kDa polyethylene glycol (PEG) as described in previous literature [80]. The size of the conjugated dye enabled it to be taken up specifically by the lymphatics upon an intradermal injection, instead of the blood vessels. The NIR dye was injected intradermally into the tip of the rat tail to facilitate easier uptake by the initial lymphatic capillaries. The dye showed up in the collecting lymphatic vessels in the ROI within a few seconds of injection (Figure 3.2a).

61

The NIR fluorescence from the dye was captured using a lymphatic NIR imaging system. The injected dye was excited by a xenon arc light source (Sutter Instrument Company®) at an 800 nm wavelength. The emitted light from the tail was passed through a bandpass filter with a center wavelength of around 830 nm (Brightline® single-band filter set, Semrock) attached to a filter cube. The filtered emitted light, centered at 830 nm was captured by a cooled EMCCD camera (Evolve® eXcelon, Photometrics) attached to a stereomicroscope with adjustable zoom (Olympus®). The images were captured at 0.63x magnification to enable the imaging of a 2.4 cm long segment of the tail.

3.2.4   Data Analysis

The captured NIR images were processed using a custom MATLAB® code. The NIR images were cropped and binarized to identify the two vessels in the ROI. Third order polynomials were fitted to the binarized images to determine the location of the two vessels. 20x20 pixel ROI were selected, centered around each point along the polynomials. This allowed for any ROI to be selected along the length of the vessel, as well as enabling the user to choose the vessel with the higher mean fluorescent intensity. The ROI closest to the pressure cuff (to the right of the tail section shown in Figure 3.2a) was chosen to quantify the changes in intensity. The mean intensity in the ROI was used for calculating the lymphatic mechanosensitivity and pumping metrics (Figure 3.2b).

The images were acquired for a total of 30 mins for each rat, divided into three windows; the first 10 mins were used for capturing the intrinsic contractility of the collecting lymphatic in vivo (pre-OPW period), followed by a 10 min period of applying OPW with the specified temporal frequency and propagation speed (OPW period). The last 10 mins were used to observe the impact of the pressure on the lymphatic function, when the OPW is removed (post-OPW period). A representative tracing of the intensity vs time data is provided in Figure 3.3a. The intensity vs time data was processed using a continuous wavelet transform (CWT) in MATLAB®, which converts the data from the time domain to the fre-
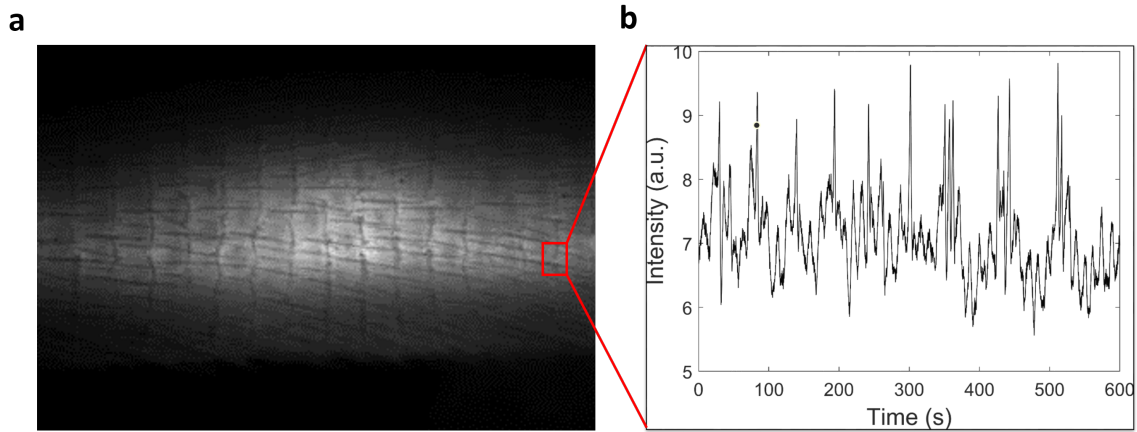
Figure 3.2: NIR image acquisition and processing. a) The PEG-conjugated IRDye®
800CW was injected intradermally into the tip of the rat tail and the fluorescence inten-
sity was recorded non-invasively using an EMCCD camera and filters designed for the
near-infrared wavelength. b) A region of interest (ROI) was selected close to the pressure
cuffs and the intensity was tracked over time. This intensity was analyzed for quantifying
entrainment and lymphatic transport function.

quency domain. Figure 3.3b shows a spectrogram of the data, with respect to frequency and
time. The colorbar represents the magnitude of the CWT coefficient at particular frequen-
cies and times. The magnitude of the CWT at a particular frequency and time corresponds
to the prevalence of that particular frequency component at the particular time and is re-
ferred to as the "power" in that frequency component. Thus, the CWT is a good way to
"resolve" the data into its constituent frequency components and find the relative impor-
tance of a particular frequency component over others. The power at the applied temporal
frequency was used a measure of the entrainment of the contractions to the applied OPW
frequency.

The area under the curve for the OPW and post-OPW time windows, normalized to the
baseline intensity (shown as the shaded area in Figure 3.3c) were calculated. The total area
was divided by the time period of OPW application to get an average packet transport as
the metric of lymphatic function. Trend lines were fitted to the intensities during the OPW
periods to observe the average intensity dynamics. The peak time (time required for the
trendline or intensity to reach maximum) and decay time (time required for the trend line

63

to reach midway between maximum and minimum) were quantified from the trend lines (Figure 3.3c).

The experimental conditions (OPW protocols) applied to the animals were randomized so that different protocols were used at different days of the week, and also at different times of the day. This was done to eliminate biases in the data that may arise from factors other than the specific parameters of the OPW. The surgeries were performed at different days of the week and the order in which the sham and ligation surgeries were done was randomized. The data analysis was automated using MATLAB® codes as described above, so that all the image processing and data analyses were performed using the same parameters of the code (e.g. averaging window of the smoothing filter and the order of the fitted polynomials were set constant across all the dataset). No user input was allowed after setting the parameters of the code and the data was plotted as is without any modification/elimination of data points.

3.2.5   Statistical Analysis

The entrainment and lymphatic function data showed a high amount of variability between the animals. Normality tests performed on the datasets did not always show that the data were normally distributed, hence non-parametric statistical tests were performed. Unpaired data (data that came from different animals), e.g. when comparing the differences in entrainment with respect to temporal frequency, were analyzed using the Mann-Whitney test. Paired data (data coming from the same animal), e.g. when comparing the change in entrainment between day 0 and day 28 for ligation animals, were analyzed using the Wilcoxon signed rank test. The alternative hypotheses included testing whether the means were greater or lesser than each other, depending on the experiment, and were tested at a significance level (α) of 5%. Linear regression analysis was used to compare the correlation between tail swelling and the power at the applied frequency. The R-squared value was used to quantify the goodness of the fit and t-test for coefficients was used to assess

whether the regression coefficients were significantly different from zero ($\alpha = 0.05$).

3.3 Results

3.3.1 In Vivo Entrainment

The behavior of collecting lymphatic vessels in vivo are different from their behavior when isolated and perfused ex vivo. In vivo collecting lymphatics do not contract as periodically as in the ex vivo condition and their contraction frequency is also much lower [80]. Hence it was first necessary to quantify the impact of an OPW on rat tail collecting lymphatic vessels to investigate whether collecting lymphatics can be entrained to this external stimulus in vivo. Using a series of three pressure cuffs placed over the tail, an oscillatory pressure wave with an amplitude of 60 mmHg, temporal frequency of 0.05 Hz, and a propagation speed of 2.55 mm/s was applied externally to the rat tail (the rationale behind selecting these particular pressure amplitude and frequency parameters are provided in the discussion section). The rats were given an intradermal injection of a near infrared (NIR) labeled, lymphatic specific, tracer and imaged using an NIR stereomicroscope which provided continuous non-invasive imaging of lymphatic contractile function during OPW application. The OPW protocol was 30 min long and divided into 3 windows: 10 mins of intrinsic contractility without any externally applied pressure (pre-OPW), 10 mins of OPW, and 10 mins of follow up after the external OPW has been stopped (post-OPW). This allowed for the characterization of the intrinsic function of the lymphatics, as well as their response to the external OPW and their contractility after the OPW was removed.

The emitted fluorescence from the injected NIR dye was imaged to capture the intensity and, consequently, the contractile function of the lymphatics. Distinct spikes in intensity were observed over time, which corresponded to lymphatic contractions and were referred to as "packets" (Figure 3.3a). A small region of the lymphatics closest to the pressure cuff was selected as the region of interest (ROI) for analyzing the intensity. The response of the collecting lymphatics to the OPW was determined through image analysis of the lymphatic
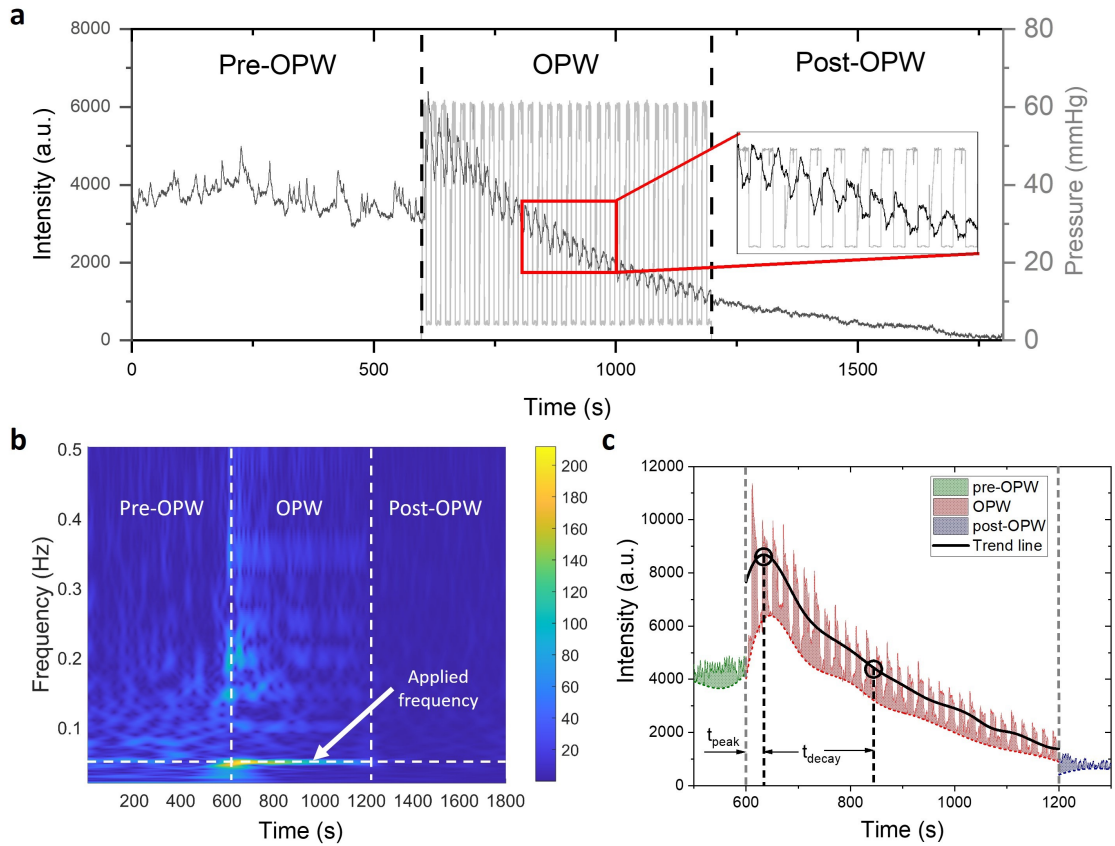
Figure 3.3: The fluorescence intensity at the chosen region of interest (ROI) is modulated by the oscillatory pressure wave (OPW) applied to the tail using the pressure cuffs. a) The intensity was recorded over a period of 30 mins (1800 s), divided into three 10 min (600 s) segments. The first 10 mins were used to record the intrinsic packet movements at the ROI (pre-OPW), followed by 10 mins of application of the oscillatory pressure wave (OPW). The final 10 mins were used to record the packet transport at the end of the pressure application, if any (post-OPW). The inset shows that the entrainment of the intensity to the OPW can be clearly observed between 10 to 20 mins. b) A representative spectrogram, obtained by continuous wavelet transform (CWT), of the intensity is plotted to showcase the entrainment at the applied frequency. The applied frequency of 0.05 Hz is highlighted by the vertical dashed line. The vertical dashed lines demarcate the segment where the OPW is applied. The colorbar represents the magnitude of the CWT coefficients at different times and frequencies, with blue corresponding to low values and yellow corresponding to high values of the CWT coefficients. c) The lymphatic function is quantified as the area under the curve of the intensity, normalized to the baseline (shown in the shaded area of the graph). This metric of lymphatic function is referred to as the average packet transport. The trend line (shown in black) shows the average intensity variation over the OPW period. The time for the trend line to reach the maximum (peak time) and subsequently fall to midway between the maximum and minimum intensity (decay time) are shown as t_{peak} and t_{decay}.

66

intensity at the ROI. For the first 10 mins, the vessels exhibited erratic and aperiodic contractility that is typical of lymphatic vessels in vivo, but they all entrained to the temporal frequency of the applied OPW as soon as the external pressure was applied. This entrainment was more apparent when looking at the power distribution in the spectrogram of the intensity signal (Figure 3.3b). The power at the applied OPW frequency was extremely low during the first 10 mins of the protocol but increased when the OPW was applied. This shows that the collecting lymphatics in the rat tail were entraining to the external OPW, and the entrainment was happening at the applied temporal frequency. The entrainment was quantified as the power at the applied frequency, which represents the prevalence of the applied frequency among the harmonics in the intensity tracings. Thus, the entrainment was defined to be a metric of the mechanosensitivity of the lymphatic vessels to the OPW.

The metric of packet transport (also referred to in the literature as pumping score) has been previously used to quantify lymphatic function [112, 113]. A similar metric, called the average packet transport, was used to quantify lymphatic function in this work. To calculate the average packet transport, the intensity at the ROI was first normalized to a baseline obtained by fitting an envelope to the intensity tracing. The area under the curve of this normalized intensity (shown in Figure 3.3c as the shaded region between the recorded and baseline intensity) was normalized by time to get the metric of average packet transport. A trendline fitted to the data also captures the average intensity dynamics of the lymphatics, which is characterized by a sharp increase in intensity that decays over time. The metrics of peak time (t_{peak}) and decay time (t_{decay}) as shown in Figure 3.3c were used to quantify the average intensity dynamics of the lymphatics. The average intensity dynamics can be used to comment on the transport function of the chain of lymphangions distal to the ROI, and this will be discussed in more details in the next chapter.
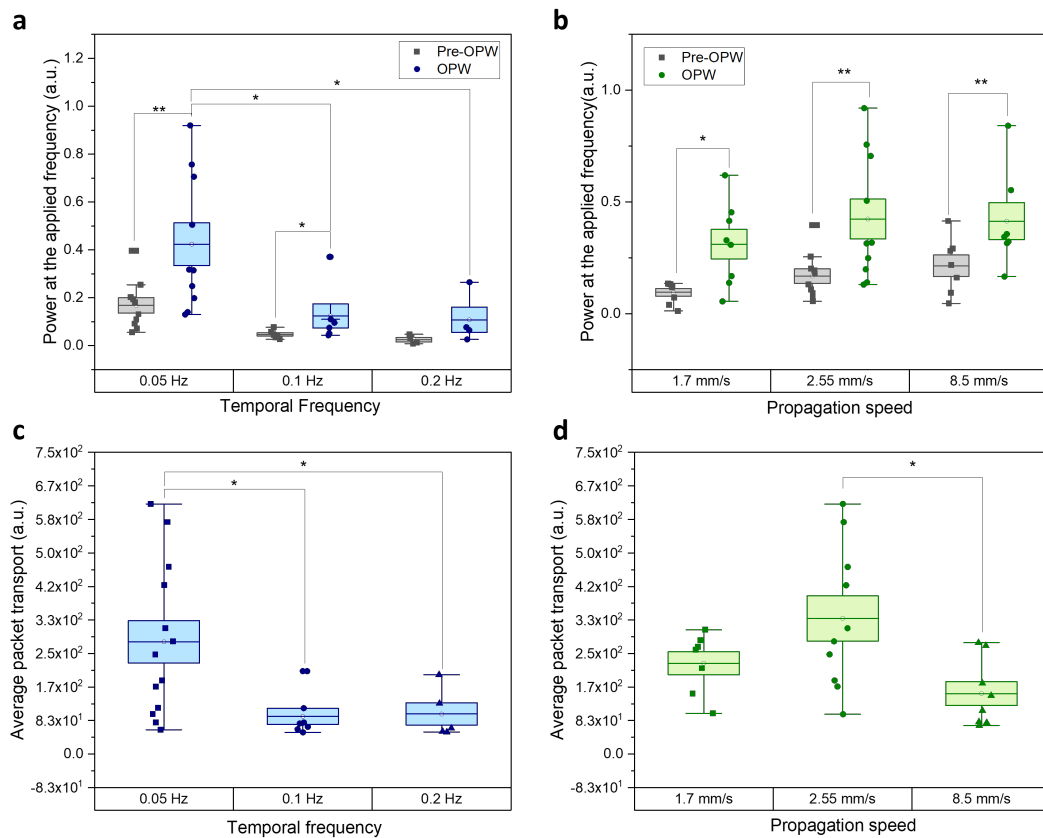
Figure 3.4: The entrainment and lymphatic transport function are modulated by the temporal frequency and the propagation speed of the OPW. A) The entrainment is summarized with respect to three temporal frequencies, 0.05 Hz (n = 10), 0.1 Hz (n = 6), and 0.2 Hz (n = 4), with the propagation speed set to 2.55 mm/s. There was a significant increase in entrainment from the intrinsic condition when the applied frequency is 0.05 Hz (p = 0.004) and 0.1 Hz (p = 0.018). The power at the applied frequency was also significantly higher at 0.05 Hz compared to 0.1 Hz (p = 0.0054) and 0.2 Hz (p = 0.014). B) The entrainment is summarized with respect to three propagation speeds, 8.55 mm/s (n = 7), 2.55 mm/s (n = 10), and 1.7 mm/s (n = 8) with the temporal frequency set to 0.05 Hz. The power at the applied frequency was significantly increased on the application of OPW for the 8.5 mm/s (p = 0.017), 2.55 mm/s (p = 0.004), and 1.7 mm/s (p = 0.007) conditions. However, the entrainment between the different groups were not significantly different from each other (p = 0.59, 0.51, and 0.45 between 8.5 mm/s and 2.55 mm/s, 2.5 mm/s and 1.7 mm/s, and 1.7 mm/s and 8.5 mm/s respectively). C) The average packet transport, representing the lymphatic transport function, was significantly higher for the 0.05 Hz temporal frequency compared to 0.1 Hz (p = 0.006) and 0.2 Hz (p = 0.019). D) The average packet transport was higher for the 2.55 mm/s propagation speed compared to 8.55 mm/s (p = 0.015) but not significantly different compared to the 1.7 mm/s condition. Mann-Whitney test was performed to compare the group means (*p<0.05, **p<0.005).

3.3.2 Impact of Temporal Frequency and OPW Propagation Speed

Massage is routinely used to stimulate collecting lymphatic contractility in mice [114, 115]. MLD, which essentially applies an OPW to the affected limb, has been shown to have a stimulating effect on the collecting lymphatics in humans [110, 116, 109] in terms of the frequency and velocity of the packets of NIR dye obtained through NIR imaging. We hypothesized that the entrainment of lymphatic function should depend on the temporal frequency and the propagation speed of the OPW. The temporal frequency (also referred to, simply, as the frequency) is the frequency of the oscillatory pressure in each pressure cuff and the propagation speed is inversely proportional to the time delay between the pressure cuffs. The modulation of lymphatic function by OPW with three different temporal frequencies (0.05 Hz, 0.1 Hz and 0.2 Hz) is shown in Figure 3.4a. We note here that the average contractile frequency of the vessels in vivo in rats, as determined by NIR, can vary between 0.02 Hz to 0.05 Hz (Figure 3.5a). Hence the 0.05 Hz condition is closest to physiological contraction frequencies, while the 0.1 Hz and 0.2 Hz conditions are supraphysiological. It should be noted that in vivo contraction frequencies can vary widely depending on the species and method of anesthesia [117]. Hence, the applied OPW frequencies were physiological or supraphysiological only in the context of the current animal model and anesthesia (Sprague-Dawley rats with a ketamine and dexmedetomidine anesthesia). Figure 3.4a shows that the lymphatic entrainment was significantly increased when the OPW was applied for the temporal frequencies of 0.05 Hz (p = 0.004) and 0.1 Hz (p = 0.018), but not 0.2 Hz. A comparison of the entrainment between the different temporal frequencies also showed that the entrainment at 0.05 Hz was significantly higher than those at 0.1 Hz (p = 0.0054) and 0.2 Hz (p = 0.014). This shows that the vessels did not effectively entrain to higher frequencies (0.2 Hz), and the entrainment was highest at the applied frequency that was closest to the intrinsic frequency.

The OPW propagation speed was not found to significantly affect lymphatic entrainment (Figure 3.4b). While at each propagation speed of 8.5 mm/s, 2.55 mm/s, and 1.7

mm/s, the entrainment was significantly increased by the application of OPW (p = 0.017, p = 0.004, and p = 0.007 respectively), there were no significant differences between the three conditions (p = 0.59, 0.51, and 0.45 between 8.5 mm/s and 2.55 mm/s, 2.5 mm/s and 1.7 mm/s, and 1.7 mm/s and 8.5 mm/s respectively). Hence the temporal frequency, and not the OPW propagation speed, had a significant impact on the entrainment of the contractions to the applied OPW.

The average packet transport, representing lymphatic transport function, was significantly higher for the 0.05 Hz temporal frequency compared to the 0.1 Hz (p = 0.006) and 0.2 Hz (p = 0.019) temporal frequency, which is concurrent with the higher entrainment at the 0.05 Hz frequency condition (Figure 3.4c). Interestingly, although the entrainment was not significantly different between any of the propagation speeds, the average packet transport was significantly higher for 2.55 mm/s, compared to 8.5 mm/s (p = 0.015) (Figure 3.4d). Taking the results together, we concluded that, for the specific experimental conditions presented here, a combination of 0.05 Hz temporal frequency and 2.55 mm/s propagation speed was optimal for stimulating lymphatic contractility for the animals, and these parameters were used for the subsequent experiments.

3.3.3 Involvement of Nitric Oxide in OPW-induced Lymphatic Modulation

Nitric oxide (NO) is a well-known vasodilator and has been extensively studied in the context of blood vasculature. Its role, typically, is to relax the blood vessels, reducing the hydraulic resistance of the vessels. In the context of lymphatics, NO plays a similar role, relaxing the lymphatic muscle cells (LMCs) and reducing the contractility of the lymphangions. The shear stress generated by lymph flow in the lymphangions typically increases NO production via endothelial nitric oxide synthase (eNOS), resulting in a reduction of contractile function. The application of a nitric oxide donor ointment (glyceryl trinitrate ointment or GTNO) has previously been shown to reduce lymphatic pumping in vivo [118, 80, 119]. A similar nitric oxide donor ointment, in the form of a nitroglycerine ointment
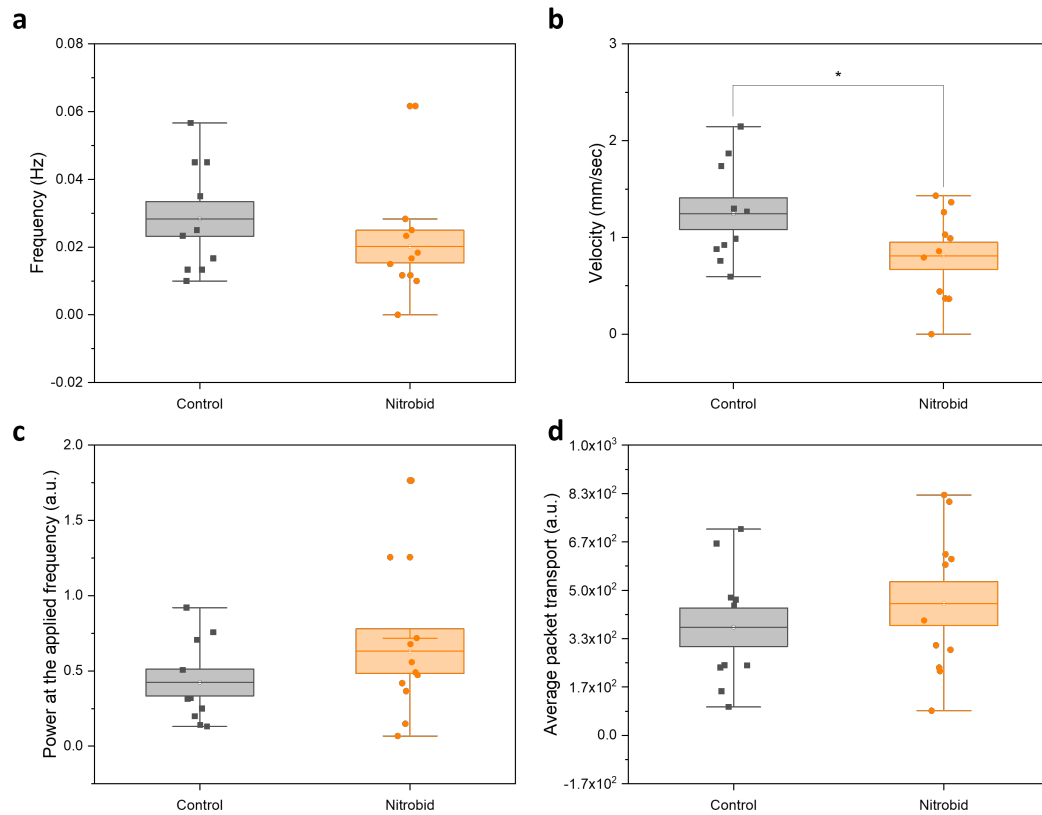
Figure 3.5: The effect of a nitric oxide (NO) donor cream (Nitrobid® nitroglycerine ointment) on the lymphatic function and entrainment. a) The packet frequency showed a decreasing trend on the application of NO ointment which was not significant (p = 0.13). b) The packet velocity was significantly reduced on the application of Nitrobid® (p = 0.029). The c) entrainment and the d) average packet transport did not show any significant changes in response to Nitrobid®. For the control conditions we had an n = 10 and for the Nitrobid® conditions we had an n = 11. Two-sample t-tests were used to compare the group means (*p<0.05).

(Nitrobid®), was used for the present study. Nitrobid® was applied to the rat tail and left on for a minute. The NIR dye was subsequently injected in the tail tip and imaging was performed after 10 mins to ensure that the lymphatic contractions reach a steady state [80]. The mean packet frequency was marginally reduced on the application of Nitrobid® (Figure 3.5a), but not significantly. The mean packet velocity was found to be significantly reduced, tested using a two-sample t test with Welch's correction (p = 0.029), as seen in Figure 3.5b. This reduction is similar to what has been observed with GTNO in the rat tail, where the reduction in packet velocity was more pronounced than the reduction in packet frequency [80]. These results showed that Nitrobid® reduces contractile function similar to what has been demonstrated previously with GTNO.

The rat tails treated with Nitrobid® were then subjected to an OPW with a frequency of 0.05 Hz and propagation speed of 2.55 mm/s. The entrainment to the applied OPW was not found to be significantly different upon application of the Nitrobid® ointment (Figure 3.5c). The average packet transport was also not found to change significantly on the application of Nitrobid® (Figure 3.5d). These results suggest that the application of exogenous NO did not interfere with the OPW induced modulation of lymphatic function.

3.4   Discussion

The present study undertakes a comprehensive investigation of the modulation of collecting lymphatic contractility in vivo using an externally applied OPW, akin to a pneumatic compression device or manual massage. The study shows, for the first time, that lymphatic contractile activity can be optimally modulated using a spatiotemporally varying oscillatory pressure wave (OPW) applied in vivo to functional collecting lymphatics. The pressure and frequencies were chosen for this study based on findings and recommendations from previous work. A previous study investigating the effect of IPC on tissue fluid pressure and flow had shown that it was necessary to use pressure waveforms with a high-pressure amplitude and low frequency to generate sufficient tissue fluid pressure to drive lymph flow [120].

Further, the tissue fluid pressure during MLD can reach up to 140 mmHg in humans [121], which is well above the lymphatic pumping pressure that has been recorded in humans (30-40 mmHg) [122]. Thus, the pressure amplitude for the experiments were chosen to be 60 mmHg, which is above the lymphatic pumping pressure of rat collecting lymphatics (30-40 mmHg) [119]. Selecting the frequency of the stimulation needed more careful consideration, since lymphatic contraction frequency in vivo can vary widely between 1 to more than 15 contractions per minute. Bachmann et al. showed that the type of anesthesia can have a significant effect on the pumping frequency in mice leg lymphatics [117]. Thus the "physiological" frequency range for the experiments is dependent on the type of anesthesia chosen, and was found to be between 0.02 and 0.06 Hz in Sprague-Dawley rats for the type of anesthesia administered for the present experiments (ketamine and dexmedetomidine). Based on the particular animal model and type of anesthesia, the OPW frequencies were chosen to vary from physiological (0.05 Hz) to supraphysiological (0.2 Hz). The OPW propagation speeds were chosen to align with the velocity of lymphatic contraction propagation under the present experimental conditions. Zawieja et al. had shown that the average conduction velocity of contractions between two lymphangions in isolated lymphatic vessels ranged between 4-8 mm/s [88]. The closest measure we have for the conduction of contractions in vivo is packet velocity, which was found to average between 0.5 mm/s and 2.2 mm/s for the experiments presented in this work (Figure 3.5b). The packet velocities reported in this work were similar to the packet velocities previously reported in rat tail lymphatics [118, 80]. Thus, similar to the temporal frequencies, the OPW propagation speeds were close to the in vivo contraction propagation speeds (or packet velocity) for 2.55 mm/s and 1.7 mm/s conditions, and supraphysiological for the 8.5 mm/s condition.

The results showed that the 0.05 Hz frequency caused a maximal increase in entrainment, compared to the frequencies of 0.1 Hz and 0.2 Hz. It is important to note that the intrinsic contractile frequency of the collecting lymphatics in vivo ranged from about 0.02 Hz to 0.06 Hz (1.2-3.6 contractions per minute), which is close to the range that has been

reported in rat tail lymphatics before [80]. In chapter 1, it was shown that the maximal entrainment to an externally applied oscillatory shear stress occurs when the applied frequency is close to the intrinsic frequency of the vessels [21]. Thus, the present work suggests that the maximal entrainment occurs at the frequency that is closest to the in vivo lymphatic contractile frequency, similar to what has been observed ex vivo (although it should be noted that in the in vivo condition, both the shear stress and transmural pressure in the lymphatics were oscillatory). While there is an optimal temporal frequency of modulation, no optimal OPW propagation speed was found that maximized entrainment. In the context of IPC, this means that the OPW propagation speed along the cuffs does not affect the entrainment of the collecting lymphatics, at least for the range of propagation speeds tested. The results thus show that slower temporal frequency of an IPC may optimally entrain the lymphatic contractions, but the OPW propagation speeds, tested within the range that many commercial IPC garments operate, will not significantly affect entrainment.

What does entrainment mean in terms of the actual lymphatic transport function? It was seen that the increase in entrainment was concurrent with an increase in the lymphatic transport function at the 0.05 Hz temporal frequency, while an optimum propagation speed of 2.55 mm/s was shown to enhance lymphatic transport function even without an accompanying increase in entrainment. These results show that while entrainment and lymphatic transport function may be related, the lymphatic transport function may be affected even without a corresponding increase in entrainment. Thus, improving the entrainment is a sufficient, but not necessary, condition for improving lymphatic transport function. Taking the results together, the OPW-induced increases in entrainment and function, dependent on the physiological lymphatic pumping conditions, show that a rational approach to physiotherapy and the design of IPC garments may be possible, by tailoring the contractile OPW to the pre-existing lymphatic transport parameters of the specific patients.

Exogenous nitric oxide is known to induce relaxation of the collecting lymphatic vessels. Application of a nitric oxide donor ointment (GTNO) has been previously shown to

slow the transit time of lymph [123] and significantly reduce lymphatic flow as well as lymphatic pumping pressure and also the frequency and velocity of the packets of NIR dye when observed in vivo [118, 80]. For the present study, a different nitric oxide donor cream in the form of a nitroglycerine ointment (Nitrobid®) was used to induce a similar reduction in collecting lymphatic function in vivo. Weiler et al. [80] showed that at steady state, there was moderate but significant reduction of packet frequency in the non-dominant collecting vessels, and a large reduction in the packet frequency for the non-dominant vessels. The dominant vessels exhibited no significant differences in frequency or velocity. In the present study, while a significant reduction in packet frequency was not observed, a significant reduction in packet velocity was seen. This is expected, given that the vessels imaged in the present study were a combination of dominant and non-dominant vessels. This was considered as evidence that the nitroglycerine ointment was causing the expected functional changes in the lymphatics. The nitroglycerine ointment did not, however, cause any significant changes in entrainment and average packet transport, which seems to suggest that NO is not involved in the OPW induced entrainment. While no analogous studies exist where exogenous NO was not found to affect lymphatic contractility, this result is supported by findings from ex vivo experiments where blocking the production of NO by inhibiting eNOS did not reduce the entrainment to oscillator shear stress [21]. Thus, NO is possibly not involved in the OPW induced entrainment of lymphatic vessels and other molecules need to be investigated for their role in this lymphatic response.

Is the entrainment to OPW caused by the active contractility of the lymphatics, or is it a passive response to the spatiotemporally varying OPW? It is important to understand that the OPW transmits a spatiotemporally varying oscillatory pressure in the rat tail tissue, whose amplitude is dependent on the amplitude of the OPW. It is also reasonable to assume that the OPW frequency is low enough that the amplitude of the transmitted oscillatory pressure does not depend on the frequency of the OPW. In the absence of any changes in the active contractility of the lymphatics by the OPW, the passive movement of lymph

due to the OPW should only depend on the changes in the tissue pressure affected by the amplitude of the OPW. To understand why this is the case, let us consider a mathematical simplification where there is a perfect entrainment of the lymphatic contractions with a sinusoidally varying OPW. Let the recorded fluorescence intensity be denoted as $I = I_{offset} + I_{amp}\sin(\omega t + \varphi)$, where I_{offset} is the DC offset in the signal, I_{amp} is the amplitude of the intensity signal, ω is the frequency, and φ is the phase of the wave. We know that the integral of $I_{amp}\sin(\omega t + \varphi)$, when integrated over a full time period, is 0. Hence the area under the curve of I is only dependent on I_{offset}, which in turn is only dictated by the amplitude of the wave. Since the amplitude of the OPW was maintained constant across all the temporal frequency and propagation speed conditions, the passive component should be equal across all the conditions. Hence, while there may be a passive component to the OPW-induced entrainment, the dependence of the entrainment and lymphatic transport function on the parameters of the applied OPW suggest a significant active component.

It should be noted that the usage of the term "entrainment" here is in a slightly different context from that described in chapter 2. While in the previous chapter the word entrainment was used to refer to a synchronization of the contractility of lymphangions to an externally applied oscillatory shear stress, here the intensity of the NIR dye synchronizes to the dynamic variations in both shear stress and transmural pressure due to the OPW. The word "entrainment" is used here as a general term that signifies the frequency matching and locking of a parameter signifying the lymphatic vessel diameter (actual diameter tracing or dye intensity) to an external modulatory signal (OWSS or OPW).

3.5 Interim Summary

This chapter showed that much like the ex vivo entrainment of lymphatic vessels to OWSS, the lymphatic contractions can be entrained in vivo as well using an externally applied OPW. The entrainment was significantly higher for the applied frequencies that were closer to "physiological" frequencies for the experimental conditions the rats were exposed to

(0.05 Hz in this particular case). The OPW propagation speed did not affect lymphatic entrainment. The lymphatic transport function (quantified by the average packet transport) was found to be significantly higher for 0.05 Hz temporal frequency and 2.55 mm/s propagation speed. Thus, lymphatic transport function may be improved by an OPW even in the absence of a similar increase in entrainment. The study shows that it might be possible to enhance lymphatic function through IPC by optimizing the frequency and wave propagation speed of the IPC garments. The molecular mechanisms behind this OPW-induced entrainment and enhancement of lymphatic function needs to be investigated further, since NO was not found to affect either entrainment or lymphatic transport function.

While the results point towards the potential optimization of IPC for enhancing lymphatic function, it should be noted that IPC is important only in the context of lymphatic dysfunction that is caused by lymphedema or other lymphatic pathologies. Although lymphedema is characterized by an aberrant microenvironment and dysfunctional lymphatic networks, little is known about how the mechanosensitivity of lymphatic vessels to OPW (such as those applied during MLD or IPC) may change due to lymphatic dysfunction. Hence in the next chapter we will be investigating the changes in the OPW-induced lymphatic entrainment and transport function in response to lymphatic injury.

CHAPTER 4

LYMPHATIC REMODELING IN RESPONSE TO INJURY

4.1 Background

In the last chapter, we saw that an externally applied OPW can entrain lymphatic contractions in vivo, and both the entrainment and lymphatic transport function depended heavily on the frequency and propagation speed of the applied OPW. The response of lymphatic contractility to an OPW, especially in the form of entrainment, can help us to quantify how the mechanosensitivity of the collecting lymphatics changes during lymphedema. Not only that, an investigation of the change in lymphatic mechanosensitivity by lymphatic injury is important since the mechanosensitivity of the lymphatics dictates to what extent the lymphatics can be modulated by an OPW akin to IPC. In the US, the most common cause of lymphedema is breast cancer related surgery, where some (or all) of the axillary lymph nodes are dissected. This injury to the lymphatics can possibly lead to a systemic failure of the lymphatic system in recirculating lymph, creating abnormal mechanical conditions within the intact lymphatic vasculature. This aberrant mechanical microenvironment associated with lymphedema can cause abnormal lymphatic formation, manifesting as both abnormal lymphangiogenesis and/or remodeled collecting vessels [65]. The short-term and long-term impact of aberrant mechanical loading on collecting lymphatic function have been investigated, and functional changes in the collecting lymphatics in response to a mechanical overload were observed [68, 70, 69, 67, 66, 60]. However, changes in the mechanosensitivity of the lymphatic vessels during lymphedema and, in turn, its impact on lymphatic transport function, are not well understood. Some studies have shown a reduction in lymphatic mechanosensitivity as a possible hallmark of lymphatic dysfunction due to ageing, obesity, and pathologies such as metabolic syndrome [124, 114, 101, 25], but

the same has not been investigated in the case of lymphedema. Hence, this chapter will look into how lymphatic injury can change the mechanosensitivity of the collecting lymphatics to OPW and what that means for lymphatic transport function. The entrainment of lymphatic contractions to OPW can be used as an important tool for studying the changes in the mechanosensitivity of lymphatics that may be caused by lymphatic injuries akin to lymphedema.

4.2   Methods

The experimental setup, protocols, data analysis and statistical analysis techniques that were used in these experiments are the same as those described in chapter 3.

4.2.1   Contralateral Lymphatic Ligation Surgery

To induce an aberrant microenvironment around the rat tail lymphatics, a unilateral tail ligation surgery was performed (schematic shown in Figure 4.1a). The surgery involved damaging the collecting lymphatic vessels on one side, while leaving the vessels on the other side intact. An incision was created around the circumference of the tail, about 2.5 cm from the base of the tail, leaving only some skin on top of the intact collecting vessels on the left side of the tail. Small sections of both collecting lymphatic vessels on the right side of the tail were then surgically excised from the animal. The incision was cauterized and an antiseptic ointment (New Skin® liquid bandage) was applied to the incision to prevent infection. The sham animals were prepared in a similar way to the ligation animals, but the collecting lymphatic vessels were left intact on both sides. After the ligation was completed, the tails were lightly massaged to make sure that there was no dye uptake past the site of incision (or conversely to ensure that there was dye uptake past the incision for the sham animals). The fluorescence in the tail past the incision site is shown for both the incised and intact side of the sham and ligation animals in Figure 4.1b. The ligated animals did not show any fluorescence past the incision site but fluorescence in collecting lymphat-
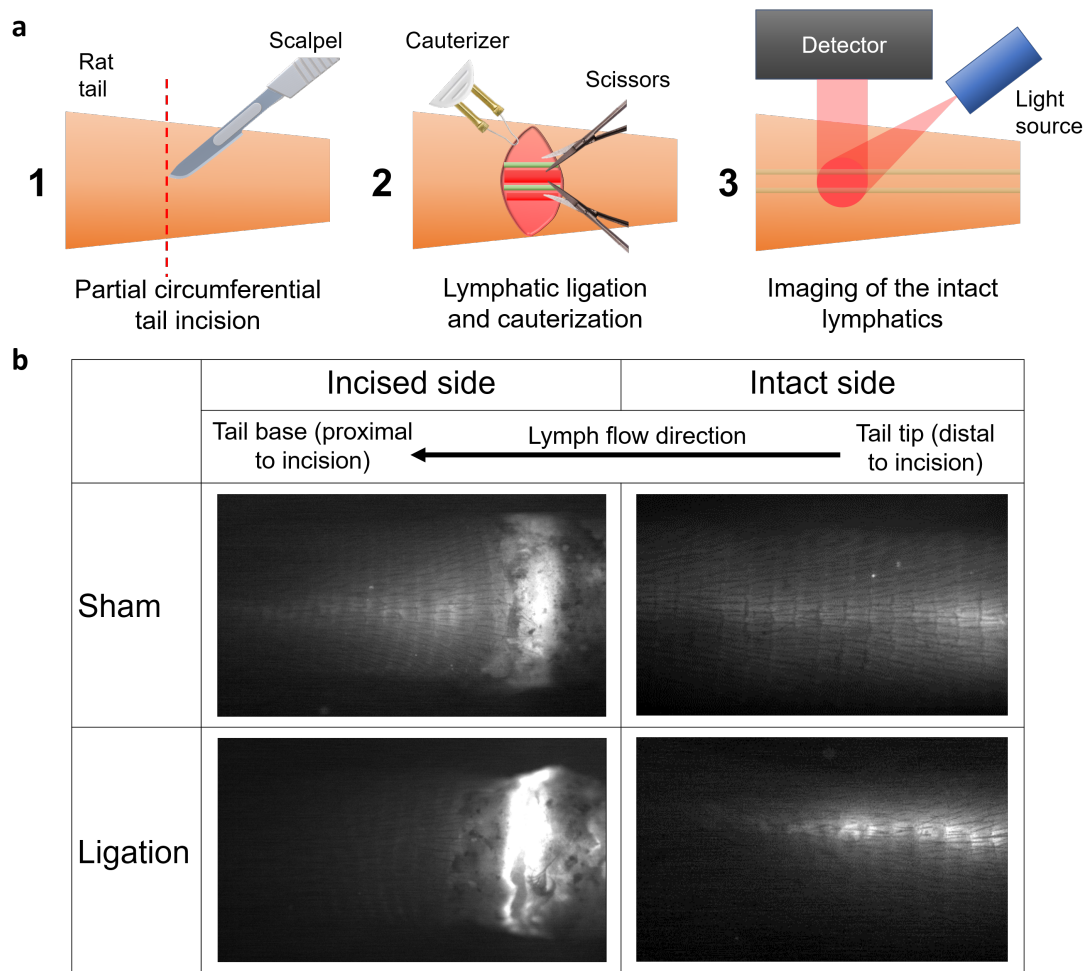
Figure 4.1: Procedure for performing the lymphatic ligation surgery on the rat tail. a) The schematic of the ligation procedure is shown. In step 1, the collecting lymphatic vessels on one side were first accessed through a skin incision. In step 2, the collecting lymphatics were then ligated and the skin was cauterized. In step 3, the intact lymphatics on the other side were subsequently imaged. The same procedure was followed for the sham animals, excluding the ligation of the collecting lymphatics. b) The collecting lymphatic vessels proximal to the incision site were visualized using NIR for the presence or absence of fluorescence. The lymph flow direction for the images shown was from the tail tip to the base of the tail as shown by the arrow, i.e. from the distal to the proximal side of the incision. The sham animals exhibited fluorescence in the collecting lymphatics past the incision site, while the ligation animals did not show any fluorescence past the incision, indicating that the collecting lymphatic vessels had been successfully ligated.

ics were clearly seen in the sham animals even past the incision, showing that the collecting lymphatics were intact in the sham animals after the skin incision.

All the animal procedures were performed in accordance with the guidelines specified by Georgia Tech's Institutional Animal and Care and Use Committee (IACUC). The protocol number for the project was A100299. The rats were anesthetized using a combination of Ketamine and Dexmedetomidine injections (40 mg/kg and 0.13 mg/kg respectively) and the anesthesia was reversed using Antisedan (1.3 mg/kg). The dosage for the injections were recommended by the institutional IACUC. All animals, post-surgery, were injected with Buprenorphine to alleviate pain. The animals were monitored for any signs of pain following the surgery, including weight loss, porphyrin around the eyes, abnormal posture (e.g. hunching) or aggressiveness. The animals were euthanized through CO2 induced asphyxiation following IACUC guidelines on reaching the end point of the study or if any of the above signs of pain were observed.

4.2.2   Histology

The morphology of the lymphatics in the sham and ligation animals was investigated using histology. An approximately 1-2 cm bundle of tissues including the vein, artery and lymphatics was isolated from the intact side of the animals, distal to the site of injury and near the ROI used for capturing the NIR images. The tissue was fixed in 4% paraformaldehyde (PFA) and frozen in optimal cutting temperature compound (OCT compound) at -80º C. The frozen tissue was subsequently cryosectioned and put on glass slides for staining and imaging. For immunohistochemistry (IHC), the frozen sections were thawed in PBS and permeabilized in a 0.3% Triton-X solution for 10 mins. Antigen retrieval was performed with 0.1% Trypsin for 5 mins at room temperature. A blocking solution consisting of 3% bovine serum albumin (BSA) and 5% goat serum was applied to the sections overnight at room temperature. The primary antibodies used for the IHC were anti-podoplanin (mouse anti-rat IgG1, Millipore, Cat# MABT850, RRID:AB_2877056

[125]) and anti-α-smooth muscle actin (αSMA) (mouse anti-rat IgG2a, Sigma-Aldrich Cat#
A2547, RRID:AB_476701 [126]). The primary antibodies were diluted in the blocking
solution (20 μg/ml for anti-podoplanin and 60 μg/ml for anti-αSMA) and applied to the
sections overnight at 4° C. Mouse IgG1 and IgG2a isotype control antibodies, diluted in
the blocking solution to 20 μg/ml and 60 μg/ml respectively, were used as negative con-
trols. The secondary antibodies that were used were goat anti-mouse IgG1 conjugated with
Alexa 633 and goat anti-mouse IgG2a conjugated with Alexa 594. Both the secondaries
were diluted to 10 μg/ml in PBS and applied to the sections for 1 hour at room temperature.
The sections were washed with PBS and sealed with Prolong gold antifade reagent with
DAPI. The stained sections were imaged at 20x magnification using a Zeiss 710 NLO laser
scanning confocal microscope with excitation wavelengths of 594 nm and 633 nm.

4.3 Results

4.3.1 Alterations in Lymphatic Entrainment and Transport Function after Lymphatic Ligation

The rat tail lymphatics are organized into two sets of two collecting vessels running along
each side of the tail. These rat tails were subjected to a unilateral lymphatic ligation surgery
(Figure 4.1a). Under this surgical model (referred to as the ligation model), the collecting
lymphatic vessels on one side of the tail were surgically ligated through an incision, and
the wound was cauterized. For a sham model, a similar incision and cauterization was per-
formed, but the collecting lymphatic vessels were left intact as confirmed by NIR imaging
(Figure 4.1b). The intact collecting vessels on the other side of the tail were imaged for
function at day 0, immediately before the ligation surgery, and at day 28 post-ligation, to
understand the long-term impact of the collecting lymphatic damage on the contralateral
intact lymphatics (quantification of the transient change in lymphatic function, if any, at day
3 was not possible due to leakage of the dye into the interstitium, which made it impossible
to differentiate the collecting lymphatics from the background (Figure D.1)). Specifically,
the modulation of lymphatic function by an applied OPW with an amplitude of 60 mmHg,

82
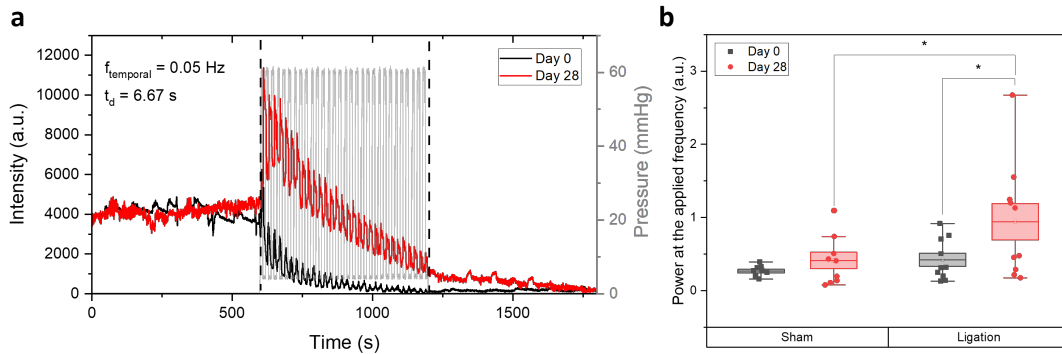
Figure 4.2: A contralateral lymphatic ligation (referred to, in short, as ligation) alters the OPW-induced entrainment of the intact lymphatics. a) A representative image of the effect of ligation is shown. The vertical dashed lines enclose the time window over which the OPW is applied. There is a clear increase in the amplitude of the entrained packets at Day 28, along with a corresponding increase in intensity. b) The entrainment data is summarized for both sham (n = 9) and ligation (n = 10) animals. The power at the applied frequency (entrainment) was significantly higher for the ligation animals at day 28 compared to day 0 ((p = 0.016). The entrainment was also significantly higher for the ligation animals compared to the sham animals at day 28 (p = 0.033). Mann-Whitney test was performed to compare the group means between the sham and ligation conditions (*p<0.05). Wilcoxon signed rank test was performed to compare the group means between day 0 and day 28 conditions (*p<0.05).

temporal frequency of 0.05 Hz and propagation speed of 2.55 mm/s was investigated (these were the optimal OPW conditions for lymphatic modulation, as shown previously).

Figure 4.2a shows a representative plot of the intensity profile at day 0 vs day 28 for a ligation animal. Some immediately noticeable differences between day 0 and day 28 include an increase in the amplitude of the packets, along with an increase in the maximum fluorescence intensity. When the entrainment data was summarized for both the sham and ligation animals, it was seen that the entrainment in the ligation animals was significantly increased at day 28 as compared to day 0 (p = 0.016), showing that the intact vessels were more sensitive to the applied OPW (Figure 4.2b). The entrainment at day 28 for the ligation animals was also increased significantly compared to the sham animals at day 28 (p = 0.033), suggesting that the change in sensitivity to OPW was due to a functional remodeling of the intact vessel in response to the ligation of the contralateral collecting lymphatics and

not merely a general response to the disruption of the superficial microcirculation, the skin barrier and cauterization.

The average packet transport was computed for the OPW and post-OPW conditions. The average packet transport was increased significantly for the ligation animals, but not the sham animals, at day 28 compared to day 0 (p = 0.0095), on the application of OPW (Figure 4.3a). This shows a higher lymphatic transport function of the intact vessels in response to an OPW at day 28 following the lymphatic ligation. Thus, the intact vessels, on average, reacted more favorably to OPW and increased their lymphatic transport at day 28 following the contralateral lymphatic ligation. In general, the vessels did not exhibit any pronounced contractility during the 10 mins after the OPW was removed (post-OPW). This decrease in contractility was not merely an artifact of the dye being diluted in the lymphatics, since contractions could be detected at even lower intensities than those typically seen during the post-OPW condition (Figure D.1). However, both the sham and ligation animals at day 28 did show an increase in contractility after the OPW was removed when compared to day 0 (p = 0.029 and p = 0.004 respectively) as can be seen from Figure 4.3b. However, the effect size of the ligation surgery between day 0 and day 28 was higher compared to the sham animals (Cohen's d of 1.56 and 0.88 respectively).

Changes were also observed in the average intensity dynamics of the lymphatics in the imaging ROI. As mentioned before, the average intensity dynamics, represented by the trend line, allowed for the calculation of a "peak time" as the time after the application of OPW when the intensity trendline reached its highest value, and a "decay time", which is the time at which the intensity trend fell to a point midway between the highest and lowest intensities. The peak time and decay time are determined by an interplay between the lymphangions at the ROI clearing the lymph and the lymphangions distal to the ROI pumping the lymph into the ROI. In a perfect equilibrium, the ROI intensity will be constant, but an overburdening of the lymphangions in the ROI by the applied OPW can cause a peak in intensity which gets cleared out over time. However, a more contractile distal lymphangion
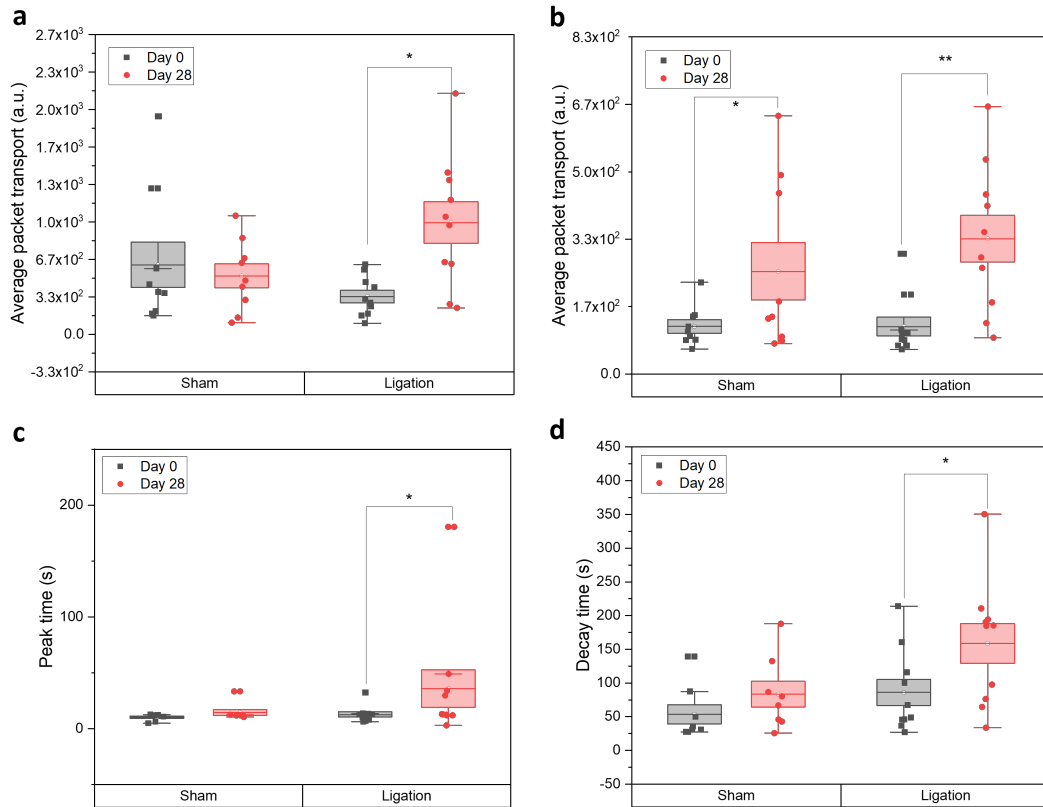
Figure 4.3: The OPW-induced change in lymphatic transport function is altered for the ligation animals at day 28 post surgery. a) The figure shows the average packet transport during the application of the OPW. The ligation animals (n = 10) showed significantly higher function at day 28 (p = 0.007). b) The figure shows the average packet transport after the OPW has been stopped (post-OPW). The ligation animals showed a significant change in function at day 28 (p = 0.0029). The sham animals (n = 9) also showed a significant change, but not as pronounced as the ligation animals (p = 0.029). c) The peak time was significantly higher for the ligation animals at day 28 (p = 0.042) unlike the sham group. d) The decay time was also significantly higher at day 28 for the ligation animals, but not the sham animals (p = 0.026). Mann-Whitney test was performed to compare the group means between the sham and ligation conditions (*p<0.05). Wilcoxon signed rank test was performed to compare the group means between day 0 and day 28 conditions (*p<0.05, **p<0.005).

chain will mean that the peak time and decay time will increase, since the lymph clearance from the ROI will be compensated by more lymph being pumped by the distal lymphangions. Thus, the peak and decay times indirectly indicate the transport function of the distal collecting lymphatics. When the data from the present study was summarized, the intact vessels in the ligation animals, but not in the sham animals, showed a significant increase in both the peak time (p = 0.042) and decay time (p = 0.026) at day 28 compared to day 0 (Figures 4.3c and 4.3d). This result is consistent with the distal lymphatic chain being remodeled to act as stronger pumps in the ligation animals.

The tail swelling in the sham and ligated animals was tracked at days 7, 14, 21, and 28 after the ligation. The percentage change in the circumference of the tail was used as a metric for swelling. The swelling typically reached a maximum at day 7, and gradually decreased till it resolved completely by day 28. The percentage change in the circumference of the tail at day 7 was used as a metric for swelling. The amount of swelling in the rats was not as pronounced as the swelling observed in mice with a contralateral lymphatic ligation [112], nor was there any significant difference in swelling (p = 0.18) between the sham and ligation animals (Figure 4.4a). Moreover, for both the sham and ligation animals, the percentage swelling at day 7 was not strongly (R-squared values of 0.0004 and 0.0257 respectively) or significantly (p = 0.96 and 0.66 respectively) correlated to the entrainment at day 28 (Figure 4.4b). Thus, the swelling of the tails was not a significant factor affecting the changes in lymphatic function in these experiments. These results demonstrate that functional changes in the collecting lymphatics could be brought on exclusively by collecting lymphatic vessel damage, even without significant swelling.

4.3.2   Histology

Immunohistochemistry (IHC) was used to quantify the changes in the morphology of the lymphatic vessels in response to the lymphatic ligation surgery. A bundle of tissues, including the vein, artery, and lymphatics, was isolated from the intact side of the rat tail
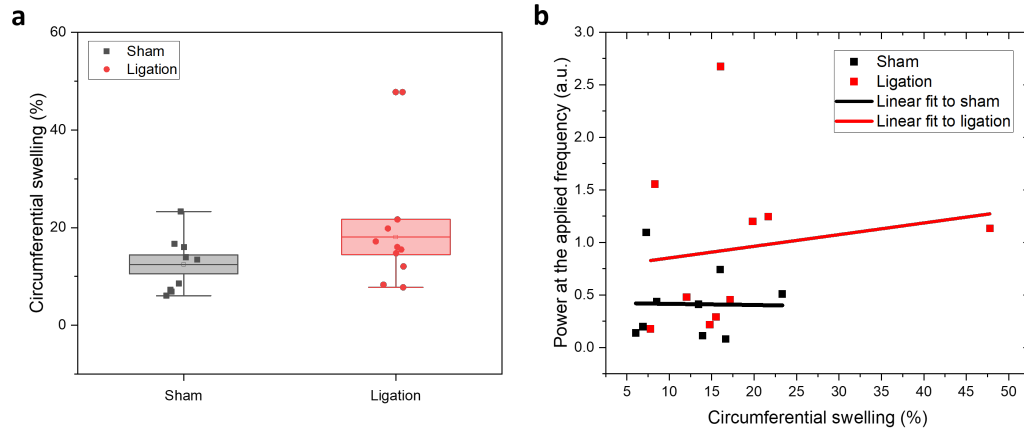
Figure 4.4: Circumferential tail swelling is not significantly different between the sham and ligation groups, and does not affect entrainment. a) The circumferential swelling of the sham (n = 9) and ligation (n = 10) animals at day 7, calculated as the percentage change in circumference at the incision site, is shown. There were no statistical differences between the two groups of animals (p = 0.18). Mann-Whitney test was performed to compare the group means between the sham and ligation conditions (*p<0.05). b) The correlation between the circumferential swelling and the entrainment at day 28, for both sham and ligation animals, is shown. For both the sham and ligation groups the R-squared value was low (0.0004 and 0.0257 respectively) and the coefficients were not significantly different from zero (p = 0.96 and 0.66 respectively). T-test for coefficients was used to conclude whether the coefficients of the regression were significantly different from zero.

posthumously on day 28 after the surgery, for both sham and ligation animals. The tissues were subsequently fixed and frozen in OCT, and sectioned for IHC. The lymphatic endothelial cells were stained for podoplanin and the lymphatic muscle cells were stained for α-smooth muscle actin (αSMA). DAPI was used to stain the nucleus. Each image thus has three distinct channels corresponding to the three stains – green for podoplanin, red for αSMA and blue for DAPI (Figure 4.5a). Negative controls were performed by i) exposing the sections to the primary, but no secondary, antibodies to determine autofluorescence at the settings used for imaging and ii) by using appropriate isotypes for the podoplanin and αSMA stains to determine any non-specific binding of the primary antibodies. Neither of the negative controls stained positive for podoplanin and αSMA, showing that the fluorescence being observed was due to specific staining for podoplanin and αSMA (Figure D.3). The collecting lymphatics were identified in the sections by looking for lumen-like struc-
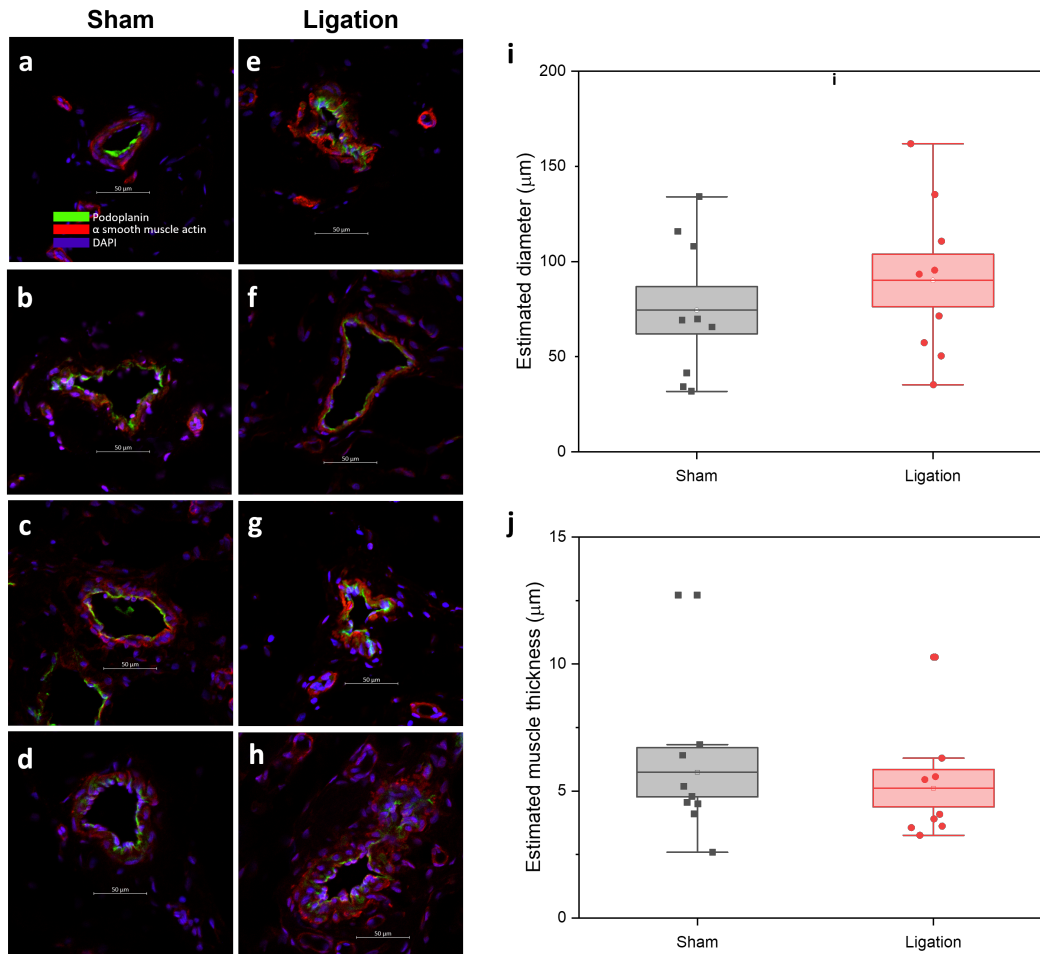
Figure 4.5: There are no significant changes in the morphology (estimated lumen diameter and estimated muscle thickness) of the lymphatic vessels between sham and ligation animals at day 28 post surgery. Representative lymphatic vessels from the tissue sections stained for podoplanin and α-smooth muscle actin (αSMA) are shown for the sham (a-d) and ligation (e-h) animals. The podoplanin stains are shown in green and are concentrated near the lumen. The SMA stain is shown in red and stain the lymphatic muscle cells surrounding the lumen. The DAPI is shown in blue and stains the nuclei. The morphology of the vessels was quantified by estimating the i) diameter and j) thickness of the lymphatic muscle cell layer and did not show any difference between the sham and ligation animals (n = 9 for both conditions). Mann-Whitney test was performed to compare the group means between the sham and ligation conditions (*p<0.05).

tures with strong podoplanin staining near the lumen, and a band of αSMA stained cells surrounding the podoplanin positive cells. Representative lymphatic vessels identified in this way are shown in Figure 4.5. Figures 4.5a-d show the lymphatic vessels in the sham animals, and Figures 4.5e-h show the lymphatic vessels in the ligation animals.

To quantify the morphology of the identified lymphatic vessels, two metrics were used: i) estimated diameter and ii) estimated muscle thickness. The lymphatic lumen in the tissues sections frequently deviated from their mechanically loaded circular geometry. Hence the circumference of the lumen (L) was first calculated by identifying the lumen from the podoplanin stain, and manually tracing the lumen in an open-source image processing software, ImageJ2 [127]. The diameter (D) was estimated from the circumference as $L/2\pi$. The cross-sectional area occupied by the lymphatic muscle cells (A) was calculated by thresholding and binarizing the channel with the αSMA stain. The muscle thickness (T) was estimated by assuming a circular vessel geometry using the following equation:

$$T = \sqrt{\frac{A + \pi D^2}{\pi} + D}$$

The estimated diameter and muscle thickness were compared between the sham and ligation groups (n = 9 for both groups, counting each vessel as a distinct data point) at day 28 and no significant differences were observed. Thus, the lymphatic ligation surgery does not cause any significant morphological remodeling of the intact collecting lymphatics compared to the sham surgery (Figure 4.5i-j).

4.4 Discussion

The alterations in lymphatic function that have been observed in the ligation animals suggest a more "pump-like" behavior of the intact collecting lymphatic vessels, 28 days after the ligation surgery. The idea of pump-conduit duality of the collecting lymphatic vessels had been previously described by Quick et al [46, 47]. Under this paradigm, the lymphatic

vessels can act as pumps (higher contractile function) or conduits (lower contractile function) depending on the mechanical microenvironment, specifically the existence of a pressure gradient that either favors or opposes lymph flow. A pump configuration is more suited for driving lymph flow against an adverse pressure gradient while a conduit configuration is more suited for a favorable pressure gradient. There were a few findings in this study which point to the reconfiguration of the collecting lymphatics to a pump configuration due to the collecting lymphatic ligation. Firstly, the animals undergoing collecting lymphatic vessel ligation exhibited an increase in the entrainment at day 28. Since the entrainment is a measure of the mechanosensitivity of the vessel to an OPW, the vessels can be considered to have increased sensitivity at day 28 following contralateral lymphatic ligation. At the same time, the lymphatic transport function of the vessels was increased both during the application of the OPW and after the application of the OPW. Further, the peak time and decay time of the intensity, which are representative of the transport function of the chain of collecting vessels distal to the ROI, was increased in the ligation animals, showing that the collecting lymphatic chain distal to the injury site was more contractile in the ligation animals. The combined increase in mechanosensitivity and transport function thus points to a remodeling of the intact collecting lymphatics into a pump-like configuration, going by the paradigm of pump-conduit duality.

What causes this reconfiguration of the lymphatics? The answer can possibly be found in an understanding of the mechanical microenvironment of the tails that have undergone collecting lymphatic ligation. The non-significant increase in tail swelling alludes to the fact that the interstitial fluid was being drained effectively by the intact collecting lymphatic network. Since there were fewer lymphatic vessels clearing the interstitial space, a normal lymph clearance means that the intact collecting vessels were exposed to a higher pressure and shear environment. It was known as early as 1976 that an elevated transmural pressure on isolated lymphatic vessels can increase their contractility [28]. Later work by Davis et al. has shown that an increase in lymphatic afterload increases the muscle contractility

[54]. A novel partial bovine lymphatic constriction model also showed that increasing the transmural pressure on the lymphatics by partially occluding the lymph flow could make the upstream lymphangions more contractile [60]. More recently, a study of lymphatic injury in the hind-limb of sheep showed that the contralateral intact collecting lymphatic vessels showed higher contractility ex vivo than lymphatics that were isolated from naive animals [66]. The present work can be interpreted in the context of these functional changes in lymphatics in response to an elevated pressure and flow environment. The intact collecting lymphatic vessels were possibly subjected to an elevated pressure and flow environment, which remodeled their response to behave more as pumps than conduits, characterized by increased mechanosensitivity and contractility. This can be a possible adaptation of the intact collecting lymphatics to their microenvironment to effectively clear the same amount of interstitial fluid with a lower number of functional collecting lymphatics.

It is interesting to note that the results from histology indicate that the collecting lymphatics did not undergo significant morphological remodeling as a consequence of the lymphatic ligation, even though there were significant changes in lymphatic mechanosensitivity and transport function. While lymphatics do undergo morphological changes during the course of human lymphedema [65], there is evidence from the literature that functional remodeling of collecting lymphatics is possible without morphological changes. Specifically, it has been shown in a model of mesenteric venous hypertension that the mesenteric lymphatics became weaker pumps, even though there were no changes in vessel morphology or collagen area [128]. What causes the functional changes in the intact collecting lymphatics possibly needs to be investigated by studying the molecular changes in the remodeled vessels. A recent study has shown that the collecting lymphatics in a contralateral lymphatic injury model in the hindlimb of sheep express markers of oxidative stress [66], which makes reactive oxygen species (ROS) promising candidates in investigating the ligation induced remodeling of the collecting lymphatics. Since the remodeling happens in the context of OPW induced entrainment, ROS should also be investigated as molecular

regulators of entrainment in vivo. Further, specific changes in the frequency and amplitude of the contractions of the lymphatic vessels may point to different molecular mechanisms of the functional remodeling, e.g. changes in the density and function of ion channels such as Ca^{2+} channels and changes in contractile proteins.

In animal models of secondary lymphedema, it can be difficult to decouple the effects of inflammation and mechanical forces in the alteration of lymphatic function, since an inflammatory environment can affect lymphatic contractility [129, 130, 131]. However, in the present animal model, minimal tail swelling of the ligated or sham animals was observed at day 7 post-ligation, and the swelling was also not significantly different between the sham and ligation animals. This is in contrast to the significantly increased swelling that is observed at day 7 for unilateral ligation surgeries in mice [112]. A recent study on a secondary lymphedema model in mice has shown that progressive edema after surgery is accompanied by an increased fibrosis and infiltration of CD4+ T cells [132]. Considering the minimal edema in the rat tail model compared to the mouse lymphedema models, it is reasonable to assume that the local inflammation and the milieu of immune responses accompanying it were also minimal. This leads us to reasonably conclude that the changes that are seen in lymphatic mechanosensitivity and function (due to a contralateral lymphatic ligation surgery) are a result of the surgery-induced altered lymphatic microenvironment and not because of local inflammation.

There are several questions arising from our study that are worth addressing in the future. Our work demonstrated that the modulation of collecting lymphatics by OPW in vivo is sensitive to the frequency of the stimulation. This sensitivity of the lymphatics to OPW is enhanced by an aberrant mechanical microenvironment induced by collecting lymphatic ligation. How does this adaptation facilitate the clearance of tissue fluid in the context of physiotherapy for the treatment of secondary lymphedema? Physiotherapy usually involves multiple sessions with a clinician to keep the arm volume in check, in conjunction with long-term CB and/or IPC by the patients themselves. Is it possible to optimize the

application of physiotherapy, especially at the early stages of lymphedema, to maximize lymphatic transport function and reduce swelling? More importantly, what are the long-term effects of this therapy on the intact collecting lymphatics network? Further studies involving the application of IPC with different OPW parameters to reduce the limb swelling during lymphedema, as well as deciphering the molecular puzzles surrounding OPW induced lymphatic modulation, can help answer these questions.

4.5   Summary

It was shown in this chapter that the collecting lymphatic vessels can remodel in response to a contralateral lymphatic injury. The remodeling is, possibly, primarily due to a change in the mechanical microenvironment brought about by the collecting lymphatic vessel ligation, and not due to a local inflammation induced by the surgery. The remodeled lymphatic vessels achieve a "pump-like" configuration characterized by increased mechanosensitivity, lymphatic transport function, and a more contractile lymphangion chain distal to the injury site. No morphological changes were observed in the intact collecting lymphatics in response to the contralateral collecting lymphatic ligation. Thus the remodeling of lymphatic function in response to lymphatic ligation is possibly a physiological and not a morphological adaptation to an aberrant mechanical microenvironment. Thus, within the 28 day window that was used for observing the changes in lymphatic function, the intact collecting lymphatics were better at responding to the applied OPW, which implies they can be more effectively modulated by MLD or IPC.

CHAPTER 5

CONCLUSIONS

This work attempts to draw a comprehensive picture of the modulation of lymphatic contractility by oscillatory forces akin to those that exist in the collecting lymphatic microenvironment or those applied during physiotherapy for lymphedema. Through a combination of ex vivo and in vivo studies, we showed that the lymphatics can sense and respond to their oscillatory microenvironment by entraining to them and this entrainment has a bearing on the lymphatic transport function as well. The entrainment, thus, is a valuable metric for quantifying the mechanosensitivity of lymphatic vessels to oscillatory forces. Ex vivo studies with isolated collecting lymphatic vessels showed that the entrainment and ejection fraction of lymphatics were maximized at optimal OWSS parameters. The optimal parameters were also found to be dependent on the intrinsic contraction frequency and mechanosensitivity of the lymphatics, thus showing that the specific lymphatic contractility of patients possibly need to be taken into account for optimally stimulating their lymphatics. These findings have been expanded upon in vivo, with sub-optimal OPW stimulation parameters having been identified which did not enhance the entrainment and/or lymphatic transport function. The relationship between lymphatic entrainment and lymphatic transport function was a little more tenuous in vivo, where an increase in entrainment was seen to be coincident with an increase in transport function, but the transport function could increase without a corresponding increase in entrainment. Lymphatic injury was found to affect the mechanosensitivity of lymphatics to OPW. Both OPW-induced lymphatic entrainment and transport function were seen to increase in the intact collecting lymphatics in response to a ligation of the contralateral collecting lymphatic vessels in a rat tail. Thus, within the time window of observation (28 days), the lymphatic function was altered to have increased mechanosensitivity and transport in response to an OPW.

94

5.1 Major Findings/Contributions

The major findings and contributions from this work are summarized below:

- Developed a novel data analysis framework using CWT to quantify the entrainment of lymphatic contractions to OWSS and OPW. The metric of entrainment was introduced, for the first time, to signify the mechanosensitivity of lymphatic contractions to external oscillatory forces.

- Quantified the mechanosensitivity of lymphatic vessels to ramped shear stress as the "critical shear stress", which serves as a metric of the intrinsic mechanosensitivity of lymphatic vessels to shear stress. The critical shear stress acts as a threshold for the entrainment of lymphatic contractility to OWSS.

- Showed that lymphatic entrainment and function is optimal for OWSS frequencies and amplitudes that are close to the physiological contraction frequency and mechano sensitivity of the lymphatic vessels. Thus the lymphatic mechanical microenvironment has a strong influence on optimal lymphatic function.

- Designed a pressure-cuff system that allows for the application of an external OPW to a rodent tail with varying frequencies and wave propagation speeds, mimicking the pressure waveforms that are applied during MLD or IPC. This system, in conjunction with an NIR imaging system, allowed for the characterization of the mechanosensitvity and function of lymphatic vessels in response to an OPW, allowing the user to determine lymphatic function in response to "massage-like" pressure waveforms.

- Showed that an externally applied OPW can optimally modulate lymphatic function depending on the parameters of the OPW (frequency and propagation speed). The optimum OPW parameters were found to be close to the "physiological" contractile parameters of the lymphatics, similar to what has been observed ex vivo. Thus,

externally applied OPWs, such as those applied during IPC, can be optimized in a patient-specific manner to enhance lymphatic function.

- Developed a contralateral lymphatic ligation surgery model in the rat tail. The ligation model allows for the investigation of the effect of a prolonged change in the lymphatic microenvironment, following lymphatic injury, on the intact collecting lymphatic network.

- Showed that the lymphatic entrainment and function, induced by OPW, in the intact collecting lymphatic vessels is enhanced during a 28 day period following lymphatic ligation surgery. Thus, the intact collecting lymphatics are more sensitive to the applied OPW and show a higher increase in transport function in response to an OPW. This implies that MLD or IPC can be effectively applied, even after the injury-induced remodeling of the intact collecting lymphatic network, to enhance lymphatic transport function. This increased collecting lymphatic function can possibly act to enhance the drainage of fluid from the affected limbs.

5.2 Future Directions

It was shown in chapter 2 that the lymphatic vessels respond to their oscillatory microenvironment by entraining to the luminal OWSS and this entrainment influences the transport function of the vessels as well. One should realize that this is an idealized scenario where the transmural pressure was held constant while the shear stress was varied, a scenario which never occurs in a lymphatic vessel under physiological conditions. Usually, the microenvironment of the lymphatic vessel is characterized by a combination of oscillatory transmural pressure, shear stress, and axial stretch. Thus the present work provides one piece of the puzzle on how lymphatics respond to these myriad of oscillatory mechanical clues. The previous knowledge of lymphatic contractility has been gradually incorporated into computational models of lymphatic contractility that help us better understand and ex-

plain the response of lymphatics to various mechanical forces. However, the entrainment of lymphatics to oscillatory shear stresses has not been translated into these computational models, despite being important in describing the dynamic contractile behavior of the lymphatics. Thus, the present work can be incorporated into existing computational models of lymphatic contractility, further refining our understanding of lymphatic vessel contractility and mechanosensitivity.

Several mathematical models have attempted to simulate the dynamics between the smooth muscle cells and endothelial cells that lead to the spontaneous contractions of lymphatic vessels. Lumped parameter models have attempted to capture the synchronized contraction of multiple lymphangions in series, and their valve dynamics, by incorporating the interdependence between lymphatic pumping and the transmural pressures that the lymphangions are exposed to [133, 134, 135, 136]. It has been shown through mathematical modeling that stretch-induced Ca^{2+} and shear-induced NO release can act as a biological oscillator, explaining the spontaneous contractility and mechanosensitivity of collecting lymphatics [90, 91]. These models have been successful at simulating the behavior of lymphatic vessels in response to a large number of pressure and shear conditions. The data from the ex vivo experiments in the present study may be incorporated into these computational models of the lymphatics to further understand how OWSS controls lymphatic contractility. These updated models can help us answer some unanswered questions such as i) how do lymphangions coordinate their contraction across the length of a chain of lymphangions while ensuring optimal flow and ii) how do dysfunctions in one or more lymphangions affect the contractility of the lymphangion chain? Thus questions pertaining to the coordination, robustness, and redundancy of the lymphatic network may be better answered through the incorporation of the present ex vivo data into computational models of the lymphatics.

While the present work has shed light on the modulation of lymphatic vessels by oscillatory pressures and has shown that lymphatic dysfunction can influence the said mod-

ulation, there are still many more questions that are left to be answered. These questions can be broadly categorized around two major themes: i) the impact of lymphatic function modulation by OPW on the clearance of interstitial fluid, and the subsequent limb volume reduction in lymphedema patients, and ii) the molecular mechanisms that dictate the mechanosensitivity of the lymphatic vessels to OWSS and OPW and the subsequent remodeling of the mechanosensitivity by lymphatic injury. These two questions are explored in the next few paragraphs in order to understand where the results from the present study can take us.

While the results in chapter 3 showed that an externally applied OPW can enhance lymphatic function, studies need to be done in the context of lymphedema physiotherapy (specifically MLD and IPC) to judge the clinical relevance of the results. We have shown that the intact collecting lymphatic vessels in the affected region of an animal may be stimulated effectively by an applied OPW. Since MLD and IPC work by applying an OPW to the affected limb of the lymphedema patient, it will be interesting to see if these techniques can be optimized based on the intrinsic contractile function of the patients' lymphatics (obtained by NIR imaging). It also needs to be seen whether an increase in the collecting lymphatic function actually translates to a significantly increased reduction in the limb volume of the patients. This can be studied by using commercially available IPC garments on lymphedema patients, where the parameters of the IPC stimulation (frequency and propagation speed) are varied to find optimal conditions that maximize the limb volume reduction.

Although the response of lymphatics to an OPW in the rat tail was altered due to a contralateral collecting lymphatic ligation, it is not known whether these changes in lymphatic mechanosensitivity are beneficial or detrimental to the long-term function of the lymphatic network. A short term increase in lymphatic function can lead to long-term maladaptive remodeling of the collecting lymphatics. This conjecture arises from studies that have shown that patients with higher rates of lymph formation, flow, and pressure are at an increased risk for getting lymphedema following lymphadenectomy [137, 138, 139, 140]. Hence, an

overworked lymphatic network may put the patient at an additional risk of eventual lymphatic failure and lymphedema. Thus, it is worth studying whether periodic stimulation of the injured tail with an OPW (similar to physiotherapy) can lead to a reversal of this functional remodeling of the lymphatics and restore the normal (or rather, pre-surgery) function of the lymphatic network. Studies can be performed using the rat tail contralateral lymphatic ligation model introduced in this work, where the injured animals can be subjected to continuous (or intermittent) OPW over the period of 28 days post-surgery (similar to the physiotherapy provided to lymphedema patients) and the changes in lymphatic function (or lack thereof) can be tracked.

Despite the extensive literature on the molecules that regulate lymphatic mechanosensitivity to shear stresses, the molecular regulators of lymphatic mechanosensitivity to OWSS or OPW have not been identified. Although NO is an important player in shear-induced inhibition of collecting lymphatics, neither blocking NO production (in the ex vivo isolated lymphatic vessels), nor the application of exogenous NO (in the in vivo studies) had any effect on the entrainment and transport function of lymphatic vessels to OWSS or OPW. Hence, further investigation is needed to delineate the molecular mechanisms of the entrainment of lymphatics to oscillatory forces. ROS are potential candidates for future studies, since they they are known to be upregulated by oscillatory flow in the blood vasculature [96] and have been shown to inhibit lymphatic contractions [43]. Hence ROS need to be investigated as regulators of OWSS and OPW induced entrainment of lymphatics.

ROS have also been shown to be involved in the collecting lymphatic remodeling in a contralateral lymphatic ligation model in sheep [66], thus implicating them in the remodeling of collecting lymphatics induced by lymphatic injury. Thus, lymphatic tissue from the animals subjected to the contralateral lymphatic ligation surgery can be obtained and the oxidative stress on these lymphatics can be quantified through polymerase chain reaction or western blot. Depending on whether the remodeling of the collecting lymphatics to a lymphatic injury is beneficial or maladaptive, future studies can investigate whether

therapeutic approaches may be designed to reduce the oxidative stress in the lymphatics to prevent their functional remodeling. Hence, an understanding of the molecular mechanisms of entrainment and adaptations of collecting lymphatic function to lymphatic injury can help us develop pharmacological approaches for treating potential lymphatic maladaptation.

Appendices

APPENDIX A

MATLAB CODES FOR IMAGE PROCESSING AND ANALYSIS OF EX VIVO

DATA

1) Image Processing and Diameter Calculation

```matlab
1  % Read the video file
2  vid_name = uigetfile();
3  % Create a videoreader object
4  cont_vid = VideoReader(vid_name);
5
6  % Read and display the first frame
7  I_init = readFrame(cont_vid);
8  I_init = rgb2gray(I_init);
9  figure
10 imshow(I_init);
11 % Select the vessel from the first frame
12 init_rect = getrect;
13 close
14
15 [¬, col] = size(I_init);
16 box_width = 10;   % Width of the window for binarizing the frame
17 n_pts = floor(col/box_width);   % Total number of binarizing windows
18 % Initialize the variables for calculating and storing the ...
       diameter data
19 dia_up_mat = [];
20 dia_down_mat = [];
21 dia_mat = [];
22
23 % Binarize and calculate the diameter for each frame
```

```matlab
24  while hasFrame(cont_vid)
25
26      I = readFrame(cont_vid);
27      I = rgb2gray(I);    % Convert the frame to grayscale
28      windows = cell(1,n_pts);
29      bw_windows = cell(1,n_pts);
30      bw_img = [];
31      for i = 0:n_pts-1
32          wind_rect = ...
                [i*box_width+1,init_rect(2),box_width-1,init_rect(4)];
33          windows{1,i+1} = imcrop(I,wind_rect);   % Divide the ...
                frame into windows
34          thresh = graythresh(windows{1,i+1});    % Calculate the ...
                hreshold
35          bw_windows{1,i+1} = im2bw(windows{1,i+1},thresh);   % ...
                Binarize the frame
36          bw_img = [bw_img bw_windows{1,i+1}];    % Stich the ...
                binarized images together
37      end
38
39      [¬, s_col] = size(bw_img);
40      dia_up = zeros(1,s_col);
41      dia_down = zeros(1,s_col);
42
43      % Calculate the upper and lower wall of the binarized image
44      for line = 1:s_col
45          dia_up(1,line) = find(¬bw_img(:,line),1,'first');
46          dia_down(1,line) = find(¬bw_img(:,line),1,'last');
47      end
48
49      dia_up_mat = [dia_up_mat; dia_up];
50      dia_down_mat = [dia_down_mat; dia_down];
51
```

103

```matlab
52  end
53
54  % Calculate the diameter
55  dia_mat = dia_down_mat - dia_up_mat;
56
57  % Save the diameter file
58  save(strrep(vid_name,'.avi','_dia_mat'),...
59      'dia_up_mat','dia_down_mat','dia_mat','-v7.3')
```

2) Wavelet Transform

```matlab
1   % Read the saved diameter file
2   dia_name = uigetfile('*.mat');
3   load(dia_name);
4   [dia_row, dia_col] = size(dia_mat);
5
6   % Low pass filter the diameter data to reduce noise
7   window = 15;
8   b = (1/window)*ones(1,window);
9   a = 1;
10  dia_avg = zeros(dia_row,dia_col);
11  for i = 1:dia_row
12      dia_avg(i,:) = filtfilt(b,a,dia_mat(i,:));
13  end
14
15  % Initialize the parameters for the wavelet transform (CWT)
16  dt = 1/15;    % Sampling Frequency (FPS of the video)
17  dia_t = dt:dt:length(dia_avg)*dt;    % Sampling time points
18
19  NumVoices = 64;
20  a0 = 2^(1/NumVoices);
21  wavCenterFreq = 5/(2*pi);
```

```matlab
22   minfreq = 0.05;

23   maxfreq = 1;

24   minscale = wavCenterFreq/(maxfreq*dt);

25   maxscale = wavCenterFreq/(minfreq*dt);

26   minscale = floor(NumVoices*log2(minscale));

27   maxscale = ceil(NumVoices*log2(maxscale));

28   scales = a0.^(minscale:maxscale).*dt;

29

30   gap = 10;    % Intervals for calculating the

31

32   % Initialize the variables for storing the CWT data

33   cwt_dia = cell(floor(dia_col/gap),1);

34   dia_spec = cell(floor(dia_col/gap),1);

35   abs_dia_spec = cell(floor(dia_col/gap),1);

36

37   % Calculate the CWT for the analysis windows

38   for p = 1:gap:floor(dia_col/gap)*gap

39       a = (p-1)/gap+1;

40       cwt_dia{a,1} = cwtft({dia_avg(:,p),dt},...

41           'wavelet','bump','scales',scales,'padmode','symw');

42       dia_spec{a,1} = cwt_dia{a,1}.cfs;    % Calculated Spectrogram

43       dia_freq = cwt_dia{a,1}.frequencies;   % Corresponding ...
             frequency array

44       % Calculate the magnitude of the CWT coefficients

45       abs_dia_spec{a,1} = abs(dia_spec{a,1});

46   end

47

48   % Calculate the frequency and phase information from the spectrogram

49   [row, col] = size(dia_spec{1,1});

50   freq_max = zeros(col,floor(dia_col/gap));

51   phase_max = zeros(col,floor(dia_col/gap));

52   for p = 1:gap:floor(dia_col/gap)*gap

53       a = (p-1)/gap+1;
```

```matlab
54      for i = 1:col
55          [dia_freq_peaks, freq] = ...
                findpeaks(abs_dia_spec{a,1}(:,i));   % Find the ...
                frequencies at which the coefficients are maximum
56          [¬, freq_loc_max] = max(dia_freq_peaks);
57          freq_max(i,a) = dia_freq(freq(freq_loc_max));   % ...
                calculate the maximum frequency
58          phase_max(i,a) = ...
                angle(dia_spec{a,1}(freq(freq_loc_max),i));   % ...
                Calculate the phase at the maximum frequency
59      end
60  end
61
62  % Save the CWT data
63  save(strrep(dia_name,'_mat','_avg_cwt'),'dia_avg','dia_spec',...
64      'abs_dia_spec','dia_freq','dia_t','freq_max','phase_max','-v7.3')
```

3) Calculation of the Wall Shear Stress

```matlab
1  % Read the saved diameter file
2  dia_name = uigetfile('*.mat');
3  load(dia_name);
4  [dia_row, dia_col] = size(dia_mat);
5
6  % Low pass filter the diameter data to reduce noise
7  window = 20;
8  b = (1/window)*ones(1,window);
9  a = 1;
10 dia_avg = zeros(dia_row,dia_col);
11 for i = 1:dia_row
12     dia_avg(i,:) = filtfilt(b,a,dia_mat(i,:));
13 end
```

```matlab
14
15  dt = 1/15;    % Sampling Frequency (FPS of the video)
16  dia_t = dt:dt:length(dia_avg)*dt;    % Sampling time points
17  dia_t = dia_t';
18
19  %% Calculation of the diastolic diameter
20
21  [dia_poly, dia_peak] = dia_envelope(dia_t, dia_avg);    % Peak ...
        diameter in pixels detected by polynomial fitting
22  dpeak = dia_poly*3.4*10^-4;    % Peak diamater in cm
23  mu = 6.78e-3; % water viscosity @ 38C, dynes-s/cm^2
24
25  %% Read the pressure and syringe position data
26  pressure_file=uigetfile('*.txt');
27  pressure_fileID = fopen(pressure_file);
28  P = textscan(pressure_fileID,'%f %f %f %f %f %f %f %f %f %f %f ...
        %f','EndOfLine','\r\n');
29  P = cell2mat(P);
30
31  % Adjust the pressure data array to the same size as the diameter ...
        array
32  td=0:1/15:(length(dia_mat)-1)/15;
33  td = td';
34  tp=P(:,1)-P(1,1);
35  actP=zeros(length(td),12);
36  actP(1,:)=P(1,:);
37  for i=2:length(td)
38      [¬, ind]=min(abs(tp-td(i,1)));
39      actP(i,:)=P(ind,:);
40  end
41
42  t = actP(:,1);    % Time array
43  x1 = actP(:,8);    % Position data for syringe 1
```

```matlab
44  x2 = actP(:,9);     % Position data for syringe 2

45  switched = actP(:,12);    % Position of the solenoid valve

46

47  %% Calculation of the wall shear stress

48

49  fps = 15;    % FPS of the video

50  wind_len = 1;    % Length of the calculation window (in sec)

51  v = ones(length(dia_t)-wind_len*fps,1);    % Initialize the ...
        velocity array

52  Q = ones(length(dia_t)-wind_len*fps,1);    % Initialize the flow ...
        rate array

53  t_diff = ones(length(dia_t)-wind_len*fps,1);    % Initialize the ...
        time array

54  tau = ones(length(dia_t)-wind_len*fps,1);    % Initialize the wall ...
        shear stress array

55  for i = 1:length(dia_t)-wind_len*fps

56      x1diff = 0;

57      x2diff = 0;

58      for j = 1:wind_len*fps

59      % Sum up the syringe positions based on the state of the ...
            solenoid valve

60          if switched(j+i,1) == 0

61              x1diff = x1diff + (x1(j+i,1) - x1(j+i-1,1));

62              x2diff = x2diff + (x2(j+i-1,1) - x2(j+i,1));

63          else

64              x1diff = x1diff + (x1(j+i-1,1) - x1(j+i,1));

65              x2diff = x2diff + (x2(j+i,1) - x2(j+i-1,1));

66          end

67      end

68      % Average velocity over the specified time window (cm/s)

69      v(i,1) = 0.5*(x1diff+x2diff)*10^-1./wind_len;

70      % Convert velocity to flow (mL/sec)

71      Q(i,1) = 0.25*pi*.146^2*v(i,1);    % inner diameter of ...
```

108

```matlab
            tubing is 1.46 mm
72      % Place time points in the middle of the calculation windows
73      t_diff(i,1) = dia_t((i-1)+floor(wind_len*fps/2),1);
74      % Average shear stress over the time window
75      tau(i,1) = 4*mu*Q(i,1)./(pi*(dpeak/2).^3);   % Convert mu to ...
            dyne-s/cm2
76  end
```

```matlab
1  clear
2  clc
3
4  % Initialize the NIDAQ for data acquisition
5  ni_daq = daq.getDevices;
6  dev_ID = ni_daq.ID;
7
8  % Define the input channel for cuff 1
9  pr_sensor_1 = daq.createSession('ni');
10 addAnalogInputChannel(pr_sensor_1, dev_ID, 4, 'Voltage');
11 % Define the output channel for switching solenoid connected to ...
       cuff 1
12 valve_switch_1 = daq.createSession('ni');
13 addDigitalChannel(valve_switch_1, dev_ID, ...
       'Port0/Line1','OutputOnly');
14
15 % Define the input channel for cuff 2
16 pr_sensor_2 = daq.createSession('ni');
17 addAnalogInputChannel(pr_sensor_2, dev_ID, 5, 'Voltage');
18 % Define the output channel for switching solenoid connected to ...
       cuff 2
19 valve_switch_2 = daq.createSession('ni');
20 addDigitalChannel(valve_switch_2, dev_ID, ...
       'Port0/Line2','OutputOnly');
21
22 % Define the input channel for cuff 3
```

110

```matlab
23  pr_sensor_3 = daq.createSession('ni');
24  addAnalogInputChannel(pr_sensor_3, dev_ID, 6, 'Voltage');
25  % Define the output channel for switching solenoid connected to ...
        cuff 3
26  valve_switch_3 = daq.createSession('ni');
27  addDigitalChannel(valve_switch_3, dev_ID, ...
        'Port0/Line3','OutputOnly');
28
29  % Define the output channels for switching the solenoids
30  % connected to the syringe pumps
31  % For pump 1
32  valve_switch_4 = daq.createSession('ni');
33  addDigitalChannel(valve_switch_4, dev_ID, ...
        'Port0/Line6','OutputOnly');
34  % For pump 2
35  valve_switch_5 = daq.createSession('ni');
36  addDigitalChannel(valve_switch_5, dev_ID, ...
        'Port0/Line7','OutputOnly');
37
38  % Initialize syringe pump 1
39  s_1 = serial('COM5');
40  set(s_1,'BaudRate',115200);
41  fopen(s_1);
42  % Initialize syringe pump 2
43  s_2 = serial('COM6');
44  set(s_2,'BaudRate',115200);
45  fopen(s_2);
46
47  %% Move syringe to the starting position
48  start_pos = 11;   % Starting position, calculated in cm from the ...
        zero position
49  start_com = ['mov abs ' num2str(start_pos) ' cm 100%'];   % ...
        Command to move the pump to the starting position
```

```matlab
50  fprintf(s_1,'?rep pos');    % Check the current position of pump 1
51  act_pos_1 = fscanf(s_1);
52  fprintf(s_2,'?rep pos');    % Check the current position of pump 2
53  act_pos_2 = fscanf(s_2);
54
55  % Get the current position of pump 1 in mm
56  act_pos_1(1:3) = [];
57  act_del_1 = findstr(act_pos_1,' mm');
58  act_pos_1(act_del_1:length(act_pos_1)) = [];
59  act_start_pos_1 = str2double(act_pos_1);    % Current position of ...
        pump 1 in mm
60  % Get the starting position of pump 2 in mm
61  act_pos_2(1:3) = [];
62  act_del_2 = findstr(act_pos_2,' mm');
63  act_pos_2(act_del_2:length(act_pos_2)) = [];
64  act_start_pos_2 = str2double(act_pos_2);    % Current position of ...
        pump 1 in mm
65
66  % Set solenoids to open to air
67  off_state = 0;
68
69  outputSingleScan(valve_switch_1, off_state);
70  outputSingleScan(valve_switch_2, off_state);
71  outputSingleScan(valve_switch_3, off_state);
72
73  % Start moving the pumps to the desired starting position
74  start = tic;
75  while abs(act_start_pos_1/10 - start_pos) > 0.05 ||...
76          abs(act_start_pos_2/10 - start_pos) > 0.05   % Move the ...
                syringe if the desired starting position is 0.5 mm ...
                away from the actual position
77      % Move syringe pump 1
78      fprintf(s_1,start_com)
```

```matlab
79      pause(0.25)
80      fprintf(s_1,'?rep pos');
81      act_pos_1 = fscanf(s_1);
82      act_pos_1(1:3) = [];
83      act_del_1 = findstr(act_pos_1,' mm');
84      act_pos_1(act_del_1:length(act_pos_1)) = [];
85      act_start_pos_num = str2double(act_pos_1);
86      if isnan(act_start_pos_num) == 0
87          act_start_pos_1 = act_start_pos_num;   % Updated actual ...
                position for pump 1
88      end

90      % Move syringe pump 2
91      fprintf(s_2,start_com)
92      pause(0.25)
93      fprintf(s_2,'?rep pos');
94      act_pos_2 = fscanf(s_2);
95      act_pos_2(1:3) = [];
96      act_del_2 = findstr(act_pos_2,' mm');
97      act_pos_2(act_del_2:length(act_pos_2)) = [];
98      act_start_pos_num = str2double(act_pos_2);
99      if isnan(act_start_pos_num) == 0
100         act_start_pos_2 = act_start_pos_num;   % Updated actual ...
                position for pump 2
101     end

103     pause(0.5)

105     elapsed = toc(start);
106     % Stop the pumps after 25 s
107     if elapsed > 25
108         break
109     end
```

113

```matlab
110  end
111
112  fprintf(s_1,'stop')
113  fprintf(s_2,'stop')
114
115  %% Solenoid diagnostics - use this section to test the solenoids
116
117  on_state = 1;
118  off_state = 0;
119
120  outputSingleScan(valve_switch_1, on_state);
121  pause(1)
122  outputSingleScan(valve_switch_1, off_state);
123  pause(1)
124
125  outputSingleScan(valve_switch_2, on_state);
126  pause(1)
127  outputSingleScan(valve_switch_2, off_state);
128  pause(1)
129
130  outputSingleScan(valve_switch_3, on_state);
131  pause(1)
132  outputSingleScan(valve_switch_3, off_state);
133  pause(1)
134
135  outputSingleScan(valve_switch_4, on_state);
136  pause(1)
137  outputSingleScan(valve_switch_4, off_state);
138  pause(1)
139
140  outputSingleScan(valve_switch_5, on_state);
141  pause(1)
142  outputSingleScan(valve_switch_5, off_state);
```

```matlab
143
144 %% Send the pressure information
145
146 % Define the pressure waveforms
147 n_wave = 3;    % Number of cuffs
148 amp = 60;    % Amplitude in mmHg
149 freq = 0.05;    % Frquency of each cuff in Hz
150 runtime = 600;    % Total duration of the pressure wave in seconds
151 dt = 0.1;    % Time resolution of the pressure waveform
152 T_frac = 3;    % Fraction of time period (to set delay between the ...
        pressure cuffs)
153 td = round(1/(T_frac*freq),1);    % Time delay between the ...
        pressure cuffs
154 t = 0:dt:runtime-dt+td*(n_wave-1);    % Total time (s)
155 duty = 50;                        % Duty cycle of the waveform in %
156 % Initialize the waveforms
157 wave_1 = zeros(1,length(t));
158 wave_1(1,1:round(runtime/dt)) = ...
        amp/2*(1+square(2*pi*freq*t(1,1:runtime/dt),duty));
159 wave_2 = zeros(1,length(t));
160 wave_2(1,td/dt+1:round((runtime+td)/dt)) = ...
        amp/2*(1+square(2*pi*freq*t(1,1:runtime/dt),duty));
161 wave_3 = zeros(1,length(t));
162 wave_3(1,2*td/dt+1:round((runtime+2*td)/dt)) = ...
        amp/2*(1+square(2*pi*freq*t(1,1:runtime/dt),duty));
163
164 % Separate the signal into 1 minute windows for switching between the
165 % syringe pumps
166 run_min = runtime/60;    % Number of windows
167 wind = 60;    % Window duration in seconds
168 % Initialize the pressure data array
169 pr_data_1 = [];
170 pr_data_2 = [];
```

115

```matlab
171  pr_data_3 = [];
172
173  % Start controlling the pumps to achieve the desired pressure ...
         waveform
174  tot_start = tic;
175  for a = 1:run_min
176      % Select which syringe pump to run, while the other resets, ...
             by setting
177      % the valve states for the solenoids connected to the syringe ...
             pumps
178      if mod(a,2) == 1
179          s_pump = s_1;
180          s_prime = s_2;
181          outputSingleScan(valve_switch_4, on_state);
182          outputSingleScan(valve_switch_5, off_state);
183      elseif mod(a,2) == 0
184          s_pump = s_2;
185          s_prime = s_1;
186          outputSingleScan(valve_switch_4, off_state);
187          outputSingleScan(valve_switch_5, on_state);
188      end
189      start_pos = 11;
190      start_com = ['mov abs ' num2str(start_pos) ' cm 100%'];
191      fprintf(s_prime,start_com)
192
193      % Send the move signal to the syringe pump
194      Fs = 1;    % Sampling rate for the pressure sensor
195      % Select the bounds for the syringe movement
196      max_right = 1;
197      max_left = 11;
198
199      % Define the on and off states of the solenoids
200      on_state = 1;
```

```matlab
201        off_state = 0;
202        % Get the starting pressures (in Volts) in the three pressure ...
              sensors
203        pr_data_1 = [pr_data_1 inputSingleScan(pr_sensor_1)];
204        pr_data_2 = [pr_data_2 inputSingleScan(pr_sensor_2)];
205        pr_data_3 = [pr_data_3 inputSingleScan(pr_sensor_3)];
206        err_thresh = 1;    % in mmHg
207
208        % Calculate the pressure and move the syringe pump within the ...
              1 min
209        % time windows
210        for i = wind*(a-1)/dt+2:wind*a*Fs/dt
211            start = tic;
212
213            % Select the states of the solenoids connected to the ...
                  pressure cuffs
214            count_1 = 0;
215            count_2 = 0;
216            count_3 = 0;
217            if wave_1(1,floor(i/Fs)+1) == amp
218                outputSingleScan(valve_switch_1, on_state);
219                count_1 = count_1 + 1;
220            else
221                outputSingleScan(valve_switch_1, off_state);
222            end
223            if wave_2(1,floor(i/Fs)+1) == amp
224                outputSingleScan(valve_switch_2, on_state);
225                count_2 = count_2 + 1;
226            else
227                outputSingleScan(valve_switch_2, off_state);
228            end
229            if wave_3(1,floor(i/Fs)+1) == amp
230                outputSingleScan(valve_switch_3, on_state);
```

```matlab
231            count_3 = count_3 + 1;
232        else
233            outputSingleScan(valve_switch_3, off_state);
234        end
235
236        % Calculate the pressure in sensor 1 and also the error ...
                compared to
237        % the desired pressure
238        pr_data_1 = [pr_data_1 inputSingleScan(pr_sensor_1)];
239        pr_data_gauge_1 = 51.71484*(7.5*(pr_data_1-0.5)-15);   % ...
                Voltage converted to psi and then to mmHg
240        err_1 = pr_data_gauge_1(1,i) - wave_1(1,floor(i/Fs)+1);
241        err_abs_1 = abs(err_1);
242
243        % Calculate the pressure in sensor 2 and also the error ...
                compared to
244        % the desired pressure
245        pr_data_2 = [pr_data_2 inputSingleScan(pr_sensor_2)];
246        pr_data_gauge_2 = 51.71484*(7.5*(pr_data_2-0.5)-15);   % ...
                Voltage converted to psi and then to mmHg
247        err_2 = pr_data_gauge_2(1,i) - wave_2(1,floor(i/Fs)+1);
248        err_abs_2 = abs(err_2);
249
250        % Calculate the pressure in sensor 3 and also the error ...
                compared to
251        % the desired pressure
252        pr_data_3 = [pr_data_3 inputSingleScan(pr_sensor_3)];
253        pr_data_gauge_3 = 51.71484*(7.5*(pr_data_3-0.5)-15);   % ...
                Voltage converted to psi and then to mmHg
254        err_3 = pr_data_gauge_3(1,i) - wave_3(1,floor(i/Fs)+1);
255        err_abs_3 = abs(err_3);
256
```

```matlab
257         % Control the pressure cuffs by moving the syringe pump ...
                as a
258         % function of the error in the pressure
259         % Control pressure cuff 1
260         if count_1 == 1
261             if err_1 < -1*err_thresh
262                 com = ['mov abs ' num2str(max_right) ' cm 100%'];
263                 fprintf(s_pump,com)
264             elseif err_1 > err_thresh
265                 com = ['mov abs ' num2str(max_left) ' cm 100%'];
266                 fprintf(s_pump,com)
267             elseif err_1 > -1*err_thresh && err_1 < 0
268                 com = ['mov abs ' num2str(max_right) ' cm ' ...
                        num2str(floor(err_abs_1*100)) '%'];
269                 fprintf(s_pump,com)
270              elseif err_1 > 0 && err_1 < err_thresh
271                 com = ['mov abs ' num2str(max_left) ' cm ' ...
                        num2str(floor(err_abs_1*100)) '%'];
272                 fprintf(s_pump,com)
273             end
274         end
275
276         % Control pressure cuff 2
277         if count_2 == 1
278             if err_2 < -1*err_thresh
279                 com = ['mov abs ' num2str(max_right) ' cm 100%'];
280                 fprintf(s_pump,com)
281             elseif err_2 > err_thresh
282                 com = ['mov abs ' num2str(max_left) ' cm 100%'];
283                 fprintf(s_pump,com)
284             elseif err_2 > -1*err_thresh && err_2 < 0
285                 com = ['mov abs ' num2str(max_right) ' cm ' ...
                        num2str(floor(err_abs_2*100)) '%'];
```

119

```matlab
                fprintf(s_pump,com)
            elseif err_2 > 0 && err_2 < err_thresh
                com = ['mov abs ' num2str(max_left) ' cm ' ...
                    num2str(floor(err_abs_2*100)) '%'];
                fprintf(s_pump,com)
            end
        end

        % Control pressure cuff 3
        if count_3 == 1
            if err_3 < -1*err_thresh
                com = ['mov abs ' num2str(max_right) ' cm 100%'];
                fprintf(s_pump,com)
            elseif err_3 > err_thresh
                com = ['mov abs ' num2str(max_left) ' cm 100%'];
                fprintf(s_pump,com)
            elseif err_3 > -1*err_thresh && err_3 < 0
                com = ['mov abs ' num2str(max_right) ' cm ' ...
                    num2str(floor(err_abs_3*100)) '%'];
                fprintf(s_pump,com)
            elseif err_3 > 0 && err_3 < err_thresh
                com = ['mov abs ' num2str(max_left) ' cm ' ...
                    num2str(floor(err_abs_3*100)) '%'];
                fprintf(s_pump,com)
            end
        end
        elapsed = toc(start);
        pause(dt/Fs - elapsed)
    end
    fprintf(s_prime,'stop')
end
tot_elapsed = toc(tot_start);
serialbreak(s_pump)
```

```matlab
316  fprintf(s_pump,'stop')
317
318  outputSingleScan(valve_switch_1, off_state);
319  outputSingleScan(valve_switch_2, off_state);
320  outputSingleScan(valve_switch_3, off_state);
321  outputSingleScan(valve_switch_4, off_state);
322  outputSingleScan(valve_switch_5, off_state);
323
324  % Release the devices
325  fclose(s_1);
326  fclose(s_2);
327  fclose(s_pump);
328  fclose(s_prime);
329  release(pr_sensor_1)
330  release(pr_sensor_2)
331  release(pr_sensor_3)
332
333   %% Plot in the axis provided
334  fig_pathname = 'C:\Users\LLBB_NIR\Desktop\Anish\01.23.19\';
335  set(0,'defaultfigurecolor',[1 1 1]) % Set figure background to white
336  pr_time = linspace(0,tot_elapsed,length(pr_data_gauge_1));
337  plot(pr_time,pr_data_gauge_1,'k')
338  hold on
339  plot(t,wave_1,'r')
340  plot(pr_time,pr_data_gauge_2,'k--')
341  hold on
342  plot(t,wave_2,'r--')
343  plot(pr_time,pr_data_gauge_3,'k-.')
344  hold on
345  plot(t,wave_3,'r-.')
346  set(gca,'FontSize',12)
347  legend('Pr_{actual} Cuff 1','Pr_{desired} Cuff 1','Pr_{actual} ...
         Cuff 2',...
```

```matlab
348         'Pr_{desired} Cuff 2','Pr_{actual} Cuff 3','Pr_{desired} Cuff 3')
349  xlabel('Time (sec)','FontSize',18)
350  ylabel('Pressure (mmHg)','FontSize',18)
351  hold off
352  fig_filename = 'Rat_10ul_f02_1sec_40mmHg_Test_2.png';
353  fig_savename = [fig_pathname fig_filename];
354  % export_fig(fig_savename, '-m5')
```

APPENDIX C

SUPPLEMENTARY FIGURES FOR CHAPTER 2
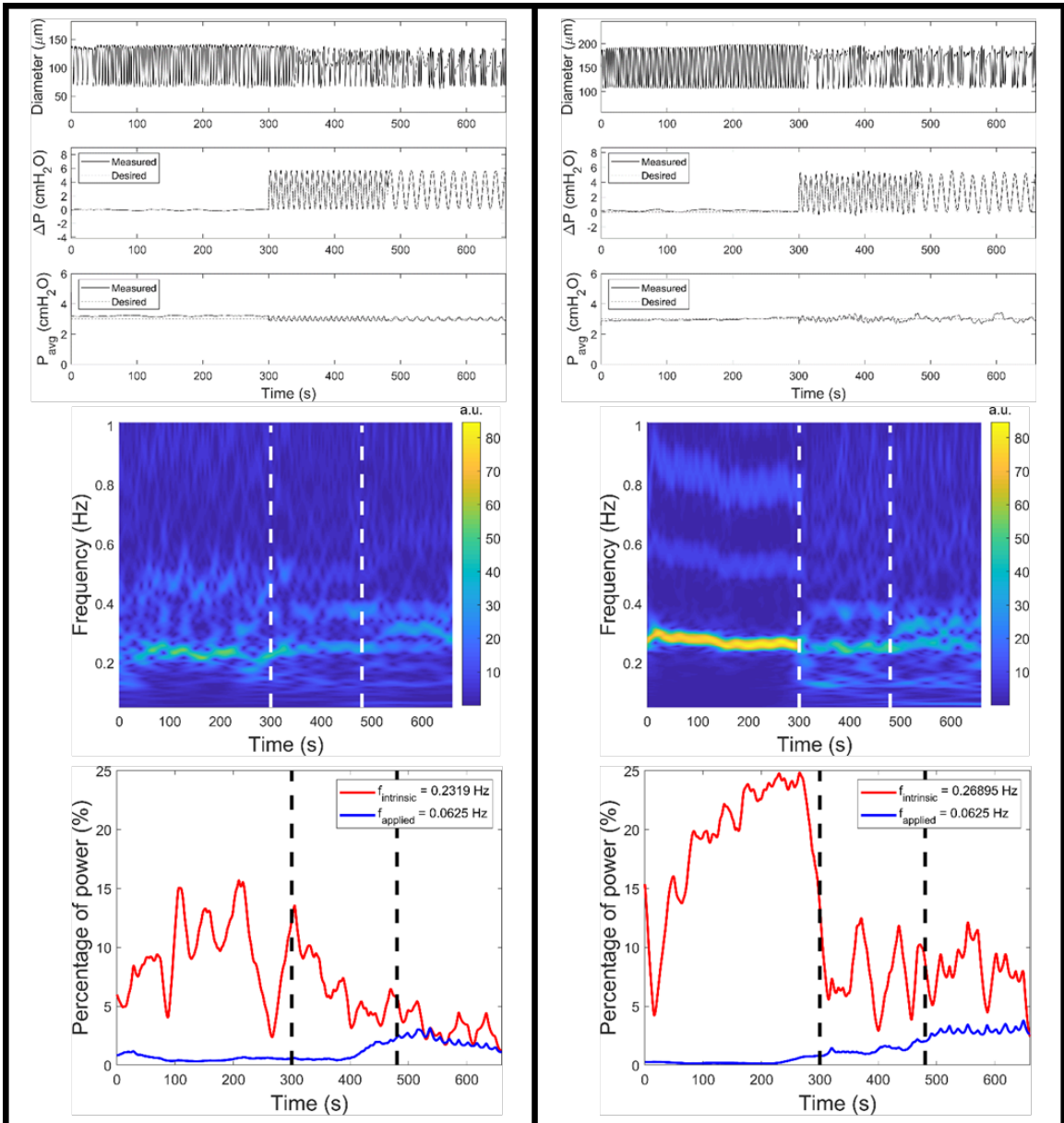
Figure C.1: The response to oscillatory pressure waveforms have been shown for two mesenteric lymphatic vessels. The top two sets of tracings show the diameter tracings along with the pressure gradient and average pressure tracings. The lower two images represent the CWT of the diameter tracing and the plot of the power at one of the applied frequencies vs time, respectively. The CWT and power tracings have been divided by the dashed lines into 3 sections: the first section corresponds to no flow (intrinsic contractility) condition, the second section had an oscillatory pressure waveform with an amplitude of 4 cmH_2O and frequency of 0.125 Hz applied to the vessel, and the third section had an oscillatory pressure waveform with amplitude of 4 cmH_2O and frequency of 0.0625 Hz applied to the vessel.
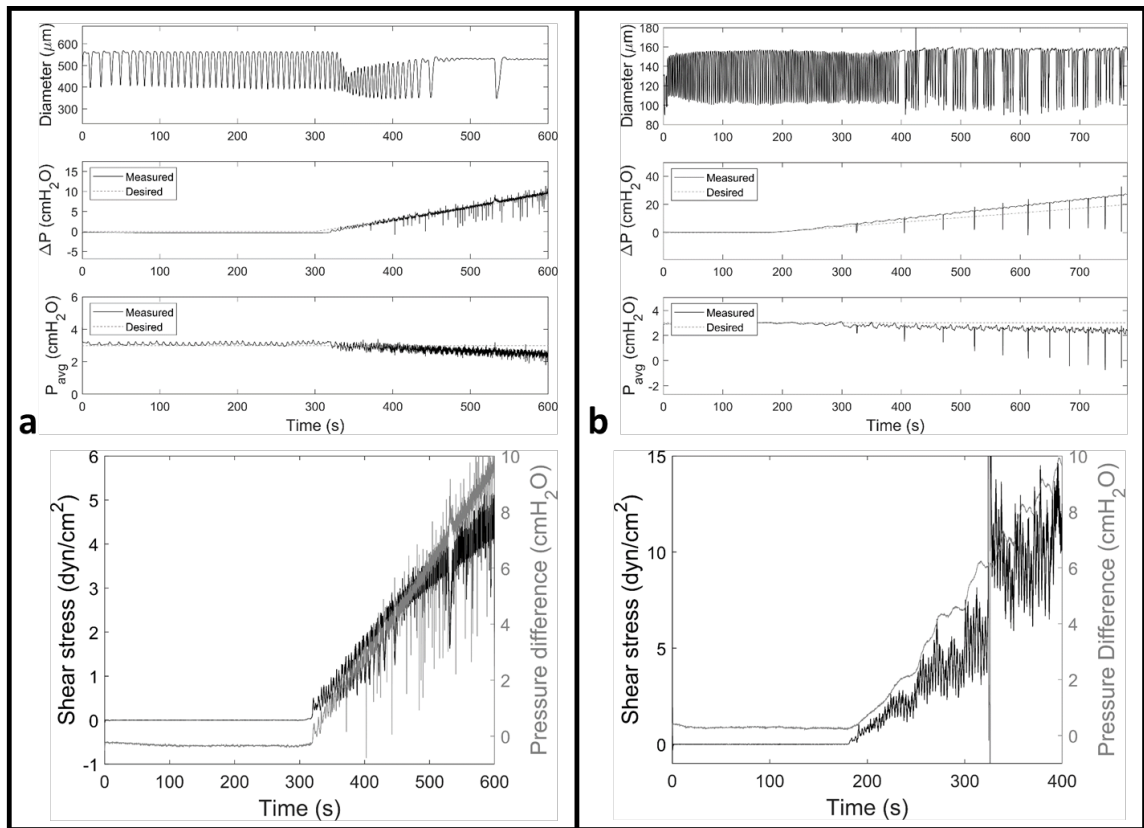
Figure C.2: The response to a ramped pressure gradient, along with the shear stresses have been shown for a) a thoracic duct and b) a mesenteric lymphatic vessel. The top graphs show the diameter tracings along with the pressure gradient and average pressure tracings. The lower two graphs show the wall shear stress on the vessel lumen plotted on top of the pressure gradient applied across the vessel chamber.
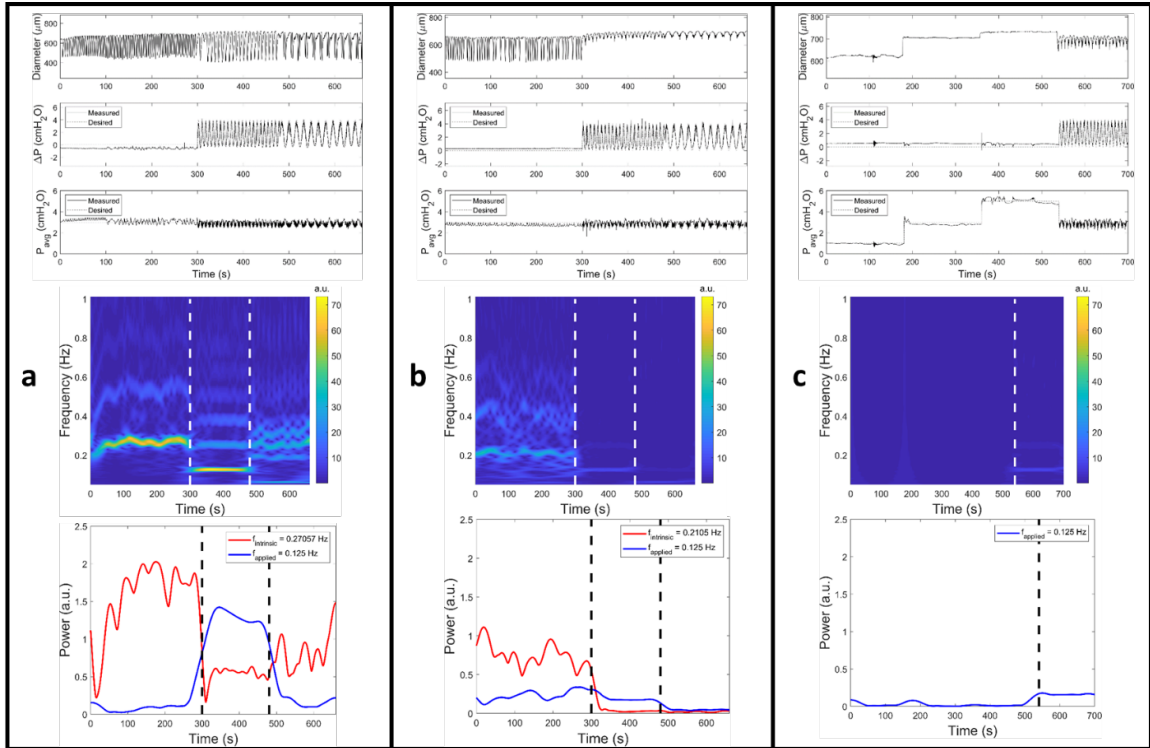
Figure C.3: The diameter and pressure tracings, CWT of diameter tracings, and power in the applied frequency vs time are shown in the top, middle and bottom panels respectively. The intact vessel (a) and denuded vessel (b) are exposed to 3 pressure conditions differentiated by the dashed lines: the first section corresponds to no flow (intrinsic contractility) condition, the second section had an oscillatory pressure waveform with an amplitude of 4 cmH_2O and frequency of 0.125 Hz applied to the vessel, and the third section had an oscillatory pressure waveform with amplitude of 4 cmH_2O and frequency of 0.0625 Hz applied to the vessel. The denuded vessel exposed to calcium free media (c) was taken through transmural pressure steps of 1, 3 and 5 cmH_2O at 0 cmH_2O pressure gradient (no flow) and subsequently exposed to an oscillatory pressure gradient with an amplitude of 4 cmH_2O and frequency of 0.125 Hz.

126

APPENDIX D

SUPPLEMENTARY FIGURES FOR CHAPTER 4
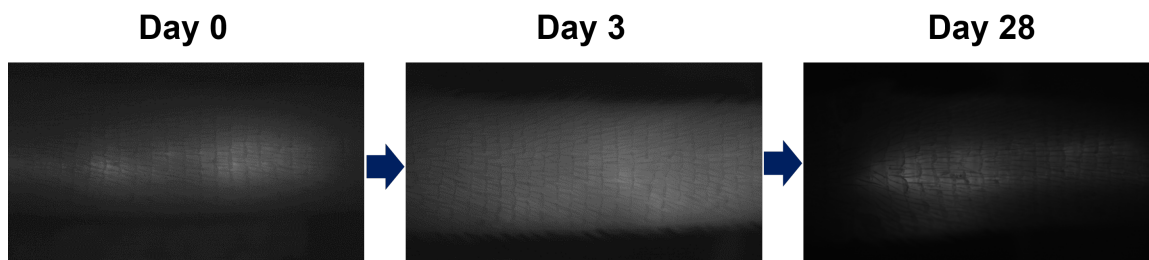
Figure D.1: Representative NIR images of the ROI (distal to the incision site) at different time points post ligation. Day 0 shows healthy collecting lymphatics prior to surgery. The vessels were easily distinguishable. Day 3 was marked by leakage of the dye into the interstitium which made it impossible to locate the collecting lymphatic vessels. By day 28, the swelling was resolved and the collecting lymphatics could be clearly located again.
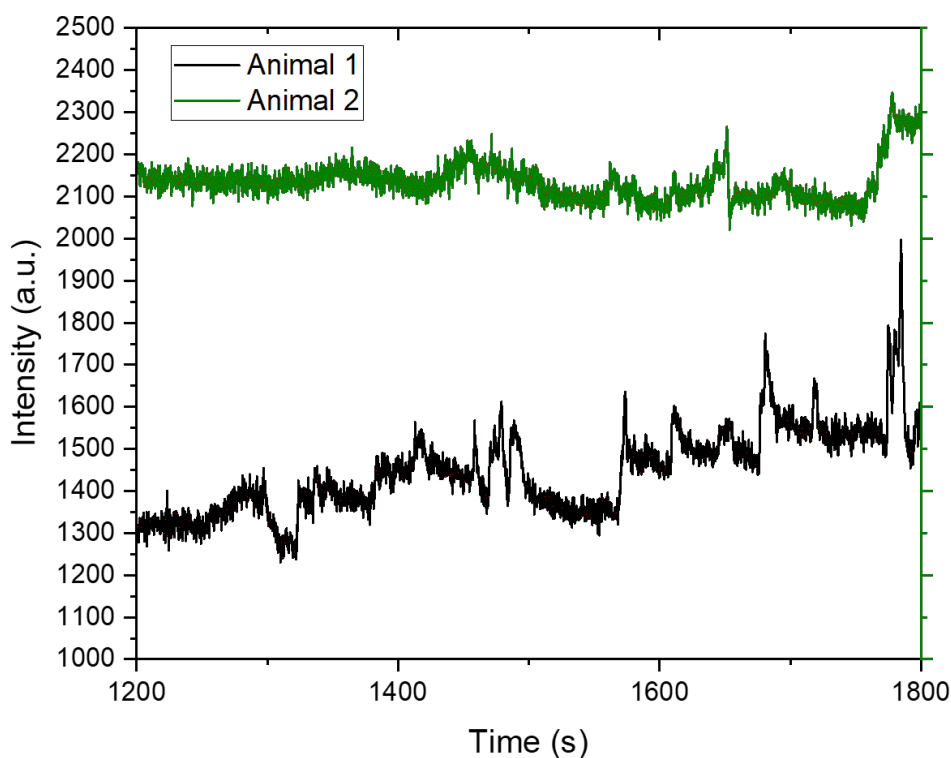
Figure D.2: The intensity during the 10 min time window after the application of OPW for two different animals. Animal 1 shows contractions while animal 2 does not, despite having a higher intensity. This shows that the inhibition of contractile activity that is observed after the OPW is removed is caused by inhibition of contractility and not because of the intensity going below the detection limit for the dye.
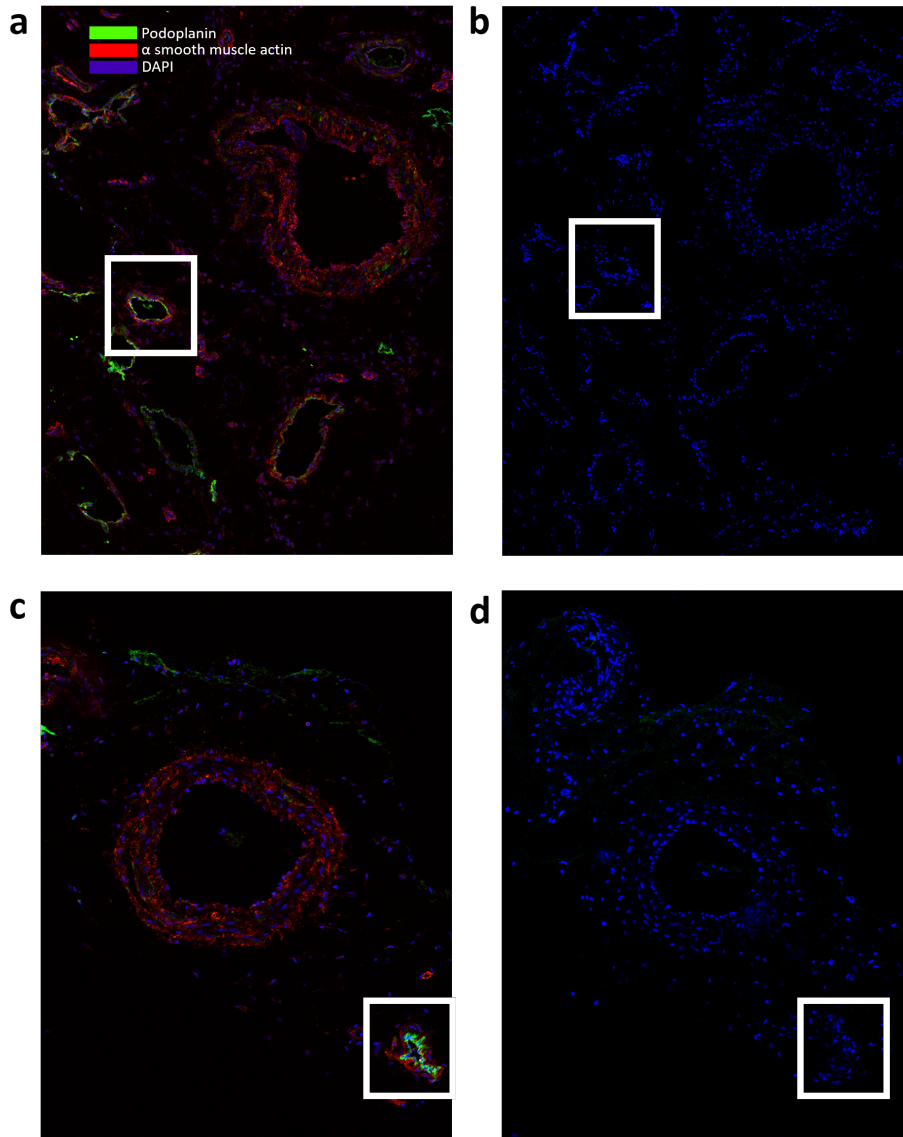
Figure D.3: Staining of the whole tissue sections, along with the corresponding negative controls. A) The tissue from a sham animal, stained with anti-podoplanin (green) and anti-αSMA (red) primary antibodies is shown. The lymphatic vessel, identified from the podoplanin stain, is marked with the white rectangle. B) An adjacent section from the same tissue sample is exposed to the primary, but no secondary, antibody to detect any autofluorescence. No detectable αSMA or podoplanin stains were found. The estimated position of the lymphatic vessel (obtained by comparing with the preceding section and the DAPI (blue) stain is marked with the white rectangle. C) A stained section from a ligation animal is shown and one of the lymphatic vessels is marked with the white square. D) An adjacent section from the tissue was stained using an isotype control for the primary (same concentration) and the same secondaries as the previous section to detect non-specific binding of the primary antibodies. No detectable fluorescence was found for podoplanin and αSMA. The estimated position of the lymphatic vessel (from the DAPI stain) is shown by the white rectangle.

REFERENCES

[1] R. Suy, S. Thomis, and I. Fourneau, "The discovery of the lymphatic system in the seventeenth century. Part II: the discovery of Chyle vessels.," *Acta chirurgica Belgica*, vol. 116, no. 5, pp. 329–335, 2016.

[2] S. P. Williams, M. G. Achen, S. B. Fox, S. A. Stacker, T. Karnezis, and R. Shayan, "Lymphangiogenesis and lymphatic vessel remodelling in cancer," *Nature Reviews Cancer*, vol. 14, no. 3, pp. 159–172, 2014.

[3] L. V. Leak and J. F. Burke, "Electron microscopic study of lymphatic capillaries in the removal of connective tissue fluids and particulate substances.," *Lymphology*, vol. 1, no. 2, pp. 39–52, 1968.

[4] L. Leak, "Electron microscopic observations on lymphatic capillaries and the structural components of the connective tissue-lymph interface," *Microvasc Res*, vol. 2, no. 4, pp. 361–391, 1970.

[5] G. W. Schmid-Schönbein and G. W. Schmid-Schonbein, "Microlymphatics and lymph flow.," *Physiological Reviews*, vol. 70, no. 4, pp. 987–1028, 1990.

[6] P. Baluk, J. Fuxe, H. Hashizume, T. Romano, E. Lashnits, S. Butz, D. Vestweber, M. Corada, C. Molendini, E. Dejana, and D. M. McDonald, "Functionally specialized junctions between endothelial cells of lymphatic vessels.," *The Journal of experimental medicine*, vol. 204, no. 10, pp. 2349–2362, 2007.

[7] J. Trzewik, S. K. Mallipattu, G. M. Artmann, F. A. Delano, and G. W. Schmid-Schonbein, "Evidence for a second valve system in lymphatics: endothelial microvalves.," *FASEB journal : official publication of the Federation of American Societies for Experimental Biology*, vol. 15, no. 10, pp. 1711–1717, 2001.

[8] L. V. Leak and J. F. Burke, "Fine structure of the lymphatic capillary and the adjoining connective tissue area.," *The American journal of anatomy*, vol. 118, no. 3, pp. 785–809, 1966.

[9] K. Aukland and R. K. Reed, "Interstitial-lymphatic mechanisms in the control of extracellular fluid volume," *Physiological Reviews*, vol. 73, no. 1, 1 LP –78, 1993.

[10] G. Sacchi, E. Weber, M. Agliano, N. Raffaelli, and L. Comparini, "The structure of superficial lymphatics in the human thigh: precollectors," *The Anatomical Record*, vol. 247, no. 1, pp. 53–62, 1997.

[11]   C. Scavelli, E. Weber, M. Aglianò, T. Cirulli, B. Nico, A. Vacca, and D. Ribatti, "Lymphatics at the crossroads of angiogenesis and lymphangiogenesis," *Journal of Anatomy*, vol. 204, no. 6, pp. 433–449, 2004.

[12]   K. H. Albertine, L. M. Fox, and C. C. C. O'Morchoe, "The morphology of canine lymphatic valves," *The Anatomical Record*, vol. 202, no. 4, pp. 453–461, 1982.

[13]   E. Bazigou, J. T. Wilson, and J. E. Moore, "Primary and secondary lymphatic valve development: Molecular, functional and mechanical insights," *Microvascular Research*, vol. 96, no. 5, pp. 38–45, 2014. arXiv: 15334406.

[14]   M. Muthuchamy, A. Gashev, and N. Boswell, "Molecular and functional analyses of the contractile apparatus in lymphatic muscle," *The FASEB journal*, no. 1, 2003.

[15]   D. C. Zawieja, "Contractile physiology of lymphatics.," *Lymphatic research and biology*, vol. 7, no. 2, pp. 87–96, 2009.

[16]   M. A. Swartz, "The physiology of the lymphatic system," *Advanced Drug Delivery Reviews*, vol. 50, no. 1-2, pp. 3–20, 2001.

[17]   T. J. Heath, R. L. Kerlin, and H. J. Spalding, "Afferent pathways of lymph flow within the popliteal node in sheep.," *Journal of anatomy*, vol. 149, pp. 65–75, 1986.

[18]   T. H. Adair and A. C. Guyton, "Modification of lymph by lymph nodes. II. Effect of increased lymph node venous blood pressure," *American Journal of Physiology - Heart and Circulatory Physiology*, vol. 245, no. 4, H616 LP –H622, 1983.

[19]   C. C. Clement, W. Wang, M. Dzieciatkowska, M. Cortese, K. C. Hansen, A. Becerra, S. Thangaswamy, I. Nizamutdinova, J.-Y. Moon, L. J. Stern, A. A. Gashev, D. Zawieja, and L. Santambrogio, "Quantitative Profiling of the Lymph Node Clearance Capacity," *Scientific reports*, vol. 8, no. 1, pp. 1–16, 2018.

[20]   M. Jafarnejad, M. C. Woodruff, D. C. Zawieja, M. C. Carroll, and J. E. Moore, "Modeling Lymph Flow and Fluid Exchange with Blood Vessels in Lymph Nodes," *Lymphatic research and biology*, vol. 13, no. 4, pp. 234–47, 2015.

[21]   A. Mukherjee, J. Hooks, and J. B. Dixon, "Physiology: Lymph Flow," in *Lymphedema*, B.-B. Lee, S. G. Rockson, and J. Bergan, Eds., Cham: Springer International Publishing, 2018, pp. 91–111, ISBN: 978-3-319-52423-8.

[22]   J. B. Dixon, S. T. Greiner, A. a. Gashev, G. L. Cote, J. E. Moore, and D. C. Zawieja, "Lymph flow, shear stress, and lymphocyte velocity in rat mesenteric prenodal lymphatics.," *Microcirculation (New York, N.Y. : 1994)*, vol. 13, no. 7, pp. 597–610, 2006.

[23] S. D. Moore-Olufemi, H. Xue, S. J. Allen, F. a. Moore, R. H. Stewart, G. a. Laine, and C. S. Cox, "Effects of primary and secondary intra-abdominal hypertension on mesenteric lymph flow: implications for the abdominal compartment syndrome.," *Shock (Augusta, Ga.)*, vol. 23, no. 6, pp. 571–5, 2005.

[24] E. Rahbar, T. Akl, G. L. Coté, J. E. Moore, and D. C. Zawieja, "Lymph Transport in Rat Mesenteric Lymphatics Experiencing Edemagenic Stress," *Microcirculation*, vol. 21, no. 5, pp. 359–367, 2014.

[25] T. Kassis, S. C. Yarlagadda, A. B. Kohan, P. Tso, V. Breedveld, and J. B. Dixon, "Postprandial lymphatic pump function after a high-fat meal: a characterization of contractility, flow, and viscosity," *American Journal of Physiology - Gastrointestinal and Liver Physiology*, vol. 310, no. 10, G776–G789, 2016.

[26] B. J. Ballermann, A. Dardik, E. Eng, and A. Liu, "Shear stress and the endothelium," *Kidney International*, vol. 54, S100–S108, 1998.

[27] H. Lipowsky, "Microvascular Rheology and Hemodynamics," *Microcirculation (New York, NY : 1994)*, vol. 12, no. 1, pp. 5–15, 2005.

[28] N. G. McHale and I. C. Roddie, "The effect of transmural pressure on pumping activity in isolated bovine lymphatic vessels.," *The Journal of physiology*, vol. 261, no. 2, pp. 255–269, 1976.

[29] J. N. Benoit, D. C. Zawieja, A. H. Goodman, and H. J. Granger, "Characterization of intact mesenteric lymphatic pump and its responsiveness to acute edemagenic stress.," *The American journal of physiology*, vol. 257, no. 6 Pt 2, H2059–69, 1989.

[30] J. B. Dixon, "Lymphatic lipid transport: sewer or subway?" *Trends in endocrinology and metabolism: TEM*, vol. 21, no. 8, pp. 480–7, 2010.

[31] A. R. Hargens and B. W. Zweifach, "Contractile stimuli in collecting lymph vessels.," *The American journal of physiology*, vol. 233, no. 1, H57–65, 1977.

[32] A. A. Gashev, "Physiologic aspects of lymphatic contractile function: current perspectives.," *Annals of the New York Academy of Sciences*, vol. 979, 178–87; discussion 188–96, 2002.

[33] A. W. Caulk, Z. V. Nepiyushchikh, R. Shaw, B. Dixon, and R. L. Gleason, "Quantification of the passive and active biaxial mechanical behaviour and microstructural organization of rat thoracic ducts.," *Journal of the Royal Society, Interface / the Royal Society*, vol. 12, no. 108, p. 20 150 280, 2015.

[34] M. S. Razavi, J. Leonard-Duke, B. Hardie, J. B. Dixon, and R. L. Gleason, "Axial stretch regulates rat tail collecting lymphatic vessel contractions," *Scientific Reports*, vol. 10, no. 1, p. 5918, 2020.

[35] A. Koller, R. Mizuno, and G. Kaley, "Flow reduces the amplitude and increases the frequency of lymphatic vasomotion: role of endothelial prostanoids.," *The American journal of physiology*, vol. 277, no. 6, R1683–9, 1999.

[36] A. A. Gashev, "[The pump function of the lymphangion and the effect on it of different hydrostatic conditions].," *Fiziologicheskii zhurnal SSSR imeni I. M. Sechenova*, vol. 75, no. 12, pp. 1737–43, 1989.

[37] A. A. Gashev, M. J. Davis, and D. C. Zawieja, "Inhibition of the active lymph pump by flow in rat mesenteric lymphatics and thoracic duct," *Journal of Physiology*, vol. 540, no. 3, pp. 1023–1037, 2002.

[38] J. A. Kornuta, Z. Nepiyushchikh, O. Y. Gasheva, A. Mukherjee, D. C. Zawieja, and J. B. Dixon, "Effects of dynamic shear and transmural pressure on wall shear stress sensitivity in collecting lymphatic vessels," *American Journal of Physiology - Regulatory, Integrative and Comparative Physiology*, vol. 309, no. 9, R1122 LP –R1134, 2015.

[39] L. V. Leak, J. L. Cadet, C. P. Griffin, and K Richardson, "Nitric-Oxide Production By Lymphatic Endothelial-Cells in-Vitro," *Biochemical and Biophysical Research Communications*, vol. 217, no. 1, pp. 96–105, 1995.

[40] J. P. Scallan and M. J. Davis, "Genetic removal of basal nitric oxide enhances contractile activity in isolated murine collecting lymphatic vessels," *Journal of Physiology*, vol. 591, no. 8, pp. 2139–2156, 2013.

[41] I. T. Nizamutdinova, D. Maejima, T. Nagai, E. Bridenbaugh, S. Thangaswamy, V. Chatterjee, C. J. Meininger, and A. A. Gashev, "Involvement of Histamine in Endothelium-Dependent Relaxation of Mesenteric Lymphatic Vessels," *Microcirculation*, vol. 21, no. 7, pp. 640–648, 2014.

[42] C. J. Morris, R. J. Kameny, J. Boehme, W. Gong, Y. He, T. Zhu, E. Maltepe, G. W. Raff, J. R. Fineman, and S. A. Datar, "KLF2-mediated disruption of PPAR-γ signaling in lymphatic endothelial cells exposed to chronically increased pulmonary lymph flow," *American Journal of Physiology-Heart and Circulatory Physiology*, vol. 315, no. 1, H173–H181, 2018.

[43] D. C. Zawieja, S. T. Greiner, K. L. Davis, W. M. Hinds, and H. J. Granger, "Reactive oxygen metabolites inhibit spontaneous lymphatic contractions.," *The American journal of physiology*, vol. 260, no. 6 Pt 2, H1935–H1943, 1991.

[44] J. Hagendoorn, T. P. Padera, S. Kashiwagi, N. Isaka, F. Noda, M. I. Lin, P. L. Huang, W. C. Sessa, D. Fukumura, and R. K. Jain, "Endothelial nitric oxide synthase regulates microlymphatic flow via collecting lymphatics," *Circulation Research*, vol. 95, no. 2, pp. 204–209, 2004.

[45] O. Y. Gasheva, D. C. Zawieja, and A. a. Gashev, "Contraction-initiated NO-dependent lymphatic relaxation: a self-regulatory mechanism in rat thoracic duct," *The Journal of physiology*, vol. 575, no. Pt 3, pp. 821–32, 2006.

[46] C. M. Quick, A. M. Venugopal, A. A. Gashev, D. C. Zawieja, and R. H. Stewart, "Intrinsic pump-conduit behavior of lymphangions.," *American journal of physiology. Regulatory, integrative and comparative physiology*, vol. 292, no. 4, R1510–8, 2007.

[47] C. M. Quick, B. L. Ngo, A. M. Venugopal, and R. H. Stewart, "Lymphatic pump-conduit duality: contraction of postnodal lymphatic vessels inhibits passive flow," *American journal of physiology Heart and circulatory physiology*, vol. 296, no. 3, H662–8, 2009.

[48] B. Li, I. Silver, J. P. Szalai, and M. G. Johnston, "Pressure-volume relationships in sheep mesenteric lymphatic vessels in situ: response to hypovolemia.," *Microvasc Res*, vol. 56, no. 2, pp. 127–138, 1998.

[49] M. K. Ferguson, U Williams, A. R. Leff, and R. W. Mitchell, "Length-tension characteristics of bovine tracheobronchial lymphatic smooth muscle," *Lymphology*, vol. 26, no. 1, pp. 19–24, 1993.

[50] R.-Z. Zhang, A. A. Gashev, D. C. Zawieja, and M. J. Davis, "Length-tension relationships of small arteries, veins, and lymphatics from the rat mesenteric microcirculation.," *American journal of physiology Heart and circulatory physiology*, vol. 292, no. 4, H1943–52, 2007.

[51] A. A. Gashev, R. Z. Zhang, M Muthuchamy, D. C. Zawieja, and M. J. Davis, "Regional heterogeneity of length-tension relationships in rat lymph vessels," *Lymphat Res Biol*, vol. 10, no. 1, pp. 14–19, 2012.

[52] M. J. Davis, A. M. Davis, C. W. Ku, and A. A. Gashev, "Myogenic constriction and dilation of isolated lymphatic vessels," vol. 65212, pp. 293–302, 2009.

[53] J. P. Scallan, J. H. Wolpers, M. Muthuchamy, D. C. Zawieja, A. A. Gashev, and M. J. Davis, "Independent and interactive effects of preload and afterload on the pump function of the isolated lymphangion.," *American journal of physiology Heart and circulatory physiology*, vol. 303, no. 7, H809–24, 2012.

[54] J. P. Scallan, A. A. Gashev, M. J. Davis, M. Muthuchamy, D. C. Zawieja, and J. H. Wolpers, "Intrinsic increase in lymphangion muscle contractility in response to elevated afterload," *American Journal of Physiology-Heart and Circulatory Physiology*, vol. 303, no. 7, H795–H808, 2012.

[55] R. Zhang, A. A. Gashev, D. C. Zawieja, M. M. Lane, and M. J. Davis, "Length-dependence of lymphatic phasic contractile activity under isometric and isobaric conditions," *Microcirculation (New York, NY : 1994)*, vol. 14, no. 6, pp. 613–625, 2007.

[56] J. P. Scallan, J. H. Wolpers, and M. J. Davis, "Constriction of isolated collecting lymphatic vessels in response to acute increases in downstream pressure," *Journal of Physiology*, vol. 591, no. 2, pp. 443–459, 2013.

[57] C. A. Hanley, R. M. Elias, and M. G. Johnston, "Is endothelium necessary for transmural pressure-induced contractions of bovine truncal lymphatics?" *Microvascular Research*, vol. 43, no. 2, pp. 134–146, 1992.

[58] F. Sachs, "Stretch-Activated Ion Channels: What Are They?" *Physiology*, vol. 25, no. 1, pp. 50–56, 2010.

[59] A. Mukherjee and J. B. Dixon, "Mechanobiology of lymphatic vessels," in *Mechanobiology in vascular physiology and disease*, M. Hecker and D. Duncker, Eds., Springer, New York, NY, In press.

[60] R. M. Dongaonkar, T. L. Nguyen, C. M. Quick, J Hardy, G. A. Laine, E Wilson, and R. H. Stewart, "Adaptation of mesenteric lymphatic vessels to prolonged changes in transmural pressure.," *American journal of physiology Heart and circulatory physiology*, vol. 305, no. 2, H203–210, 2013.

[61] S. G. Rockson, "Lymphedema," *American Journal of Medicine*, vol. 110, no. 4, pp. 288–295, 2001.

[62] S. H. Ridner, "Pathophysiology of Lymphedema," *Seminars in Oncology Nursing*, vol. 29, no. 1, pp. 4–11, 2013.

[63] K. Radhakrishnan and S. G. Rockson, "The clinical spectrum of lymphatic disease," *Annals of the New York Academy of Sciences*, vol. 1131, pp. 155–184, 2008.

[64] A. G. Warren, H. Brorson, L. J. Borud, and S. A. Slavin, "Lymphedema: a comprehensive review," *Annals of plastic surgery*, vol. 59, no. 4, pp. 464–472, 2007.

[65] M. Mihara, H. Hara, Y. Hayashi, M. Narushima, T. Yamamoto, T. Todokoro, T. Iida, N. Sawamoto, J. Araki, K. Kikuchi, N. Murai, T. Okitsu, I. Kisu, and I. Koshima, "Pathological steps of cancer-related lymphedema: histological changes in the col-

lecting lymphatic vessels after lymphadenectomy.," *PloS one*, vol. 7, no. 7, e41126, 2012.

[66] T. S. Nelson, Z. Nepiyushchikh, J. S. T. Hooks, M. S. Razavi, T. Lewis, C. C. Clement, M. Thoresen, M. T. Cribb, M. K. Ross, R. L. Gleason, L. Santambrogio, J. F. Peroni, and J. B. Dixon, "Lymphatic remodelling in response to lymphatic injury in the hind limbs of sheep," *Nature Biomedical Engineering*, vol. 4, no. 6, pp. 649–661, 2020.

[67] E. Gousopoulos, S. T. Proulx, J. Scholl, M. Uecker, and M. Detmar, "Prominent Lymphatic Vessel Hyperplasia with Progressive Dysfunction and Distinct Immune Cell Infiltration in Lymphedema.," *The American journal of pathology*, vol. 186, no. 8, pp. 2193–2203, 2016.

[68] W. L. Olszewski, "Contractility patterns of normal and pathologically changed human lymphatics," *Annals of the New York Academy of Sciences*, vol. 979, no. 1, 52–63; discussion 76–79, 2002.

[69] S. Modi, A. W. B. Stanton, W. E. Svensson, A. M. Peters, P. S. Mortimer, and J. R. Levick, "Human lymphatic pumping measured in healthy and lymphoedematous arms by lymphatic congestion lymphoscintigraphy.," *The Journal of physiology*, vol. 583, no. Pt 1, pp. 271–285, 2007.

[70] W. L. Olszewski, "Contractility patterns of human leg lymphatics in various stages of obstructive lymphedema," *Annals of the New York Academy of Sciences*, vol. 1131, pp. 110–118, 2008.

[71] S. A. Datar, W. Gong, Y. He, M. Johengen, R. J. Kameny, G. W. Raff, E. Maltepe, P. E. Oishi, and J. R. Fineman, "Disrupted NOS signaling in lymphatic endothelial cells exposed to chronically increased pulmonary lymph flow.," *American journal of physiology Heart and circulatory physiology*, vol. 311, no. 1, H137–45, 2016.

[72] H. Cai and D. G. Harrison, "Endothelial dysfunction in cardiovascular diseases: The role of oxidant stress," *Circulation Research*, vol. 87, no. 10, pp. 840–844, 2000.

[73] L. L. Munn and T. P. Padera, "Imaging the lymphatic system," *Microvascular research*, vol. 96, pp. 55–63, 2014.

[74] J. C. Rasmussen, I.-C. Tan, M. V. Marshall, C. E. Fife, E. M. Sevick, E. M. Sevick-Muraca, and E. M. Sevick, "Lymphatic Imaging in Humans with Near-Infrared Fluorescence," *Curr Opin Biotechnol*, vol. 20, no. 1, pp. 74–82, 2010.

[75] R. Sharma, W. Wang, J. C. Rasmussen, A. Joshi, J. P. Houston, K. E. Adams, A. Cameron, S. Ke, S. Kwon, M. E. Mawad, and E. M. Sevick-Muraca, "Quantitative

imaging of lymph function.," *American journal of physiology Heart and circulatory physiology*, vol. 292, no. 6, H3109–18, 2007.

[76] N. Unno, K. Inuzuka, M. Suzuki, N. Yamamoto, D. Sagara, M. Nishiyama, and H. Konno, "Preliminary experience with a novel fluorescence lymphography using indocyanine green in patients with secondary lymphedema," *J Vasc Surg*, vol. 45, no. 5, pp. 1016–1021, 2007.

[77] N. Unno, M. Nishiyama, M. Suzuki, N. Yamamoto, K. Inuzuka, D. Sagara, H. Tanaka, and H. Konno, "Quantitative Lymph Imaging for Assessment of Lymph Function using Indocyanine Green Fluorescence Lymphography," *European Journal of Vascular and Endovascular Surgery*, vol. 36, no. 2, pp. 230–236, 2008.

[78] N. Unno, M. Nishiyama, M. Suzuki, H. Tanaka, N. Yamamoto, D. Sagara, Y. Mano, and H. Konno, "A novel method of measuring human lymphatic pumping using indocyanine green fluorescence lymphography," *Journal of Vascular Surgery*, vol. 52, no. 4, pp. 946–952, 2010.

[79] E. A. Maus, I.-C. Tan, J. C. Rasmussen, M. V. Marshall, C. E. Fife, L. A. Smith, R. Guilliod, and E. M. Sevick-Muraca, "Near-infrared fluorescence imaging of lymphatics in head and neck lymphedema," *Head & Neck*, vol. 34, no. 3, R. B. Smith, Ed., pp. 448–453, 2012.

[80] M. Weiler and J. B. Dixon, "Differential transport function of lymphatic vessels in the rat tail model and the long-term effects of indocyanine green as assessed with near-infrared imaging," *Frontiers in Physiology*, vol. 4 AUG, no. August, pp. 1–10, 2013.

[81] H. Tsunemoto, F. Ikomi, and T. Ohhashi, "Flow-Mediated Release of Nitric Oxide from Lymphatic Endothelial Cells of Pressurized Canine Thoracic Duct.," *The Japanese Journal of Physiology*, vol. 53, no. 3, pp. 157–163, 2005.

[82] A. A. Gashev, M. J. Davis, M. D. Delp, and D. C. Zawieja, "Regional variations of contractile activity in isolated rat lymphatics.," *Microcirculation (New York, N.Y. : 1994)*, vol. 11, no. 6, pp. 477–92, 2004.

[83] J. A. Kornuta and J. B. Dixon, "Ex vivo lymphatic perfusion system for independently controlling pressure gradient and transmural pressure in isolated vessels.," *Annals of biomedical engineering*, vol. 42, no. 8, pp. 1691–704, 2014.

[84] J. E. Moore and C. D. Bertram, "Lymphatic System Flows," *Annual Review of Fluid Mechanics*, vol. 50, no. 1, pp. 459–482, 2018.

[85] Y. Kawai, Y. Yokoyama, M. Kaidoh, and T. Ohhashi, "Shear stress-induced ATP-mediated endothelial constitutive nitric oxide synthase expression in human lym-

phatic endothelial cells," *American Journal of Physiology-Cell Physiology*, vol. 298, no. 3, pp. C647–C655, 2009.

[86] M. Jafarnejad, W. E. Cromer, R. R. Kaunas, S. L. Zhang, D. C. Zawieja, and J. E. Moore, "Measurement of shear stress-mediated intracellular calcium dynamics in human dermal lymphatic endothelial cells," *American Journal of Physiology-Heart and Circulatory Physiology*, vol. 308, no. 7, H697–H706, 2015.

[87] N. G. McHale and M. K. Meharg, "Co-ordination of pumping in isolated bovine lymphatic vessels," *The Journal of physiology*, vol. 450, pp. 503–512, 1992.

[88] D. C. Zawieja, K. L. Davis, R Schuster, W. M. Hinds, and H. J. Granger, "Distribution, Propagation, and Coordination of Contractile Activity in Lymphatics," *American Journal Of Physiology*, vol. 264, no. 4, H1283–H1291, 1993.

[89] E. J. Behringer, J. P. Scallan, M. Jafarnejad, J. A. Castorena-Gonzalez, S. D. Zawieja, J. E. Moore, M. J. Davis, and S. S. Segal, "Calcium and electrical dynamics in lymphatic endothelium," *Journal of Physiology*, vol. 595, no. 24, pp. 7347–7368, 2017.

[90] C. Kunert, J. W. Baish, S. Liao, T. P. Padera, and L. L. Munn, "Mechanobiological oscillators control lymph flow.," *Proceedings of the National Academy of Sciences of the United States of America*, vol. 112, no. 35, pp. 10 938–43, 2015.

[91] J. W. Baish, C. Kunert, T. P. Padera, and L. L. Munn, "Synchronization and Random Triggering of Lymphatic Vessel Contractions," *PLoS Computational Biology*, vol. 12, no. 12, pp. 1–23, 2016.

[92] D. Lu and G. S. Kassab, "Role of shear stress and stretch in vascular mechanobiology," *Journal of the Royal Society, Interface*, vol. 8, no. 63, pp. 1379–1385, 2011.

[93] K. E. Pyke and M. E. Tschakovsky, "The relationship between shear stress and flow-mediated dilatation: Implications for the assessment of endothelial function," *Journal of Physiology*, vol. 568, no. 2, pp. 357–369, 2005.

[94] A. Gnasso, C. Carallo, C. Irace, M. S. De Franceschi, P. L. Mattioli, C. Motti, and C. Cortese, "Association between wall shear stress and flow-mediated vasodilation in healthy men," *Atherosclerosis*, vol. 156, no. 1, pp. 171–176, 2001.

[95] D. C. Zawieja and K. L. Davis, "Inhibition of the active lymph pump in rat mesenteric lymphatics by hydrogen peroxide," *Lymphology*, vol. 26, no. 3, pp. 135–142, 1993.

[96] H.-J. Hsieh, C.-A. Liu, B. Huang, A. H. H. Tseng, and D. L. Wang, "Shear-induced endothelial mechanotransduction: the interplay between reactive oxygen species

(ROS) and nitric oxide (NO) and the pathophysiological implications," *Journal of Biomedical Science*, vol. 21, no. 1, p. 3, 2014.

[97] S. Chatterjee and A. B. Fisher, "Mechanotransduction in the Endothelium: Role of Membrane Proteins and Reactive Oxygen Species in Sensing, Transduction, and Transmission of the Signal with Altered Blood Flow," *Antioxidants & Redox Signaling*, vol. 20, no. 6, pp. 899–913, 2014.

[98] K. Pyke, D. J. Green, C. Weisbrod, M. Best, L. Dembo, G. O'Driscoll, and M. Tschakovsky, "Nitric oxide is not obligatory for radial artery flow-mediated dilation following release of 5 or 10 min distal occlusion," *AJP: Heart and Circulatory Physiology*, vol. 298, no. 1, H119–H126, 2010.

[99] M. J. Crowe, v. d. W. P. Y, J. A. Brock, and V. H. D. F, "Co-ordination of contractile activity in guinea-pig mesenteric lymphatics.," *The Journal of Physiology*, vol. 500, no. 1, pp. 235–244, 1997.

[100] S. D. Zawieja, W. Wang, X. Wu, Z. V. Nepiyushchikh, D. C. Zawieja, and M. Muthuchamy, "Impairments in the intrinsic contractility of mesenteric collecting lymphatics in a rat model of metabolic syndrome," *American journal of physiology Heart and circulatory physiology*, vol. 302, no. 3, H643–H653, 2012.

[101] S. D. Zawieja, O. Gasheva, D. C. Zawieja, and M. Muthuchamy, "Blunted flow-mediated responses and diminished nitric oxide synthase expression in lymphatic thoracic ducts of a rat model of metabolic syndrome.," *American journal of physiology Heart and circulatory physiology*, vol. 310, no. 3, H385–93, 2016.

[102] A. A. Gashev and D. C. Zawieja, "Hydrodynamic regulation of lymphatic transport and the impact of aging," *Pathophysiology*, vol. 17, no. 4, pp. 277–287, 2010.

[103] V. Zolla, I. T. Nizamutdinova, B. Scharf, C. C. Clement, D. Maejima, T. Akl, T. Nagai, P. Luciani, J. C. Leroux, C. Halin, S. Stukes, S. Tiwari, A. Casadevall, W. R. Jacobs, D. Entenberg, D. C. Zawieja, J. Condeelis, D. R. Fooksman, A. A. Gashev, and L. Santambrogio, "Aging-related anatomical and biochemical changes in lymphatic collectors impair lymph transport, fluid homeostasis, and pathogen clearance," *Aging cell*, vol. 14, no. 4, pp. 582–594, 2015.

[104] G. C. Goats, "Massage–the scientific basis of an ancient art: Part 2. Physiological and therapeutic effects.," *British journal of sports medicine*, vol. 28, no. 3, pp. 153–6, 1994.

[105] S. H. Ridner, "Pathophysiology of Lymphedema," *Seminars in Oncology Nursing*, vol. 29, no. 1, pp. 4–11, 2013.

[106] M. L. McNeely, D. J. Magee, A. W. Lees, K. M. Bagnall, M. Haykowsky, and J. Hanson, "The addition of manual lymph drainage to compression therapy for breast cancer related lymphedema: A randomized controlled trial," *Breast Cancer Research and Treatment*, vol. 86, no. 2, pp. 95–106, 2004.

[107] R. Koul, T. Dufan, C. Russell, W. Guenther, Z. Nugent, X. Sun, and A. L. Cooke, "Efficacy of complete decongestive therapy and manual lymphatic drainage on treatment-related lymphedema in breast cancer," *International Journal of Radiation Oncology Biology Physics*, vol. 67, no. 3, pp. 841–846, 2007.

[108] G. Szolnoky, B. Lakatos, T. Keskeny, E. Varga, M. Varga, A. Dobozy, and L. Kemény, "Intermittent Pneumatic Compression Acts Synergistically With Manual Lymphatic Drainage in Complex Decongestive Physiotherapy for Breast Cancer Treatment-Related Lymphedema," *Lymphology*, vol. 42, pp. 188–194, 2009.

[109] C. Lopera, P. R. Worsley, D. L. Bader, and D. Fenlon, "Investigating the Short-Term Effects of Manual Lymphatic Drainage and Compression Garment Therapies on Lymphatic Function Using Near-Infrared Imaging.," *Lymphatic research and biology*, vol. 15, no. 3, pp. 235–240, 2017.

[110] I. C. Tan, E. A. Maus, J. C. Rasmussen, M. V. Marshall, K. E. Adams, C. E. Fife, L. A. Smith, W. Chan, and E. M. Sevick-Muraca, "Assessment of lymphatic contractile function after manual lymphatic drainage using near-infrared fluorescence imaging," *Archives of Physical Medicine and Rehabilitation*, vol. 92, no. 5, 756–764.e1, 2011.

[111] J. Rasmussen, C. Fife, and E. Sevick-Muraca, "Imaging the Lymphatic Response to Manual Lymphatic Drainage and Pneumatic Compression Devices," *Journal of Vascular Surgery: Venous and Lymphatic Disorders*, vol. 7, no. 2, p. 285, 2019.

[112] M. J. Weiler, M. T. Cribb, Z. Nepiyushchikh, T. S. Nelson, and J. B. Dixon, "A novel mouse tail lymphedema model for observing lymphatic pump failure during lymphedema development," *Scientific Reports*, vol. 9, no. 1, pp. 1–15, 2019.

[113] C. Chong, F. Scholkmann, S. B. Bachmann, P. Luciani, J. C. Leroux, M. Detmar, and S. T. Proulx, "In vivo visualization and quantification of collecting lymphatic vessel contractility using near-infrared imaging," *Scientific Reports*, vol. 6, 2016.

[114] K. S. Blum, S. Karaman, S. T. Proulx, A. M. Ochsenbein, P. Luciani, J.-C. Leroux, C. Wolfrum, and M. Detmar, "Chronic high-fat diet impairs collecting lymphatic vessel function in mice.," *PloS one*, vol. 9, no. 4, e94713, 2014.

[115] Y. Nakajima, K. Asano, K. Mukai, T. Urai, M. Okuwa, J. Sugama, and T. Nakatani, "Near-Infrared Fluorescence Imaging Directly Visualizes Lymphatic Drainage Path-

ways and Connections between Superficial and Deep Lymphatic Systems in the Mouse Hindlimb," *Scientific reports*, vol. 8, no. 1, pp. 1–9, 2018.

[116] J. H. Groenlund, N. Telinius, S. N. Skov, and V. Hjortdal, "A Validation Study of Near-Infrared Fluorescence Imaging of Lymphatic Vessels in Humans," *Lymphatic research and biology*, vol. 15, no. 3, pp. 227–234, 2017.

[117] S. B. Bachmann, S. T. Proulx, Y. He, M. Ries, and M. Detmar, "Differential effects of anaesthesia on the contractility of lymphatic vessels in vivo," *Journal of Physiology*, vol. 597, no. 11, pp. 2841–2852, 2019.

[118] M. Weiler, T. Kassis, and J. B. Dixon, "Sensitivity analysis of near-infrared functional lymphatic imaging," *Journal of Biomedical Optics*, vol. 17, no. 6, p. 066 019, 2012.

[119] T. S. Nelson, R. E. Akin, M. J. Weiler, T. Kassis, J. A. Kornuta, J. B. Dixon, M. J. Weiler, J. B. Dixon, T. Kassis, R. E. Akin, T. S. Nelson, R. E. Akin, M. J. Weiler, T. Kassis, J. A. Kornuta, J. B. Dixon, M. J. Weiler, J. B. Dixon, T. Kassis, R. E. Akin, and T. S. Nelson, "Minimally invasive method for determining the effective lymphatic pumping pressure in rats using near-infrared imaging," *American Journal of Physiology-Regulatory, Integrative and Comparative Physiology*, vol. 306, no. 5, R281–R290, 2014.

[120] M. Zaleska, W. L. Olszewski, P. Jain, S. Gogia, A. Rekha, S. Mishra, and M. Durlik, "Pressures and Timing of Intermittent Pneumatic Compression Devices for Efficient Tissue Fluid and Lymph Flow in Limbs with Lymphedema," *Lymphatic Research and Biology*, vol. 11, no. 4, pp. 227–232, 2013.

[121] W. L. Olszewski, P. Jain, G. Ambujam, M. Zaleska, M. Cakala, and T. Gradalski, "Tissue fluid pressure and flow in the subcutaneous tissue in lymphedema - hints for manual and pneumatic compression therapy," *Phlebolymphology*, vol. 17, no. 3, pp. 144–150, 2010.

[122] N Unno, H Tanaka, M Suzuki, N Yamamoto, Y Mano, M Sano, T Saito, and H Konno, "Influence of age and gender on human lymphatic pumping pressure in the leg.," *Lymphology*, vol. 44, no. 3, pp. 113–120, 2011.

[123] M. E. Saul, P. A. Thomas, P. J. Dosen, G. K. Isbister, M. A. O'Leary, I. M. Whyte, S. A. McFadden, and D. F. van Helden, "A pharmacological approach to first aid treatment for snakebite.," *Nat Med*, vol. 17, no. 7, pp. 809–811, 2011.

[124] E. S. Weitman, S. Z. Aschen, G. Farias-Eisner, N. Albano, D. A. Cuzzone, S. Ghanta, J. C. Zampell, D. Thorek, and B. J. Mehrara, "Obesity impairs lymphatic fluid transport and dendritic cell migration to lymph nodes.," *PloS one*, vol. 8, no. 8, e70703, 2013.

[125] H. Oki, R. Honma, S. Ogasawara, Y. Fujii, X. Liu, M. Takagi, M. K. Kaneko, and Y. Kato, "Development of Sensitive Monoclonal Antibody PMab-2 Against Rat Podoplanin.," *Monoclonal antibodies in immunodiagnosis and immunotherapy*, vol. 34, no. 6, pp. 396–403, 2015.

[126] O. Skalli, P. Ropraz, A. Trzeciak, G. Benzonana, D. Gillessen, and G. Gabbiani, "A monoclonal antibody against alpha-smooth muscle actin: a new probe for smooth muscle differentiation.," *The Journal of cell biology*, vol. 103, no. 6 Pt 2, pp. 2787–2796, 1986.

[127] C. T. Rueden, J. Schindelin, M. C. Hiner, B. E. DeZonia, A. E. Walter, E. T. Arena, and K. W. Eliceiri, "ImageJ2: ImageJ for the next generation of scientific image data," *BMC Bioinformatics*, vol. 18, no. 1, p. 529, 2017.

[128] C. M. Quick, J. C. Criscione, A. Kotiya, R. M. Dongaonkar, J. Hardy, E. Wilson, A. A. Gashev, G. A. Laine, and R. H. Stewart, "Functional adaptation of bovine mesenteric lymphatic vessels to mesenteric venous hypertension.," *American journal of physiology. Regulatory, integrative and comparative physiology*, vol. 306, no. 12, R901–7, 2014.

[129] S. Liao, G. Cheng, D. A. Conner, Y. Huang, R. S. Kucherlapati, L. L. Munn, N. H. Ruddle, R. K. Jain, D. Fukumura, and T. P. Padera, "Impaired lymphatic contraction associated with immunosuppression," *Proc Natl Acad Sci U S A*, vol. 108, no. 46, pp. 18 784–18 789, 2011.

[130] S. Liao and P.-Y. von der Weid, "Inflammation-induced lymphangiogenesis and lymphatic dysfunction," *Angiogenesis*, vol. 17, no. 2, pp. 325–334, 2014.

[131] J. S. Torrisi, G. E. Hespe, D. A. Cuzzone, I. L. Savetsky, M. D. Nitti, J. C. Gardenier, G. D. Garc\'\ia Nores, D. Jowhar, R. P. Kataru, and B. J. Mehrara, "Inhibition of Inflammation and iNOS Improves Lymphatic Function in Obesity.," *Scientific reports*, vol. 6, p. 19 817, 2016.

[132] C. Zhou, W. Su, H. Han, N. Li, G. Ma, and L. Cui, "Mouse tail models of secondary lymphedema: fibrosis gradually worsens and is irreversible.," *International journal of clinical and experimental pathology*, vol. 13, no. 1, pp. 54–64, 2020.

[133] S. Jamalian, C. D. Bertram, W. J. Richardson, and J. E. Moore, "Parameter sensitivity analysis of a lumped-parameter model of a chain of lymphangions in series," pp. 1709–1717, 2013.

[134] S. Jamalian, M. J. Davis, D. C. Zawieja, and J. E. Moore, "Network Scale Modeling of Lymph Transport and Its Effective Pumping Parameters.," *PLoS one*, vol. 11, no. 2, e0148384, 2016.

[135] C. Contarino and E. F. Toro, "A one-dimensional mathematical model of collecting lymphatics coupled with an electro-fluid-mechanical contraction model and valve dynamics," vol. m, 2017. arXiv: 1702.05830.

[136] C. D. Bertram, C. Macaskill, M. J. Davis, and J. E. Moore, "Contraction of collecting lymphatics: organization of pressure-dependent rate for multiple lymphangions," *Biomechanics and Modeling in Mechanobiology*, vol. 17, no. 5, pp. 1513–1532, 2018.

[137] A. W. B. Stanton, S. Modi, R. H. Mellor, J. R. Levick, and P. S. Mortimer, "Recent advances in breast cancer-related lymphedema of the arm: lymphatic pump failure and predisposing factors," *Lymphatic research and biology*, vol. 7, no. 1, pp. 29–45, 2008.

[138] A. W. B. Stanton, S. Modi, T. M. Bennett Britton, A. D. Purushotham, A. M. Peters, J. R. Levick, and P. S. Mortimer, "Lymphatic drainage in the muscle and subcutis of the arm after breast cancer treatment," *Breast cancer research and treatment*, vol. 117, no. 3, pp. 549–557, 2009.

[139] S. K. Bains, A. W. B. Stanton, V. Cintolesi, J. Ballinger, S. Allen, C. Zammit, J. R. Levick, P. S. Mortimer, A. M. Peters, and A. D. Purushotham, "A constitutional predisposition to breast cancer-related lymphoedema and effect of axillary lymph node surgery on forearm muscle lymph flow," *Breast*, vol. 24, no. 1, pp. 68–74, 2015.

[140] V. Cintolesi, A. W. Stanton, S. K. Bains, E. Cousins, A. M. Peters, A. D. Purushotham, J. R. Levick, and P. S. Mortimer, "Constitutively Enhanced Lymphatic Pumping in the Upper Limbs of Women Who Later Develop Breast Cancer-Related Lymphedema," *Lymphatic Research and Biology*, vol. 14, no. 2, pp. 50–61, 2016.

VITA

Anish Mukherjee grew up in the city of Kolkata in West Bengal, India. While studying in high school, he had an early exposure to research when he participated in an engineering project with a friend which won him a National Award in 2008. He went on to win a Second Grand Award at the Intel International Science and Engineering Fair (ISEF) in 2009 for this project, and the minor planet 25629 was named Mukherjee to recognize his achievement. This experience sparked an interest in engineering in him, after which he went on to complete his undergraduate degree in Electrical Engineering from Jadavpur University, West Bengal, India. During his undergrad, he worked on a paper-based microfluidic point-of-care device for an undergraduate research internship which motivated him to get involved in interdisciplinary research. Anish joined the Bioengineering program at Georgia Tech in the lab of Dr. J. Brandon Dixon in 2014, where we worked on unraveling the mechanosensitivity of lymphatics to their oscillatory microenvironment for his PhD. His work and contributions to the field have been recognized through numerous awards including the American Heart Association Predoctoral Fellowship - a highly prestigious fellowship granted to doctoral students working on cutting-edge research in improving global cardiovascular, cerebrovascular and brain health. His work has produced one first author publication and another study which is currently under review, and two book chapters. Apart from his research, Anish has also been heavily involved in teaching, having been a teaching assistant for 3 semesters and earned the Center for the Integration of Research, Teaching and Learning (CIRTL) Associate certificate from Georgia Tech. He has also been an active volunteer of Asha for Education, an international nonprofit organization that works towards the education and empowerment of underprivileged children and women in India. Anish will be joining as a postdoc in Dr. Melody Swartz's lab, which is the next step in his pursuit of a career in academia.